Design of Low-Frequency acGIC Voltage Stability Laboratory Protocol

Prepared by:

Ngcebo S. Sithebe

STHNGC001

Department of Electrical Engineering
University of Cape Town

Supervisor: Dr David Oyedokun

University of Cape Town

November
2021

Dissertation presented for the degree of ***Master of Science in Engineering***
Department of Electrical Engineering
University of Cape Town

Declaration

1. I know that plagiarism is wrong. Plagiarism is to use another's work and pretend that it is one's own.
2. I have used the IEEE convention for citation and referencing. Each contribution to, and quotation in, this dissertation from the work(s) of other people, has been attributed and has been cited and referenced.
3. This dissertation is my own work.
4. I have not allowed, and will not allow anyone to copy my work with the intention of passing it off as their own work or part thereof

Name: **Ngcebo Simphiwe Sithebe**

Signature: **N.Sithebe** **Date:** 09 June 2022

Abstract

Geomagnetically Induced Currents (GICs) are formed as a direct consequence of space weather phenomena and have detrimental effects on power systems. GICs enter the power system through transformers' grounded neutrals, causing an array of problems ranging from transformer overheating to voltage instability. There have been extensive studies on the effects of GICs, particularly on power transformers as they are the power systems' most susceptible components to GICs. The effects on transformers then affect the rest of the power system and may lead to voltage instability and blackouts. Recent studies have shown that a real GIC is not necessarily a dc as it has been previously modelled in literature. In reality, GICs are multi-frequency, multi-amplitude currents. At the same time, voltage stability analysis due to GICs with low frequency ac as a GIC representative has not been explored in detail in the literature. This dissertation assesses the effects of GICs on the voltage stability of power systems using a low-frequency ac (acGIC) model as a GIC representative. This is different from the conventional dc model (dcGIC).

A laboratory and simulation protocol using a frequency-dependent transmission line with resistive and inductive elements in each phase, and a novel low-frequency ac injection circuit was designed and tested. This single frequency, single amplitude acGIC injection circuit is a first approximation of the real signal GIC. The effects and differences in the response of the power system to dc and low-frequency ac injections are explored and presented. The implementation of the protocol in the laboratory and simulation environments showed that there is a fundamental difference in the response of the power system when subjected to ac injection compared to dc injection.

The research showed that the dc model for GIC is a worst-case scenario, constantly at the 'prospective GIC. Contrarily, low-frequency ac model for GIC is constantly changing, never reaching the prospective GIC and, therefore, the extreme dc settling point. This study shows that with a low-frequency ac model, though being a first approximation, the network parameter response is not constant and the effect of the GIC on the network parameters varies with respect to the magnitude of the GIC at an instance. Furthermore, the implications on voltage stability revealed that the loadability effect on the system due to GIC is also not constant as the dc model depicts. It is, however, dependent on the current flow of GIC at a particular instance during a geomagnetic storm. This research showed that for better power systems modelling with GIC, a varying current injection is necessary to fully understand the effects on the system.

Acknowledgements

I would like to express my sincere gratitude to the Lord Jesus, Son of the Almighty God for who He is in my life, and His help in this journey. Without His help through His Spirit, I wouldn't be here.

To Prof Gaunt, for believing in me and affording me the necessary funding and extremely valuable insight during this Journey.

To my Supervisor Dr David Oyedokun, for your guidance throughout this journey despite all the challenges faced. Thank you for the support and guidance.

To Dr Hilary Chisepo, thank you so much for the help and assistance with the FEM analysis for the inductor designs. You have been my co supervisor honestly, from assistance in the lab, to providing much needed guidance in literally everything pertaining this research.

To Akshay, for his expert analysis and review of this dissertation and all along guidance and support throughout this journey. I sincerely appreciate it Sir.

To Maysam Soltanian,Riyaad Jacobs and Hoosein Salie for your outmost help in this journey in providing ideas, material and assisting with the design of the components and circuits. I am very grateful for your help and I pray God really blesses you Sir. May God come through for you when you are in need, as you have helped one of His own.

To my parents and the rest of the family, thank you for the unwavering support through your prayers and words of encouragement. I'm super grateful.

Table of Contents

List of Tables

List of Figures

NOMENCLATURE

I_{mag}	Magnetizing Current
V_{knee}	Knee point voltage
Q	Reactive Power
3p3L	Three phase ,3 limb transformer
3p5L	Three phase, 5 limb transformer.
GIC	Geomagnetically Induced Currents
GMD	Geomagnetic Disturbance
acGIC	Low frequency ac model of GIC representation
dcGIC	dc model of GIC representation
THD	Total Harmonic Distortion
TUT	Transformer under Test
GSU	Generator Step-up Unit
SIL	Surge Impedance Loading

1. Introduction

1.1 Background to the study

Geomagnetic Disturbances (GMDs) which occur as a result of abnormal space weather conditions, induce currents in the earth known as geomagnetically induced currents (GICs) [1]. When GICs enter the grounded neutrals of transformers, they cause part-wave saturation [2]. If the GIC is severe enough it causes harmonics, transformer overheating and sometimes voltage instability [3]. The response of transformers to GIC is core-type dependent i.e. some core types are more susceptible to part-wave saturation than others [4].

In March 1989, a severe GMD occurred and caused a blackout in the Hydro-Quebec power grid. The flow of GICs caused the transformers to produce excessive harmonics, which flowed to the nearby static var compensators (SVCs) and the bulk of the transmission network [5],[6],[7]. As a protective measure, seven SVCs tripped leaving about 9500 MW (44% of the province's total generated power demand) without voltage regulation. This loss of SVCs coupled with the increased reactive power demand from the transformers due to part-wave saturation led to serious voltage depressions and eventually the whole power system collapsed. A total of 21 500 MW of generation and load were lost due to the storm. Furthermore, what aggravated the effects of the GMD was that in North America, most utilities relied on very long transmission lines to supply scattered demand centres, hence making them even more vulnerable to the storm. This is because long transmission lines consume large quantities of reactive power when the MW loading exceed surge impedance loading (SIL) [8], and hence SVCs are needed to maintain acceptable voltage levels. The harmonics produced during part-wave saturation cause tripping on SVCs which may lead to voltage collapse. In addition, transformer inductance drops with increasing GIC leading to large draws of reactive power [9].

There is increasing pressure on power utilities to provide quality power supply to their customers [10]. This means that the voltage level, frequency, and power factor must be at or near the nominal values to ensure an acceptable quality of power delivery. Utilities can experience problems in their power systems when a combination of factors results in the voltage instability phenomenon. Voltage stability is defined as the ability of a power system to maintain acceptable voltages at all buses in the power system before and after being subjected to a disturbance [11],[12],[13],[14]. Voltage instability occurs when a disturbance in the power system causes a progressive and uncontrollable decrease in voltage, ultimately resulting in system collapses despite the availability of local compensation devices. This study aims to develop a laboratory testing protocol to analyse the effects of GICs on the voltage stability of a power system using low frequency as a GIC representative.

The events in Hydro-Quebec highlight the need for rigorous voltage stability analysis. Therefore, studies involving both simulation and laboratory work, modelling long high voltage frequency-dependent transmission lines, power transformers and GICs need to be conducted. These analyses will provide further insight into the voltage stability problem caused by GICs. Unfortunately, there is a limited number of GIC studies on voltage instability and so a better understanding of the system response is necessary before adequate mitigation strategies can be proposed. Although a lot of work has gone into the study of the effects of GICs on power transformers [15],[16],[17], very few studies have been conducted on the system voltage stability with GIC. These studies are briefly discussed below.

In a study with very small bench-scale laboratory transformers [18], a greater trend towards voltage instability due to dc is identified. The transformer saturation characteristics, however, were not related to the levels of dc injection that were used. Furthermore, the study was limited to a steady-state dc and the transformers had butt joints and poor grade electrical core steel. This core construction is not representative of real power transformers with multi-step lap mitred joints; a key consideration in saturation studies with GIC [16].

Overbye *et al.* [19] discussed the effects of GICs on the small disturbance voltage stability on the power system. For small disturbance voltage stability, the importance of the assumed static load model is considered. A study to investigate small disturbance voltage stability was conducted on a five-bus network in PowerWorld Simulator. The small disturbance of a system due to GICs was determined by sequentially increasing the modelled electric field until a point is reached where either the power flow converges (e.g point of maximum loadability) or the bus voltages drop to below the specified limit. The results showed that an increase in GIC injection leads to an increase in Mvars absorbed by the transformer, although the LTC (load tap changing transformer) does well to regulate the voltage, it also reaches its limit, and this leads to the system voltage collapse. The limitation of this study is that it was conducted in a simulation environment with no physical results for comparison. Furthermore, the transformer core types are not specified making it difficult to obtain detailed insights into the voltage stability problem due to GICs.

In this study, the practical implementation of a low-frequency alternating ac injection will be used to investigate a more representative response as real GIC is not dc. This approach is novel as no laboratory study on the dynamic effects of GICs has been reported. Furthermore, the model transformers simulating a power system are constructed with high-quality grain-oriented electrical core steel (GOES) with MSL core joints, just like a real power transformer. Even though a real GIC is a complex mixture of frequencies, an ac signal of frequency less than 50 mHz [20] will be used to analyse the actual real-time response, as a first approximation. Also, it has been identified that the much lower frequency components less than 10 mHz have the highest power densities (magnitudes).

1.2 Hypothesis

Based on the aspects outlined above, the hypothesis of this study is as follows:

"**The design and implementation of a laboratory test protocol to represent GIC as a non-zero frequency current can be used to better understand the real-time effects of GICs on the voltage stability of power systems**"

1.3 Research Questions

The following research questions that will enable the testing of this hypothesis are given:

i) How can GIC be emulated in the laboratory?

ii) What is a typical frequency for GIC and how can it be have emulated in the laboratory?

iii) How can the power systems' real time response to acGIC be assessed?

iv) How is the voltage stability of the power system impacted as a result of dcGIC compared to acGIC

1.4 Research Objectives

The following are the research objectives of this study:

i) To design and implement a novel low-frequency ac circuit for injecting GIC in a model power system.

ii) To design and implement a laboratory protocol suitable to investigate the effects of acGIC on the voltage stability of power systems.

iii) To contrast the system response to dc injection and low-frequency ac representation of GIC.

iv) To compare the response obtained in the laboratory to existing literature on GICs and draw conclusions.

1.5 Scope and Limitations

i) This research will use a three-phase three limb and three-phase five limb transformer for voltage stability analysis.

ii) This research will only consider unity power factor conditions hence only resistive loading configurations will be analyzed.

iii) The ac injection circuit will consist of a single frequency with varying amplitudes.

iv) The simulation aspect of this project was limited to PSCAD/ EMTDC.

1.6 Dissertation Outline

The dissertation is presented below.

Chapter 2 gives the literature review of GICs and their effects, voltage stability and GIC related laboratory studies.

Chapter 3 gives the methodology which will be undertaken effectively carry out this investigation.

Chapter 4 presents the design of the transmission line, acGIC injection circuit, and load rig to be used for the laboratory protocol.

Chapter 5 presents the laboratory protocol which gives details of preliminary tests undertaken, test system set up, voltage stability assessment and experimental procedure.

Chapter 6 presents the simulation protocol to be performed on PSCAD/EMTDC. The chapter first presents the available transformer models in the simulation software. Next, no-load tests are presented before the GIC modelling is described. The chapter then concludes with details on the voltage stability analysis to be performed in the laboratory.

Chapter 7 presents the results of the laboratory and simulation protocols and their discussions. The chapter then concludes with a comparison of simulation and laboratory results.

Chapter 8 presents the discussion and conclusion of both the laboratory tests and simulations performed throughout this investigation. This chapter answers to the research questions and then assesses the validity of the hypothesis.

2. Literature Review

2.1 GIC Overview

2.1.1 Geomagnetic Storms and Geomagnetically Induced Currents

The flow of GICs on the earth's surface is a result of complex solar events. Corona Mass Ejections (CMEs) travel from the surface of the sun and collide with the earth's magnetosphere [21]. This collision results in compression of the earth's magnetosphere which can generate large electric fields (E-fields) along the boundaries of the magnetosphere. These electric fields result in the flow of ionospheric currents causing a rapid change in the magnetic field on the earth's surface [22]. This changing magnetic field then induces an electric field on the earth surface according to Faraday's law of electromagnetism. The E-fields generate currents along the earth's surface and on grounded conductive conductors [23]. This process is summarised in the following Figure 2.1.

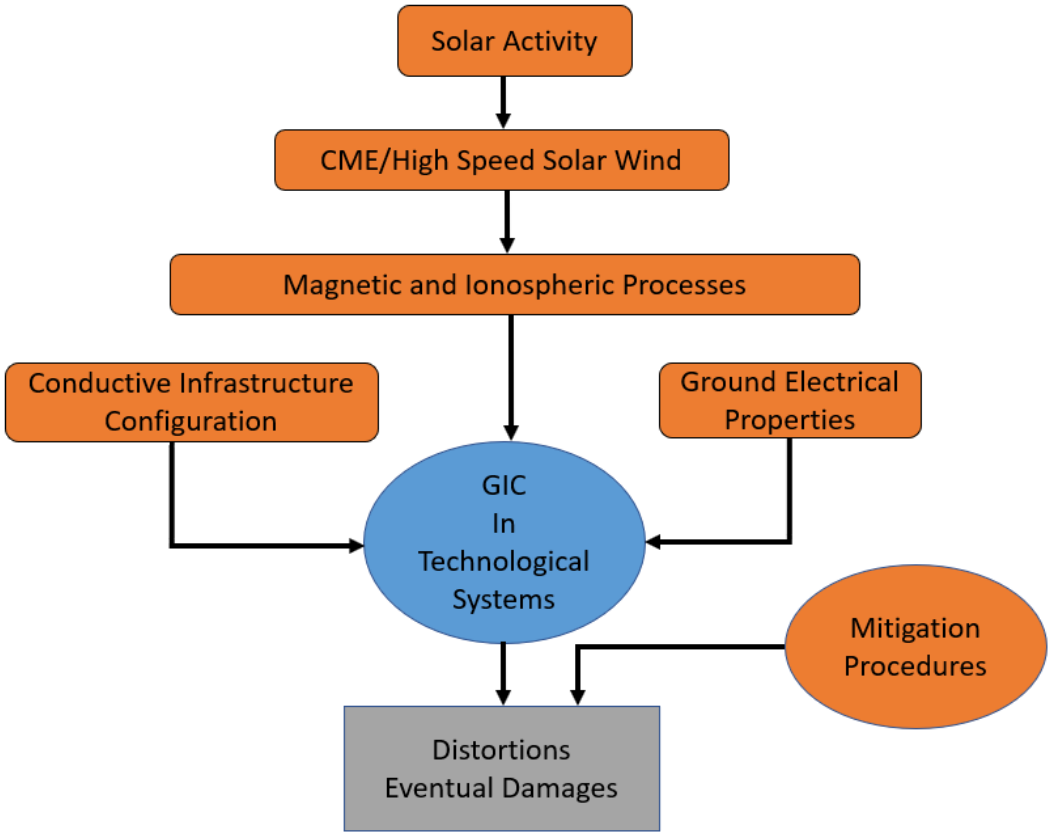

Figure 2.1: A schematic showing a chain of processes that result in the flow of GICs adapted from Caraballo [23]

The currents that flow in the earth's surface (driven by the geoelectric fields) are referred to as Geomagnetically Induced Currents (GICs). GICs have usually been modelled as "quasi-dc" due to the variation of the electric field being in minutes, and the fact that they have dominant low frequencies (0-50 mHz) relative to the power systems frequency of 60 Hz or 50 Hz [17], [24]. GICs have been previously known to be prevalent in high latitude regions like North America and Scandinavia [7],[25]. However, Gaunt and Coetzee [26] showed that the Halloween storm of 2003 caused transformer failures in South Africa, which was previously considered to be a low risk due to being a low latitude.

Geomagnetically Induced Currents have been a point of interest due to their effects on various systems on which economies depend on. These include power systems, railway lines, pipelines and

telecommunications [22],[27]. However, power systems have been the most affected [28] out of all the systems and a lot of research has been conducted on the effects of GICs on power systems. The Hydro-Quebec blackout in Canada [29] and the Malmo blackout in Sweden [30] are some examples showing the effects of GICs in power systems, and these have been the drive to increased GIC research. GICs enter power systems through the grounded neutrals of the power transformers leading to undesirable effects like part wave saturation, harmonic pollution, voltage instability, increased reactive power demand and transformer overheating [31],[32],[33],[34]. These impacts are discussed in detail in the following subsections.

2.1.2 Impacts of GICs on Power Systems

i. Transformer Part Wave Saturation

One of the major impacts of the GIC flow in power systems is part-wave saturation of the transformer core. When dcGIC flows in the transformer, the system is subjected to dc flux in the transformer core which is dependent on the reluctance path of this flux, dcGIC magnitude and the number of turns [35]. This GIC flux adds to the AC flux in one half-cycle and subtracts from the ac flux in the other half cycle thereby pushing the transformer into part wave saturation [36]. This is illustrated in Figure 2.2.

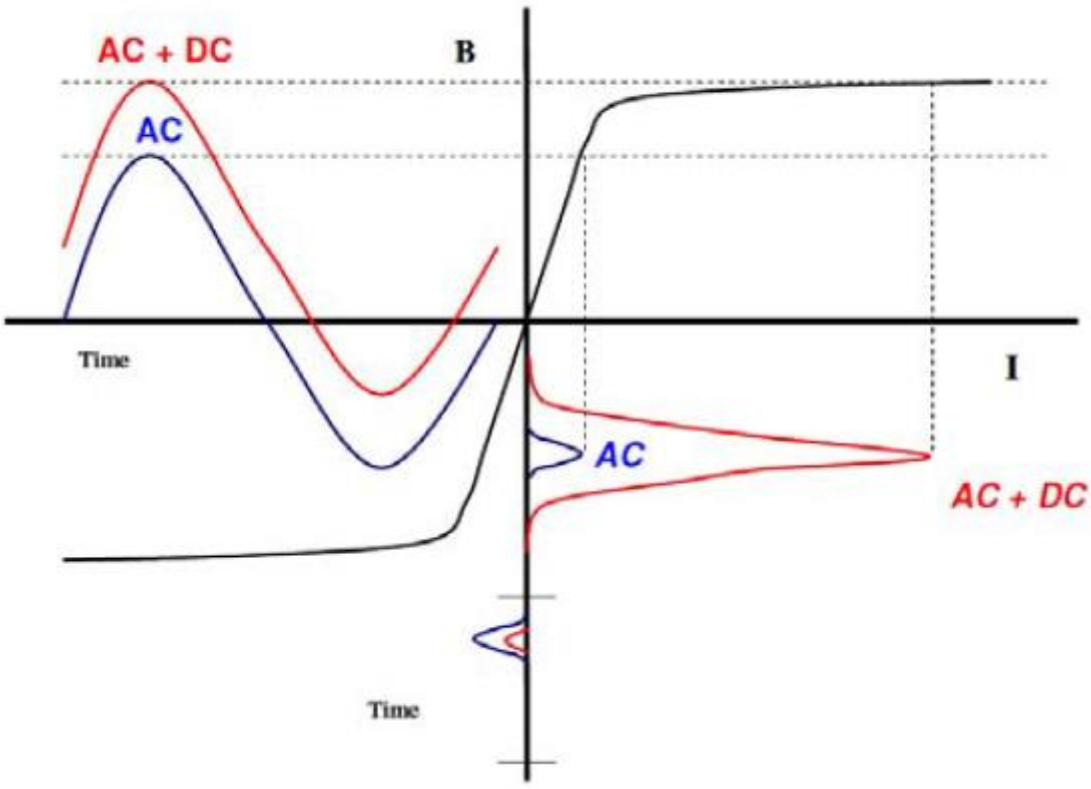

Figure 2.2: Graph shows part wave saturation of transformer core under symmetric excitation [35]

Different transformer core structures have varying susceptibilities to saturation due to the flow of dc flux in the core. The three-phase three-limb (3p3L) transformer is used in a majority of transmission networks and has been identified as one with the least susceptible to part wave saturation [37]. This is due to the high reluctance path offered by the core compared to other models such as the three-phase five-limb (3p5L) and the three-phase bank (3(1p3L)).

A study by Takasu *et al.* [38] was conducted on small bench transformers with the following core structures:

- Three-phase bank (3(1p3L))

- Three-phase five limb (3p5L)
- Three-phase three limb (3p3L)

These three transformer cores were subjected to dc excitation and their response was recorded. The results showed that the 3(1p3L) was the most susceptible to dc excitation, followed by the 3p5L and lastly the 3p3L.

Koen and Gaunt [39], however, discovered in a study conducted on a substation that a three phase three limb transformer showed signs of unexpected saturation in the presence of GICs. This was surprising because it contradicted the conventional thinking that a 3p3L is not susceptible to GICs. The study concluded that there is a need for more research before the responses can be accurately predicted.

*ii. **Harmonics***

Harmonic distortion is one of the most devastating effects of GIC flow in the power system. The harmonics are produced in the system due to high magnetizing currents of the power transformers driving them into the saturation region [31]. The magnetizing current pulse injects higher-order odd and even current harmonics into the power system to which the transformer is connected [15]. The harmonics results in the tripping of relays and var compensators connected in the power system. The effect of harmonics due to GICs was clearly seen in the Hydro Quebec power system in 1989 where a GMD caused the tripping of Static VAR Compensators and this led to the collapse of the grid due to a lack of var support [40],[41].

*iii. **Reactive Power***

The flow of GICs in the power system results in an increase in the effective reactive power absorbed by transformers. This is caused by an increase in the fundamental component of the exciting current in the power transformer under the influence of GICs [42]. The effects of this reactive power increase include voltage depression, generator tripping due to overexcitation, line disconnection and eventually voltage collapse. The impacts of the reactive absorbed are core type dependant. The single-phase transformer has been discovered to be more susceptible to GIC, drawing up to three times more reactive power compared to the 3p3L [43].

The effects of GICs on reactive power resulted in increased research effort with the aim to understand the reactive power response of a transformer under GIC stress. The need to characterise and understand the relationship between reactive power and GICs led to certain relationships being formulated. Sheyte and Overbye [44] described the relationship between the reactive power loss (Q_{Loss}) in the transformer and the GICs as:

$$Q_{Loss} = V_{pu} K I_{GIC} \tag{2.1}$$

Where, Q_{Loss} is the reactive power loss
V_{pu} is the pu voltage of the high voltage side
I_{GIC} is the "effective" per phase GIC in the transformer winding in Amps
K is a transformer specific constant in MVars/Amps. K is also core-specific

2.2 GIC Laboratory Studies

To further improve the understanding of GIC effects on power systems, a considerable amount of effort conducting laboratory studies have been done. In each of these studies, certain aspects of GIC effects on power systems have been studied. As mentioned previously, there has been only a single laboratory study analysing the effects of GICs on the voltage stability of power systems. The rest of the studies have been focused on transformer response to GICs and details of each study are discussed in detail in the following sections.

2.2.1 Chisepo

Chisepo [45] conducted a detailed laboratory protocol investigating the response of transformers to GICs. The study was conducted at the 'machines laboratory' at the University of Cape Town. It discussed the implementation and development of a laboratory protocol to characterize and test bench-scale transformers' responses due to GICs based on their magnetization characteristics. The study was conducted on the following transformers:

- Source transformer of nameplate rating: ΔY,120/230 V, 900 VA
- Load transformer of nameplate rating: YY, 120/230 V, 300 VA

To model the flow of GICs in a transmission network, a 1.5 V dc battery was used as a source to inject current into the transformer neutrals. The current to be injected was per unitized based on the load transformer magnetization (I_{mag}). A Yokogawa WT1600 Power Analyzer was used to measure readings of voltage, current, reactive power, real power and harmonics. The supply voltage to the source transformer was from a 6 kVA, 380 V variac which drew from the wall supply. The study made the following conclusion:

- There is a large amount of reactive power drawn with an increase in the dc injected into the system. This agreed with the literature on the effects of GICs on transformers.
- Reducing the voltage during a GMD event is not a suitable mitigation strategy as tests revealed that dc injections comparable to the transformer magnetization current still pushed the transformer into saturation.
- Reactive power increased linearly with increasing dc magnitude. This key finding was also in agreement with other studies showing a linear relation between reactive power drawn and GICs.
- The differences in transformer response between 3p3L and 3p5L were investigated. As the magnitude of dc increases, the 3p3L generate higher levels of harmonic distortion compared to the 3p5L. This was of interest because previously in literature it was known that the 3p3L is the least susceptible core structure to GICs.

2.2.2 Heindl et al

Heindl *et al.* [21] conducted a laboratory investigation analysing the effects of GICs by injecting dc into a three-phase power transformer. This study presented the effects of the dc offset on the partial discharge (PD) appearance, core hysteresis and transformer vibration behaviour. The transformer under test (TUT) was a 30 kVA, YNyn6, distribution transformer with a maximum output voltage of 7.5 kV. A variable ratio transformer was used to supply the TUT with a three-phase AC voltage range of 0-

400 V. The transformer was loaded with a star load with a per phase resistance of 40 kΩ. To emulate a GIC event, a dc source was connected at the load star point of the transformer. The dc voltage had a maximum value of 1.5 kV and 150 mA dc injected, with 50 A in each phase. The laboratory set up is shown in Figure 2.3.

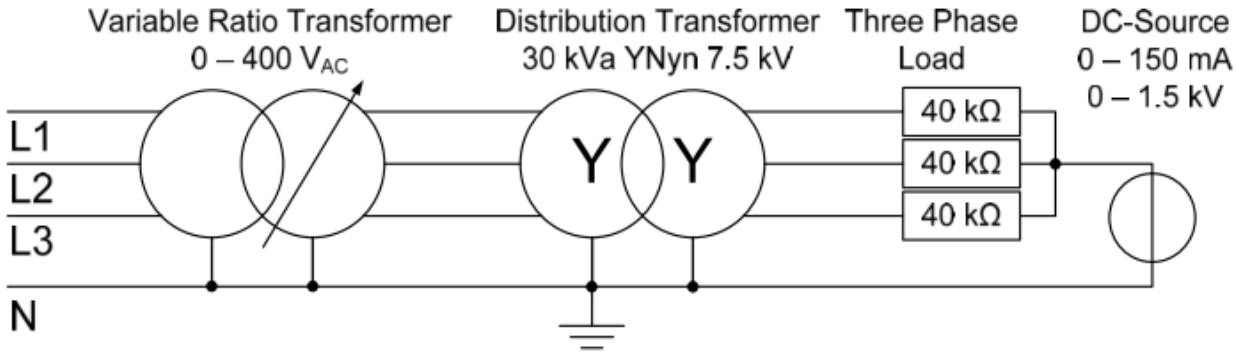

Figure 2.3: Circuit set used to investigate the GIC effects on the distribution transformer as a TUT and dc source used a GIC representative.

The results of the study revealed that the increase in GIC leads to a change in the hysteresis curve. The change and shift of the hysteresis curve increased loss of energy in the core. The study concluded that GICs can be detected by a change in the transformer's vibration spectrum. This can be done by mounting sensors onto to the transformer tank and enabling onsite, online monitoring. Furthermore, there was a correlation between the amount of dc and the partial discharge (PD) activity during the experiment.

2.2.3 Rezaei-Zare

A laboratory experiment was conducted by Rezaei-Zare [46] to validate results obtained from an analytical and simulation analysis of GIC effects on single phase transformers. The investigation set out to estimate parameters such as reactive power and harmonics in the absence of direct measurements and compare these results with the laboratory experiment. The GIC was modelled as a variable dc source connected to the HV windings. The GIC laboratory tests were performed on two single phase transformers of ratings 350 MVA-230 kV and 350 MVA-230 kV. The transformers were connected in back-to-back connection shown in Figure 2.4. The GIC is circulated in the HV windings, and the ac is applied in the parallel connection of LV windings. The back-to-back connection was done to eliminate odd harmonics in the source current which resulted in lower voltage distortion and prevented voltage asymmetry. The neutral point was grounded to prevent overvoltage.

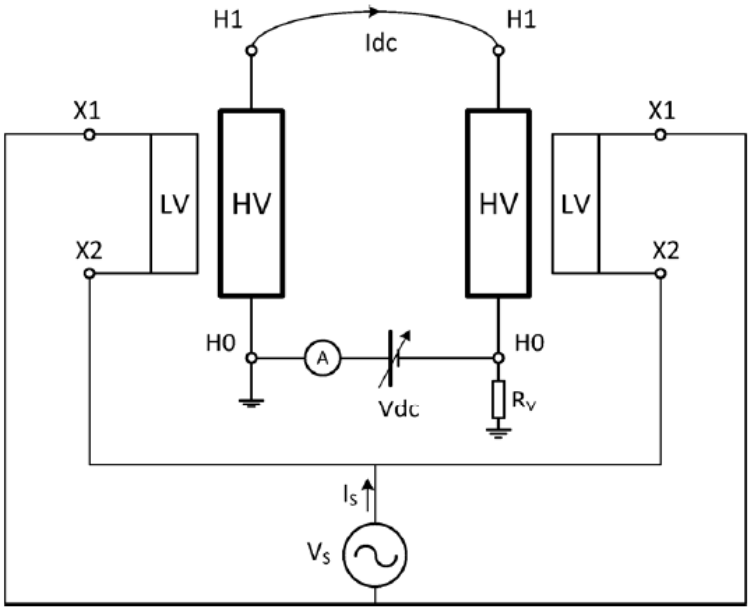

Figure 2.4: Back to back GIC test with a dc source connected at the HV windings [46]

The reactive power of the transformers was plotted against the GIC. The results obtained from the laboratory and simulations were in agreement. The reactive power increased with increasing GIC injection. The voltage and current source harmonics from both laboratory and simulation showed an agreement with, with even-order harmonics successfully eliminated due to the back-to-back configuration. The results also further revealed that the reactive power increases with GIC with an initial slope equal to the transformer peak voltage equivalent to 2.0 pu.

2.2.4 Oyedokun

Oyedokun [47] introduced a new way of calculating GICs which incorporated time response into the calculations. In this study, a laboratory protocol and simulation protocol were used to derive piecewise equations needed in transformer time response calculation. In the laboratory, three core structures were tested for analysis:

- 100 VA, 120 V/230 V,3(1p3L)
- 100 VA, 120 V/230 V 3p3L
- 100 VA, 120 V/230 V 3p5L

In each test, the source and load transformer had the same core structure. The primary side of the source transformer was connected in delta to avoid the need for a neutral connection. The secondary side of the source transformer and both sides of the load transformer were connected in wye with grounded neutrals. To emulate GIC in the laboratory, a 12V / 7.2Ah dc battery and several 1.5 V dc touch cell batteries were used to inject dc into the transformer neutrals. A programmable logic controller (PLC) was used to control the amount of dc being injected into the transformer neutrals.

The results of the experiment revealed the following:

- For the 300 VA transformer, the core structure that had the shortest response time is 3p3L, followed by 3p5L and 3(1p3L)
- For the 500 MVA transformer, the order of response in the cores structures is 3p3L, 3(1p3L), and 3p5L; with the 3p3L permitting the flow of GIC over a shorter length of time
- A response time to GIC in 3p3L, 3(1p3L), and 3p5L are load-dependent

- The shortest response time to dc was with a GSU at light load consistent across all three transformer core types

The results validated the notion that power systems could withstand GMD effects when all generating units are online.

2.3 Voltage Stability

As power systems become more expanded due to increased demands placed on them, they are forced to operate at their stability and thermal limits due to economic and environmental constraints [48]. Utilities are faced with a problem operating so close to system instability and thereby compromising effective power delivery and risking experiencing power systems blackouts. As a result, power system stability studies have become necessary considering numerous contingencies that affect the power system. This brings a need for proper definitions and classifications to understand and deal with such contingencies. In a report by Hatziargyriou *et al.* [49] which is an updated version of an initial report by Kundur *et al.*[50] , power systems stability was defined as the following:

"*Power system stability is the ability of an electric power system, for a given initial operating condition, to regain a state of operating equilibrium after being subjected to a physical disturbance, with most system variables bounded so that practically the entire system remains intact*"

Figure 2.5 shows the different classifications of power systems stability which has been updated from previous report to include resonance stability and converter-driven stability

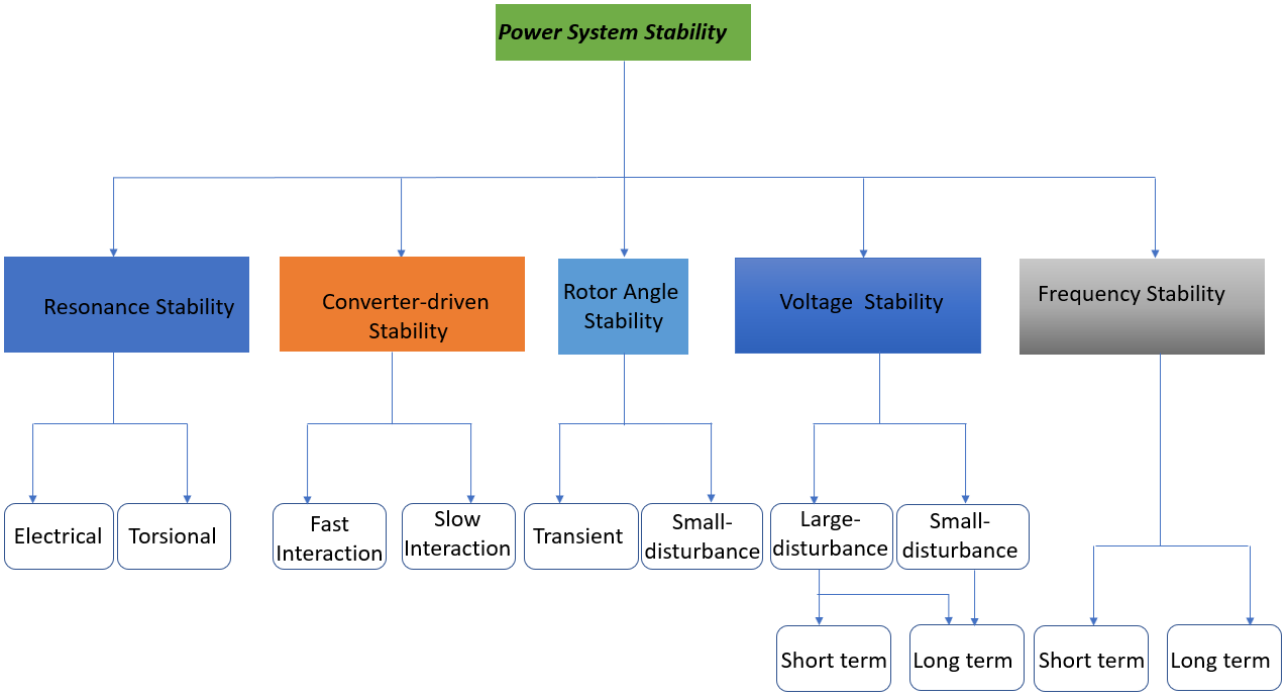

Figure 2.5: Power System Stability Classification adapted from [47]

In this study, voltage stability analysis is of particular interest due to the documented effects of GICs on the power system. Voltage instability is therefore defined as a situation whereby a perturbation in the power system causes a progressive and uncontrollable decrease in the voltage magnitude at the load bus. Voltage stability can be classified under either long-term voltage stability or short-term voltage

stability. Short term voltage stability involves dynamics of fast acting load components like HVDC links, and the study period is in the order of seconds [47]. Long term voltage stability involves slower acting equipment like transformers and its study period of interest is in the order of minutes [51]. Under these classifications, the approaches to evaluate the voltage stability can either be static or dynamic. The dynamic approach methods like time domain simulation can be applied in both long term and short term voltage stability analysis, whereas the static approach methods like PV curves are mostly applied in long term stability analysis [52], [53]. The system dynamics that result in voltage stability can occur after long periods and their snapshots of the conditions can be used to evaluate voltage stability. This approach uses static methods to evaluate voltage stability and is effective in loading effects analysis. The static approach takes into account sensitivity studies and power flow methods and has been studied extensively in literature [54]. The dynamic approach of evaluating voltage stability involves time-domain simulations which includes transient voltage behaviour of the system during a disturbance. A summary of the two voltage stability evaluations methods is shown in Figure 2.6.

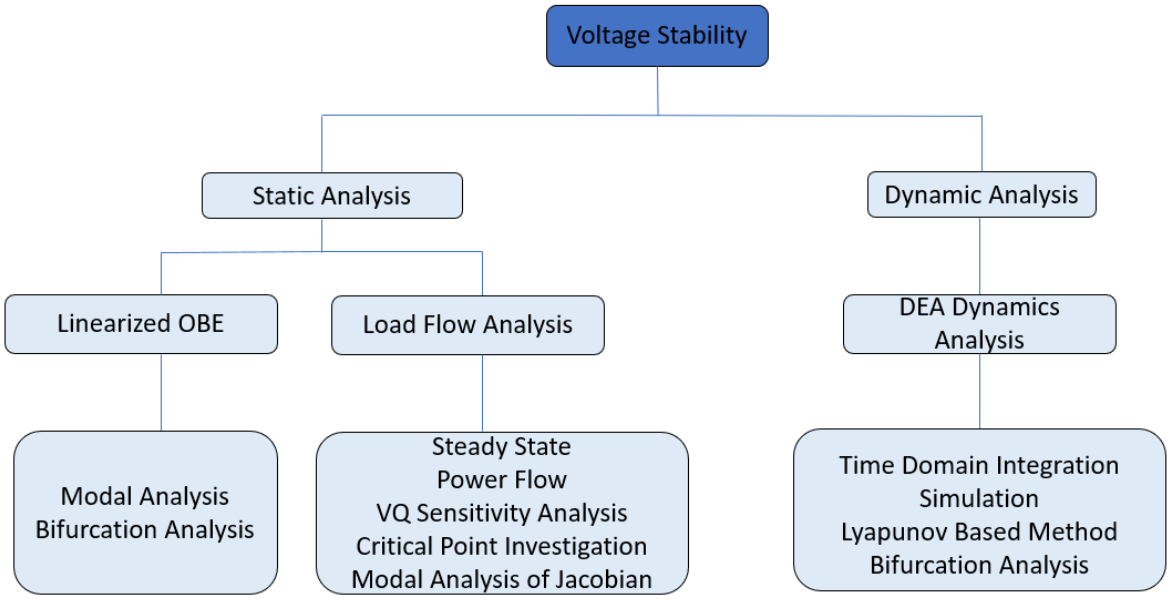

Figure 2.6: Voltage Stability Assessment Methods adapted from [55]

The two approaches are explained further in the sections 2.3.1 and 2.3.2.

2.3.1 Dynamic Voltage Stability

Dynamic voltage stability assessment involves time domain simulations and considers the dynamic modelling of loads, generators, LTCs and other components in the power system. Time-domain simulations show the real-time behaviour components such as loads, protection equipment and automatic and frequency controllers [55].

In modelling dynamic voltage stability, a model characterised by nonlinear and differential equations is used [56]. The differential equation is given by:

$$\dot{\boldsymbol{x}} = \boldsymbol{f}\,(\boldsymbol{x}, \boldsymbol{V}) \tag{2.2}$$

and the following algebraic equation:

$$\boldsymbol{I}(\boldsymbol{x}, \boldsymbol{V}) = \boldsymbol{Y_N}\,\boldsymbol{V} \tag{2.3}$$

Where $\boldsymbol{x}$ is a state vector, where $\boldsymbol{V}$ is the bus vector, $\boldsymbol{I}$ is the current injection vector and $\boldsymbol{Y_N}$ is the network node admittance matrix. Dynamic voltage stability analysis is used to verify results from static voltage analysis because it considers several network parameters.

2.3.2 Static Voltage Stability

Static voltage stability evaluates the voltage stability and loadability margins of the power system after a disturbance has occurred without analysis of the transients during the disturbance [57]. Power flow methods are used in the evaluation and analysis involved in static voltage stability. The methods used in static analysis often deploy voltage collapse points to determine the loadability margins of the system. The different conventional methods for static voltage stability analysis can be generally classified [58],[48]:

- PV Curve Analysis
- QV Curve Analysis and Reactive Power Reserve
- Minimum Singular Value Method
- Continuation Power Flow Method

For this study, PV curve analysis will be used to evaluate the effects of GICs on the voltage stability of the power system. PV and QV curve and analysis are explained in detail in the following section.

i. PV Curves

PV curve analysis is one of the most widely used methods of evaluating voltage stability and are used to evaluate the load margin of the power system. The PV curve analysis shows the amount of available active margin before the point of voltage collapse [59]. The power system load is gradually increased and, at each increment, is necessary to recalculate to power flows until the maximum loadability point of the PV curve is reached [60].

Figure 2.7 shows a PV curve and the important indicators used to evaluate voltage stability. The PV curve has two regions, a stable region, and an unstable region. These regions are separated by the Voltage Collapse Point. This is the point of maximum loadability and any loading beyond this point results in the system entering the voltage unstable region. In the voltage unstable region, any further increase in loading results in an uncontrollable decrease in both real power and voltage.

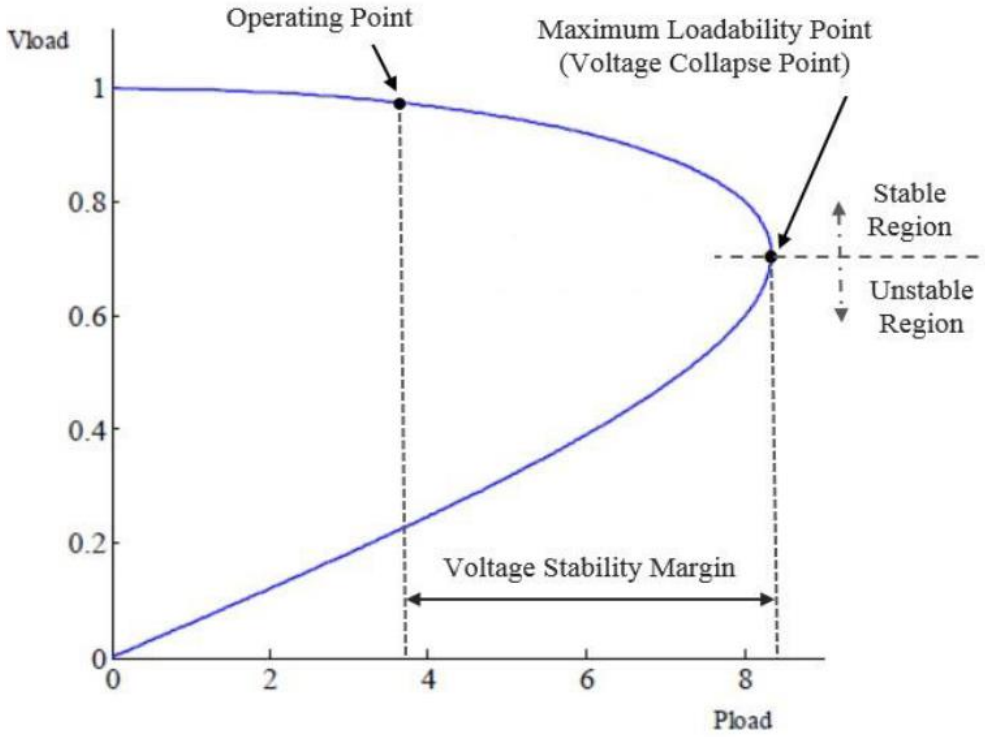

Figure 2.7: PV curve analysis showing the assessment of the loadability of the load bus [61]

It is important to note that in PV curve analysis, the power factor plays a very important role in the determination of the critical point. In a voltage stability study conducted by Neha [62], the results of different power factors connected showed that a real power transfer increased from lagging to leading power factor. The results showed that the power factor has a critical effect on the loadability and critical voltage at the load. These results were in agreement with a similar study conducted by Parihar *et al.* [63] and Figure 2.8 shows the effects of different effects of power factor on PV curve analysis.

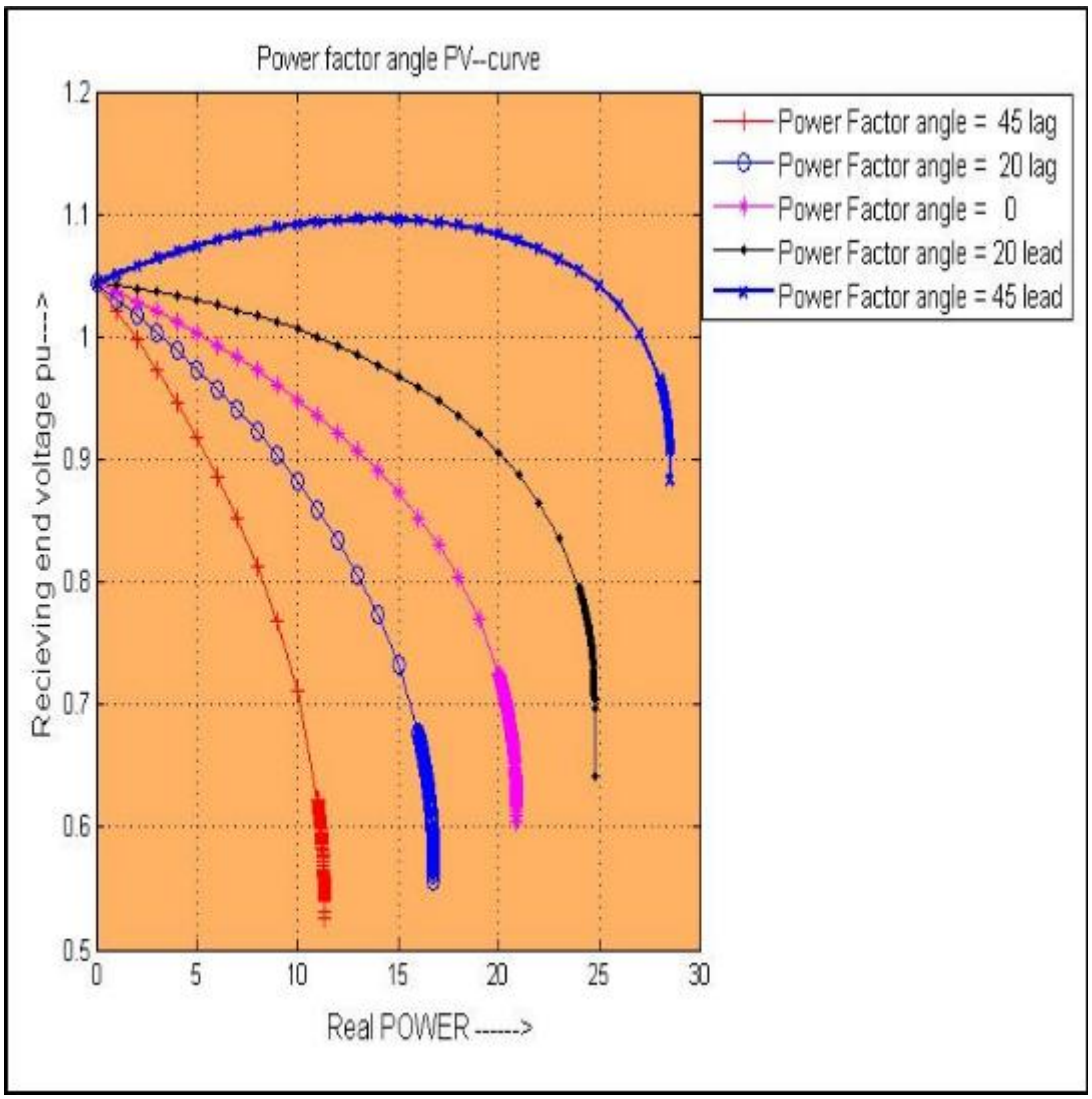

Figure 2.8: PV curves at different power factors [63]

ii. *QV Curves*

The QV curve are used to determine the voltage stability of a bus under consideration and the available reactive power reserve. The reactive power at a bus is calculated from the solutions of load flow computations and the hence plotted against specified voltage [59]. The QV curves give the reactive power margin which indicates how much further the loading can be increased on a particular bus before the system experiences voltage collapse [64]. Figure 2.9 shows that, in conjunction with PV curve analysis, the critical operating point indicates the point whereby any increase in loading the system may result in voltage instability due to a progressive decline in voltage below regulatory limits.

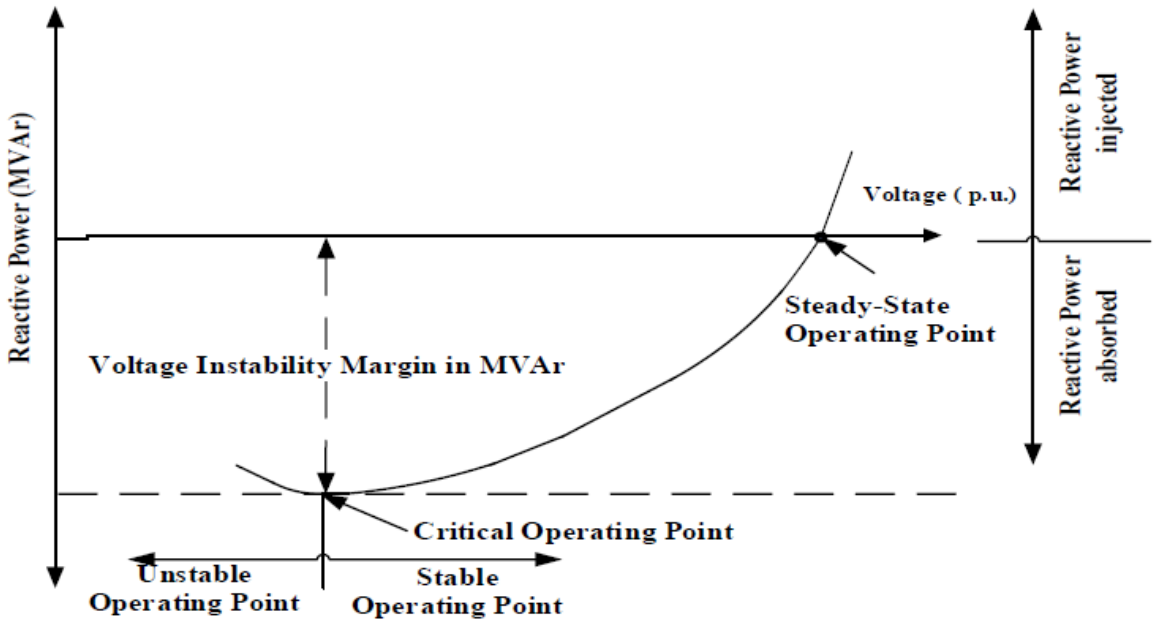

Figure 2.9: A QV curve showing the assessment of the reactive power margin [65]

2.4 Literature Review Summary

The literature review conducted on GICs, and voltage stability analysis addressed some of the research questions posed chapter 1. The key finding from this review was that all laboratory work analysing GIC effects have used dc as a GIC representative. Voltage stability studies due to acGIC have not been explored in-depth, particularly in the laboratory. The need for more representative voltage stability studies due to GICs is pointed out in this literature review. To fill this gap, this dissertation presents a design and implementation of a laboratory protocol in which a novel low-frequency ac injection (acGIC) is used to emulate GICs in the laboratory. This acGIC will be used to evaluate and assess the effects of GIC in the laboratory and key findings will be compared to the conventional dc method shown in this literature review.

3. Methodology

This chapter presents the methodology framework which guided this research. This methodology was primarily aimed at the laboratory section of the protocol and was then adapted to match the simulation protocol. The literature review outcome led to a formulation of research questions that offer guidance on how to successfully test the proposed hypothesis. This then led to the design and implementation of simulation and laboratory protocol. The chapter first describes the low-frequency ac injection acGIC. The chapter then evaluates the analytical tools that would be necessary to evaluate the impact of GICs on the voltage stability of power systems. Lastly, the chapter provides details on the test system on which tests will be carried out both in the laboratory and simulation environments.

3.1 Low Frequency AC Injection(acGIC)

It has been established from the literature that a real GIC signal is a multi-frequency, multi amplitude signal and not a dc signal. In power systems analysis, the modelling of GICs has always been the use of dc as a representative of GIC in both laboratory and simulation environments. This dc assumption stems from the low-frequency nature of the GIC signal relative to the 50 Hz/60 Hz frequency of the power system [66]. However, a recent study investigating geomagnetic pulsations that induce GICs concluded that for more accurate modelling of GICs effects in engineering studies, a low-frequency ac signal is needed to be used as a GIC representation [67]. Moreover, recent studies reveal the different power system responses when GICs are modelled as ac compared to dc [68].

This knowledge presented the need to design a low-frequency GIC representative model that gives a more accurate response of the power system. In this study, a portion of a GIC profile was considered to be built in the laboratory as a representative of the real GIC signal. Figure 3.1 shows the real signal with the section of the signal at a particular point during a Geomagnetic storm to be designed in the laboratory.

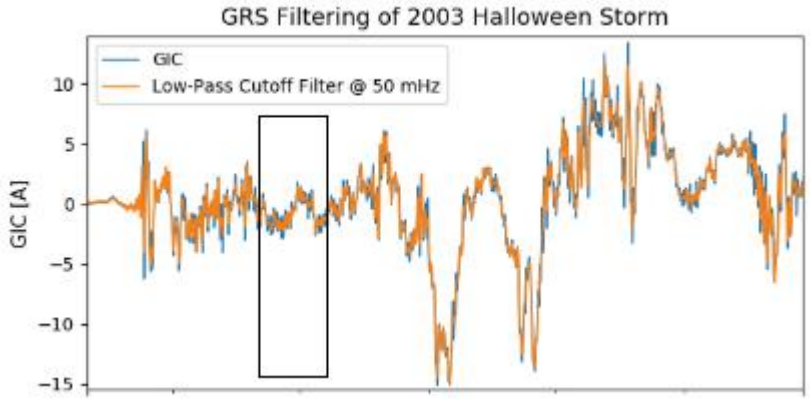

Figure 3.1: Section of GIC profile measured in a transformer neutral at Grassridge power station in South Africa during the 2003 Halloween storm - to be built in the laboratory adapted from [20].

Given the time constraints and complexity in designing a multi-frequency multi-amplitude signal in the laboratory, a 10 mHz ac circuit was designed in the laboratory as a first approximation to model real GIC. This circuit was to be connected to the transformer neutrals to inject the acGIC in the circuit to model the GIC loop. This acGIC will be used to carry out investigations of voltage stability and power systems' response with GIC. The results will be compared to the conventional dc injection to enable comparison between the response of the system due to both acGIC and dcGIC.

3.2 Parameters Measurement under acGIC

The use of acGIC presents a unique challenge as it identifies a question to be addressed: "When should measurements be taken when using an acGIC model to make voltage stability analyses?". Unlike with dcGIC, acGIC is a time-varying signal and hence parameters have to be measured in real-time throughout the cycle. For dcGIC analysis, the results can be recorded after the system has reached steady state. To capture the laboratory response over the full ac cycle, a data logging function on the Yokogawa Power Meter (YPM) was used to record the readings of voltage, current, active, and reactive power and harmonics. In PSCAD, the real-time response was captured using the parameter output channels available in the software. The Yokogawa Power Meter sampling rate is at 200Ks/s. However, for the measurements, the data logging function stores 2 samples per second to capture data of one acGIC cycle of 100s.

The data obtained from the meter will be extracted as a CSV file and stored for further post-processing. For steady-state analysis, measurements will be taken at the following three crucial points shown on Figure 3.2:

- Peak Magnitude (90 Degrees) - occurs at t = $\frac{n\pi}{2}$
- 45 Degrees - occurs at t = $\frac{n\pi}{4}$
- Zero Crossing – occurs at t = $n\pi$

Where *n=1, 3,5,……n*
and 2π represents the full GIC cycle

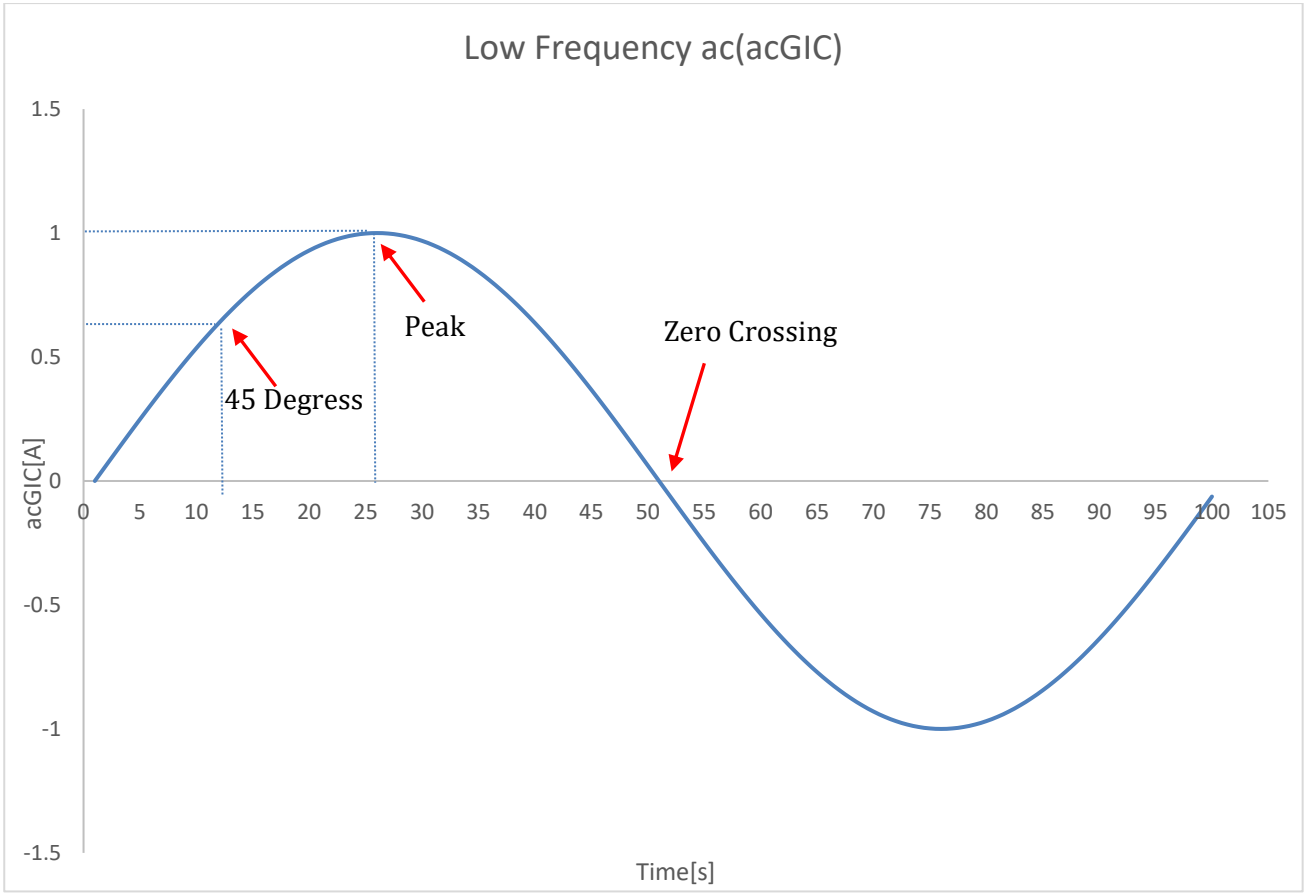

Figure 3.2: The points of the acGIC curve where measurements will be taken

Regardless of whether dcGIC or acGIC being injected into the system, the recording of parameters in the laboratory was conducted over a 100s time period using the YPM to capture a full cycle acGIC. The dcGIC was measured over 100s despite the expected constant response to allow plotting and comparison of system response with acGIC response. The acGIC and dcGIC signal was monitored using an oscilloscope which was clamped on the wire connecting the GIC injection circuit to the transformer neutrals. The readings obtained on the oscilloscope were confirmed by the readings on the YPM which measured the per phase magnitude of current flowing in the transmission line.

3.3 Voltage Stability Assessment

The system was designed and simulated on PSCAD/EMDTC v4.6.3 Educational, an Electromagnetic Transients Program (EMTP). A four-bus network was then designed in the laboratory and tests were carried out on it which were the same as the simulation protocol. To assess the voltage stability of the power system due to both acGIC and dcGIC, PV curve analysis was the tool used. PV curve analysis falls under steady state voltage stability and was used to assess the loadability of the power system through the real power load margins [63]. Given that PV curve analysis is used for steady state voltage stability analysis, an assumption of quasi-steady state was made when capturing parameters necessary for PV curve analysis. This is important particularly in acGIC injection analysis where the system response is varying with respect to the voltage.

Regardless of whether dcGIC or acGIC is being injected into the system, the recording of values in the laboratory and PSCAD was conducted over a 100s time period using the YPM and the PSCAD output channel respectively. The following are the steps that were taken in PV curve analysis in the laboratory and simulation:

1. Connect and vary the load from no load to maximum load, recording real power and voltage at each load configuration through the YPM logging function and plotting as described earlier. Plot the PV curve.
2. Introduce minimum GIC in the system. Keep the GIC value constant and repeat varying the loading from no load to maximum available load and record the real power and voltage.
3. Increase the GIC in steps till maximum GIC is determined. For each GIC increment, load the system from no load to maximum load and record the values.
4. For dcGIC injection, plot each PV curve on the same axis based on each GIC injection level, including the 0 GIC condition described in step 1.
5. For acGIC injection, 3 sets of PV curves will be plotted depending on where on acGIC cycle measurements were taken. This means that sets of PV curves will be drawn using the above measurements taken at peak, 45 degrees and zero crossing of the acGIC cycle.

3.4 THD and Reactive Power Analysis

It has been noted from literature that some of the effects of GIC flow in power systems is an increase in harmonic pollution and increase in reactive power drawn by transformers. These effects were also investigated for both acGIC and dcGIC injections. The total harmonic distortion (THD) is a measure of harmonic distortion in a power system. The voltage and current THD analysis were conducted in the laboratory to measure the amount of real time distortion experienced by the load due to both acGIC and

dcGIC. The measurements were taken over 100 s which is the duration of the acGIC cycle. Reactive power analysis was conducted in both laboratory and simulation for both acGIC and dcGIC. Studies have shown that reactive power increases linearly with increasing GIC and that will be investigated for both dcGIC and acGIC. The measurements for acGIC were done at the three points on the acGIC cycle described in section 3.2.

4. System and Component Design

This chapter details the design process of the following laboratory components to be used in the laboratory protocol:

i) Low-Frequency ac Injection Circuit

ii) Frequency-Dependent Transmission Line

iii) Load Rig

The preliminary part of the laboratory protocol involved designing the above-mentioned components for effective analysis of the laboratory protocol. The design procedure of each of the components is explained in sections 4.1 – 4.3.

4.1 Low-Frequency ac Injection Circuit

Previous studies investigating the effects of GICs on transformers and the voltage stability in the laboratory have only used dcGIC as a representation of real GIC injection. However, from literature, it has been outlined that a real GIC is not a simple dc assumption. From these studies, it was clear that the dc assumption does not provide accurate systems response as the effect of dynamic change in the injected GIC is not captured. There was therefore a need to design a circuit that has accurately depicted the GIC response by being as close to the real GIC as possible. A real GIC is a multi-frequency signal and not a single frequency signal as previously thought. Therefore, as a first approximation of real GIC, a 10 mHz ac signal was designed in the laboratory to model a varying GIC consistent with the literature and more realistic compared to dcGIC.

To accomplish this design requirement, a full bridge Sinusoidal-Pulse Width Modulation (SPWM) inverter with bipolar switching method was designed in the laboratory to emulate a 10 mHz ac signal. The circuit diagram of this set-up is shown in Figure 4.1. In these inverters a triangular carrier wave is compared with a sinusoidal reference wave (also called modulation signal) of the desired frequency and the intersection of carrier and modulation waves determines the switching instants and commutation of the modulated pulse. The magnitude ratio of the “modulation signal/carrier signal”, is called the modulation index. The frequency of the modulation signal controls the frequency of the output voltage (which controls the frequency of the acGIC). The magnitude of the fundamental component of output voltage (which controls the magnitude of the acGIC) is proportional to the modulation index (and so proportional to the magnitude of the modulation signal). The input dc signal therefore which is the modulating index is the one that controls the magnitude of the signal. Figure 4.2 shows the acGIC waveform measured using an oscilloscope. The magnitude of the GIC can be controlled by controlling the modulation index or by controlling the input dc signal.

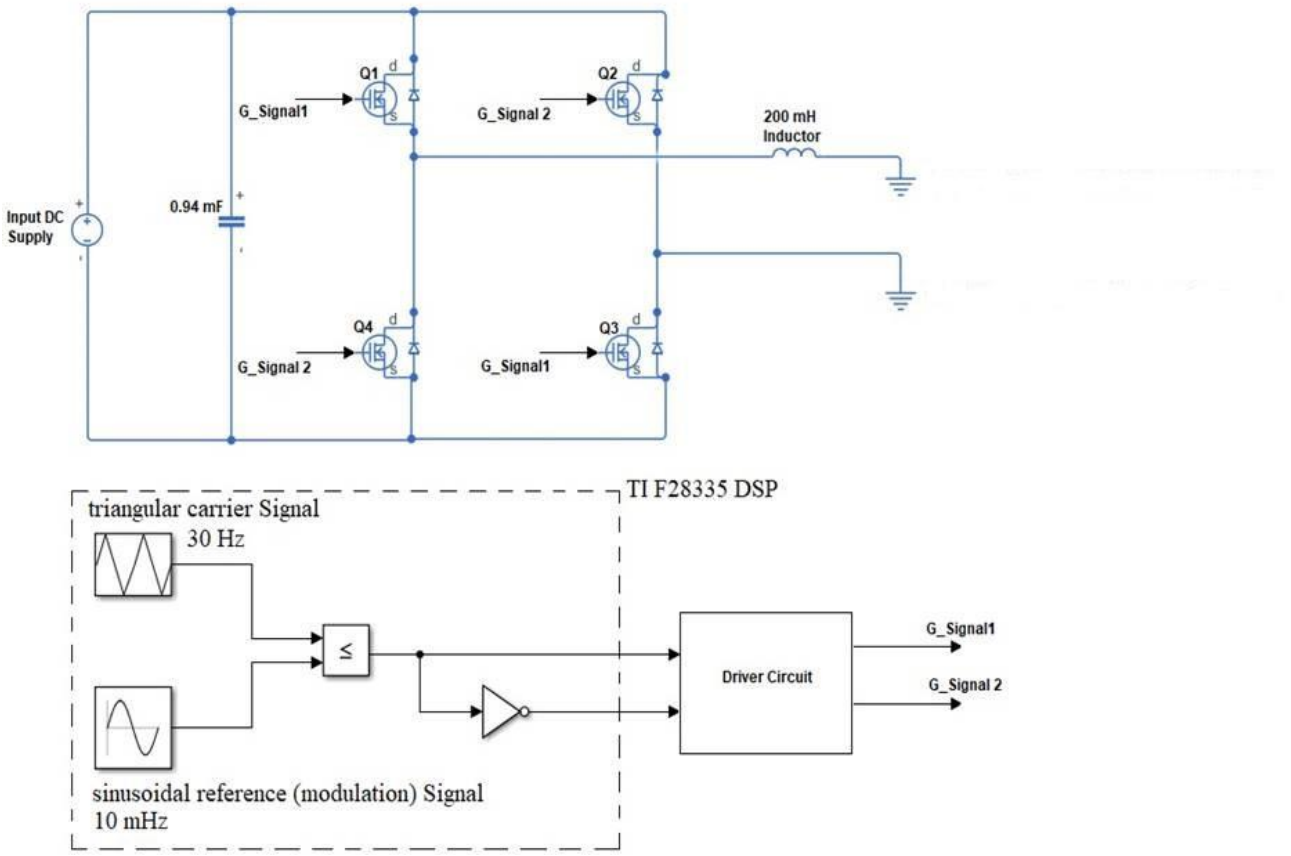

Figure 4.1: ac injection circuit

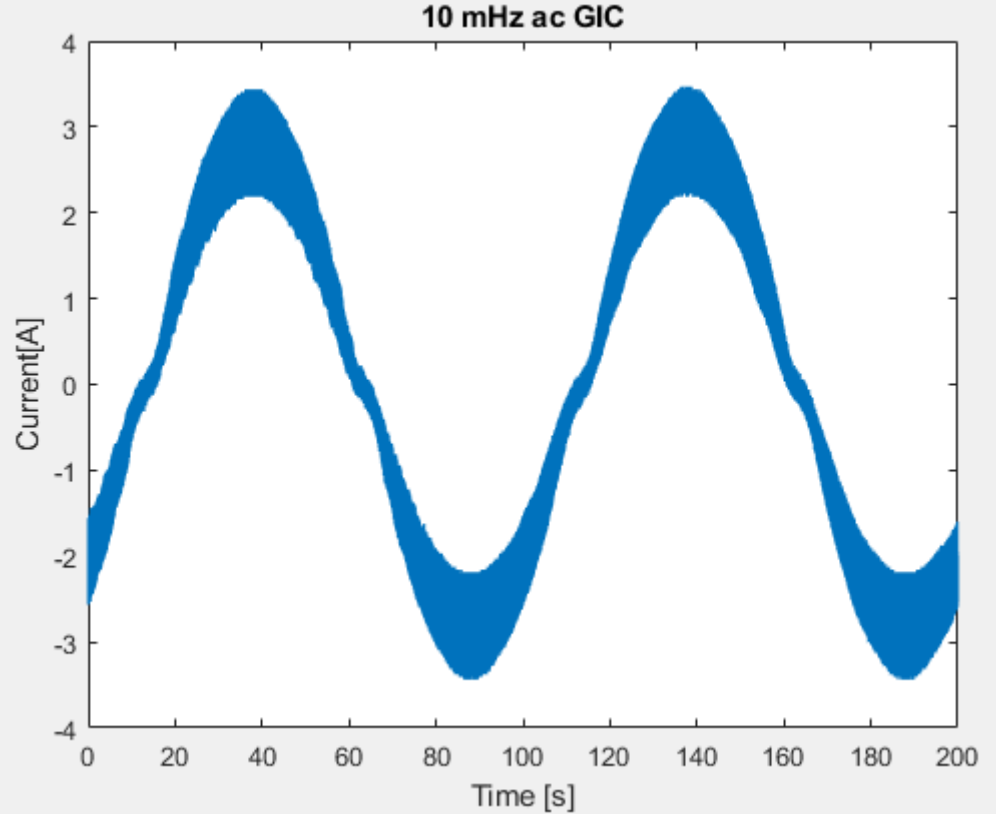

Figure 4.2: 10 mHz ac signal plotted on MATLAB measured at the neutral

A FFT of the signal shown in Figure 4.2 was conducted in MATLAB to assess the nature of any additional high frequency components superimposed on the acGIC signal in the neutral. The magnitude of each frequency component was of particular interest in this analysis. Figure 4.3 shows the results of the FFT. As seen in figure 4.3, the FFT results show that the 10 mHz signal has greater magnitude (0.705 A) compared to any frequency components present in the neutral, including the switching frequency of 30 Hz, which has a magnitude of 0.015 A. The magnitude of GIC flowing at the neutral at any given time drives the transformer to half cycle saturation which produces the GIC effects observed during the experiment. Therefore, the FFT shows that any observed response in the power system will be due to the GIC 10 mHz GIC flowing in the neutral and not the higher order frequency components.

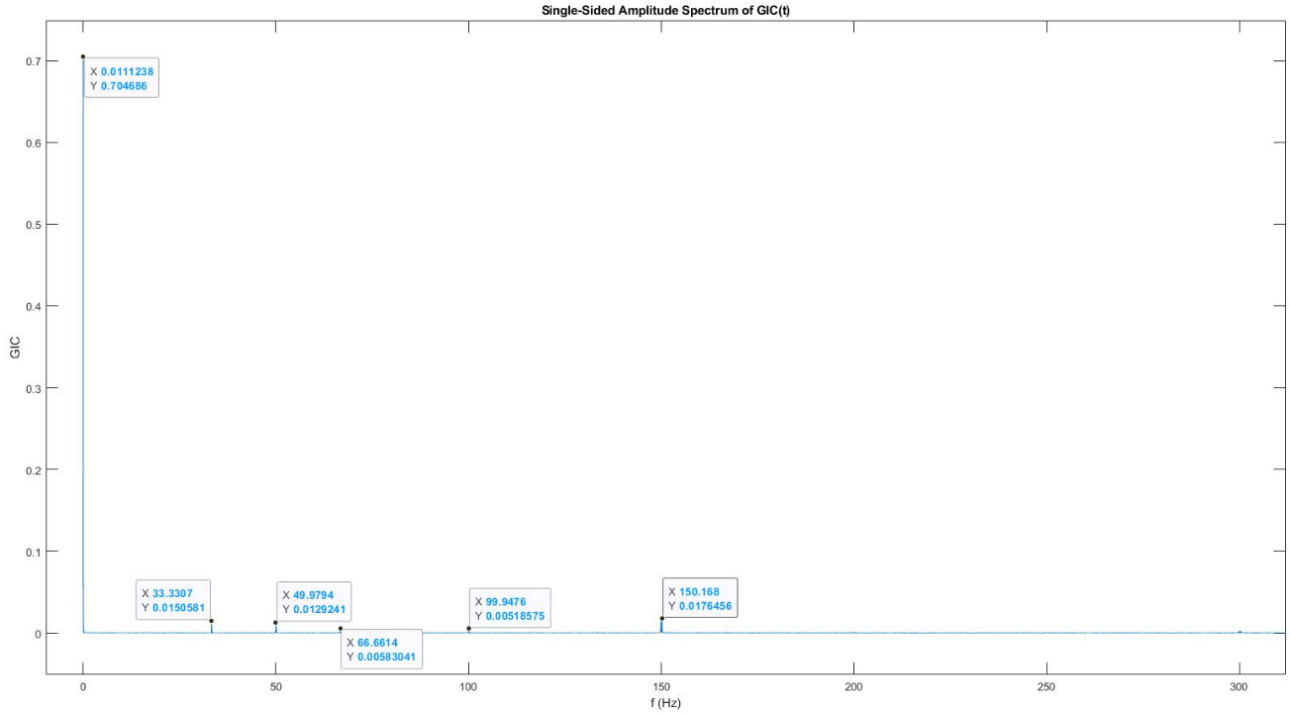

Figure 4.3: FFT on the GIC signal measured at the neutral which shows the spectrum for taken over 270s

4.2 Software Design of Laboratory Components

To model a non-saturable transmission line in the laboratory, air-core inductors for each phase were designed to give the desired XR ratio of 11. The inductors were to be designed on a software environment according to the desired specification and the software analysis would provide optimal dimensions of the air core inductor. Microsoft Excel and FEM were the two software platforms considered to design the inductors. An excel spreadsheet containing equations used for inductor design was first considered to be used to provide specifications to build the inductors. The equations are classical equations of inductance, resistance, line length and resistivity and they were entered into the spreadsheet to output optimal inductor dimensions. The spreadsheet had been used to design other inductors before this work. The inductors built from the results obtained from the spreadsheet had an inductance of about 55% of the desired value. This was an issue because the desired XR ratio of 11 would not be obtained from the design which was crucial for this research. The next option considered was the FEM designed inductor which was eventually used for the experiment. The design is explained in the next section.

4.2.1 Frequency Dependency Transmission Design Using FEM

A frequency dependant transmission line with both inductor and resistive elements per phase was designed in the laboratory. Linear “air core” inductors were chosen as the transmission lines given that they would not saturate as a result dcGIC or acGIC as opposed to normal inductors. To obtain the desired

XR ratio of 11, the design data specified an inductance of 11.74 mH and hence the air-core inductors were designed. The inductors were designed using a FEM optimization protocol which adjusted the winding height, number of turns and number of layers.

During the construction phase physical limitations like limited wire availability resulted in the number of layers being reduced to 6 layers, as opposed to the FEM specified 7 layers, ultimately resulting in inductance of approximately 8.4 mH (see Figure 4.4). Even though the fabricated inductors have lower inductance than what was expected, there has been a significant improvement from the previous designs and the circuits can still be tuned to give acceptable XR ratios.

The wire used for the design was chosen based on the calculations of the maximum current drawn in the system. Accounting for asymmetric excitation, the calculations yielded a peak current value of 37.25A. The copper wire used in the inductor design was of diameter 3mm. Based on the available wire sizes and corresponding current limits, the closest wire size is chosen was an APIi wire single strand with a maximum carrying capacity of 46.25 A. This was the next option as the closest current rating was 42.5A which was deemed to be close to the maximum current of 37.25A, hence the next current limit available was 46.25A.

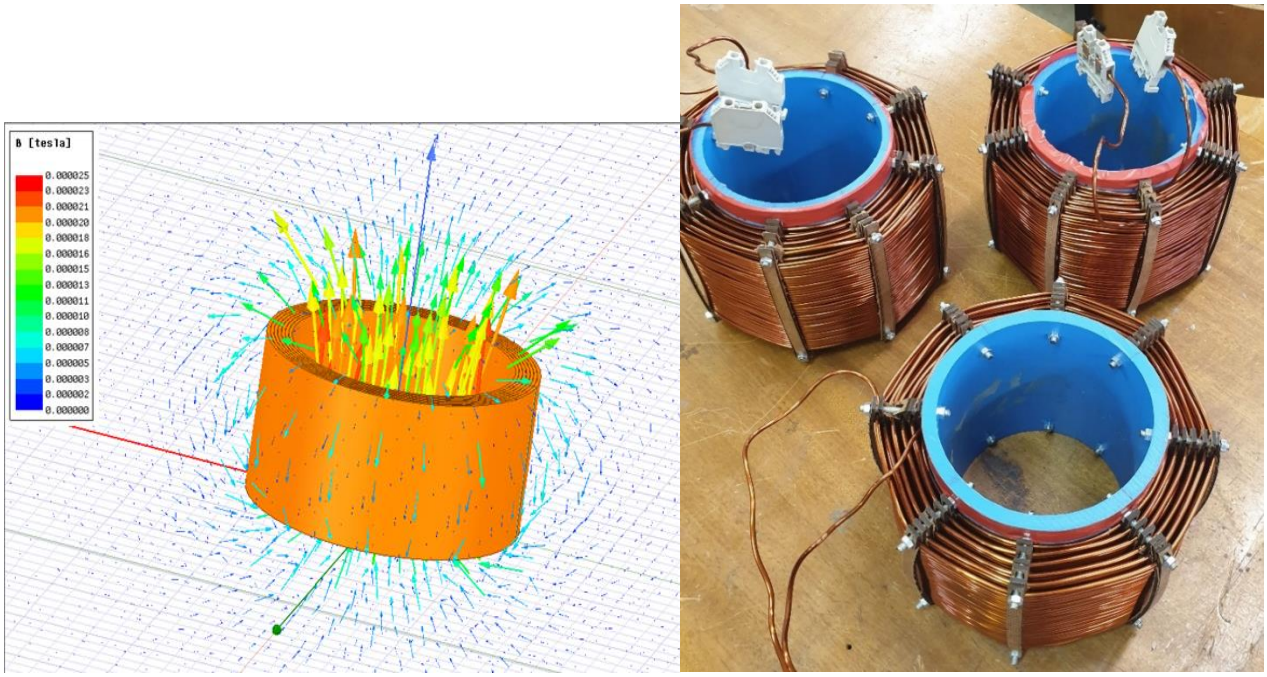

Figure 4.4: FEM models and the "air core" inductors designed in the laboratory

4.3 Load Rig

The load in this laboratory protocol chosen was purely resistive. A resistive load was chosen to achieve a power factor of 1 so that any effects on the load voltage is due to GIC injections and the effects of loading. An inductive or capacitive load causes excessive drops or increases in voltage which are not observed in a resistive load. Given that this study is an analysis of voltage stability due to GICs, it is important that any voltage change in the load is caused by the variation of GIC flow and not the nature of the load. The effect of the power factor and voltage stability was shown in the literature review section of this study. An inductive or capacitive load would result in incorrect observations leading to inaccurate conclusions. To illustrate this effect of load type and power factor, a simulation was conducted on PSCAD investigating the effect of power factor on the load voltage. A four-bus network with a 15 kVA rated load

transformer was connected with different power factor loads and load flow simulations were run with two different loading capacities. The results of these simulations showing the different power factors and load voltage at different loading levels are shown in Table 4.1.

Table 4.1: Table showing results of a simulation illustrating the effects of different load types on the voltage for the same loading capacity

5 kVA		10 kVA	
Power Factor	Load Voltage [pu]	Power Factor	Load Voltage [pu]
1	0.983	1	0.967
0.9(Leading)	1	0.9(Leading)	1.02
0.9(Lagging)	0.962	0.9(Lagging)	0.928
0.85(Leading)	1.01	0.85(Leading)	1.03
0.85 (Lagging)	0.958	0.85 (Lagging)	0.921

The results clearly illustrate the effect of the power factor on the load voltage. With a leading power factor, the voltage increases at the load and decreases considerably with a lagging power factor relative to the most efficient power factor of 1. The use of either an inductive or capacitive load would offset the results of load voltage and hence the effects of GICs would not be fully and accurately accounted for in the analysis. For this reason, this study uses a resistive load for the voltage stability analysis to be carried out in the laboratory and simulation protocols.

In the laboratory, 50 Ω, 1 kW single-phase heaters were arranged in a load rig to be connected to the load transformer in the four-bus network. The load rig containing the resistors and a cooling fan to be used are shown in Figure 4.5. The load rig has connection terminals that allow both series and parallel combinations of connections to be realised depending on the load requirements. The connection limit and combination are however subject to individual resistor power limit.

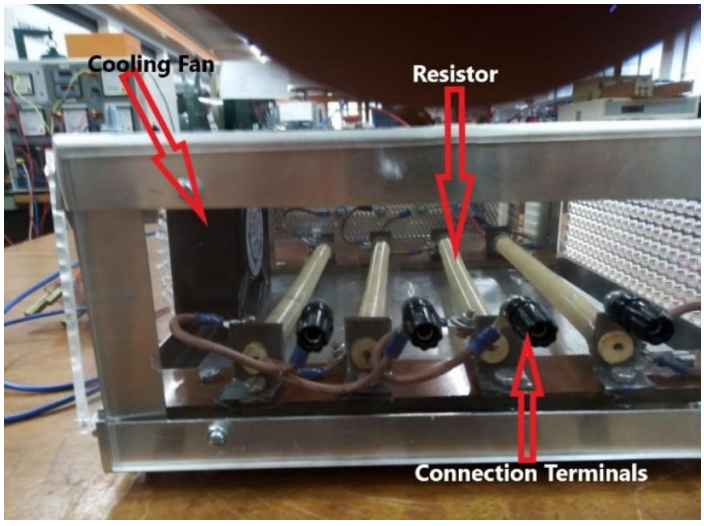

Figure 4.5: Load rig of resistors

5. Laboratory Protocol

This chapter presents the laboratory protocol conducted at the 'machines' laboratory' at the University of Cape Town. The protocol firstly presents preliminary tests which involve no-load test and short circuit tests conducted on:

- 15 kVA, 380/380 V, 3 phase, three limb transformer (3p3L)
- 15 kVA, 380/380 V, 3phase, five limb transformer (3p5L).

The transformers to be used for the laboratory protocol are shown in Figure 5.1.

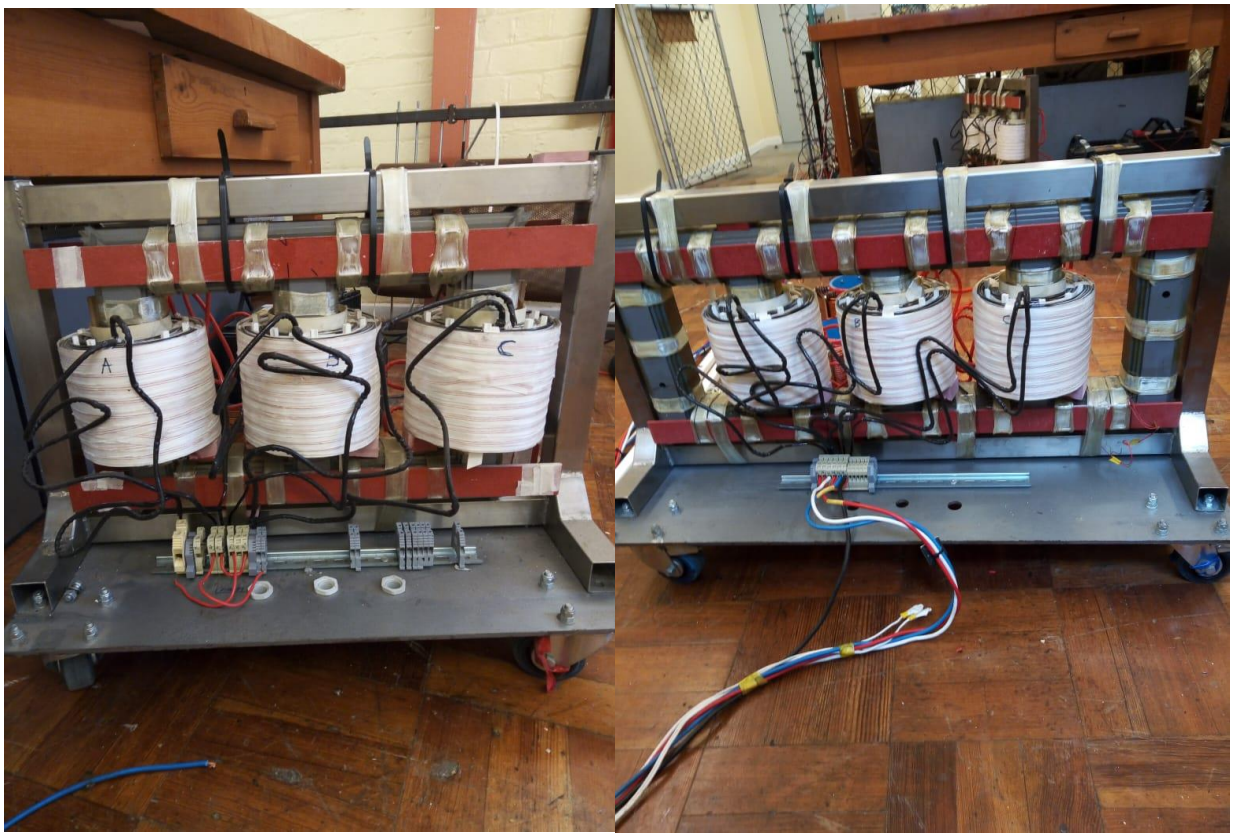

(a) *(b)*

Figure 5.1: Test transformers. (a) 3p3L. (b) 3p5L.

These transformers will be connected through a non-saturable transmission line and circuit diagram to form a four-bus test network to be used for voltage stability assessment. The 3p3L transformer was used as the source transformer, and the 3p5L was used as a load transformer. The protocol then describes a detailed setup of the laboratory and outlines the tests procedure to be carried on the four-bus network for voltage stability analysis. The procedure details steps taken in testing for both dcGIC and acGIC injections.

5.1 Preliminary Transformer Tests

The transformer is the most crucial component in GIC studies [69] and hence the accurate understanding of the transformer response is required for results analysis. Therefore, it is necessary to conduct tests on the transformers which will enable the extraction of certain parameters required to analyse the transformer performance. These parameters can also be entered into simulation models and the two transformer models will be matched for improved simulation accuracy. The tests conducted on each transformer model were open circuit and short circuit tests.

The voltage to be used in the laboratory was controlled by a 380 V, three-phase 60 A variac (variable autotransformer) which drew power from the main supply. The source was checked for harmonics to ensure that it complied with the IEEE 519-2014 standard [70]. The results confirmed that the THD was below 5% and therefore the source voltage was as classified as clean. A 6 channel Yokogawa Power Meter (YPM) WT1800 was used to measure the phase voltages and harmonics from the source.

5.1.1 Magnetization Characteristics

The no-load test was done on the two transformers described above. Unfortunately, these transformers were manufactured with holes in their cores that were used to position the core laminations for stacking purposes. The stacking holes introduce additional complexity when determining the transformer responses under simultaneous ac and dc excitation. The transformer nameplate data is therefore unreliable and preliminary testing is required to determine the actual capability of the transformers.

For simultaneous ac-dc excitation studies, it is important to first determine the operating voltage of the system to be applied under unsaturated conditions and the levels of dcGIC/acGIC to be injected into the system [71]. To obtain these parameters, an open circuit test was conducted on the both the 3p3L and 3p5L. During the test, the voltage was varied slowly from 0 V to over excitations conditions, and the values of input voltage and current were measured and recorded and used to generate a v-i curve. From the v-i curve, the following parameters were extracted:

- Knee Point Voltage
- Magnetizing Current (I_{mag})

Each transformer was energized on both the outer and inner windings using both YY or ΔY configurations and the corresponding v-i curves were plotted. This was done to confirm the reversibility of model transformers. A summary of these configurations to be tested is shown in Table 5.1.

Table 5.1: Table showing the different possible connections for each transformer to be tested to obtain their v-i curves

3p3L		**3p5L**	
1 Y'Y"	3 Δ'Y"	1 Y'Y"	3 Δ'Y"
2 Y"Y'	4 Δ"Y'	2 Y'Y"	4 Δ"Y'
Key: (")-Outer winding; (')-Inner winding			

The objectives were to study the full magnetization characteristics (v-i curves) of each transformer and determine which transformer would be used as the source or load transformer in a 4-bus test network. From the options in Table 5.1, the chosen source transformer would be connected in delta star configuration to suppress any triplen harmonics produced as a result of GIC. The load transformer would be connected in star-star configuration with the primary side connected to the GIC circuit, and the secondary to the load. Furthermore, the transformer with the lowest IEC 61689-2-2012 [72] defined knee point between the two transformers would be chosen to be the source transformer to ensure that, neither the system nor transformer is in saturation during symmetric excitation. The

chosen transformers would then have their magnetization characteristics entered in the PSCAD UMEC transformer model.

The test set-up for the magnetization characteristics is shown in Figures 5.2 and 5.3. The source impedance type is a series RLC, where R is the resistance, L is inductance and C is capacitance. The capacitance was set to zero to match the lab impedance parameters.

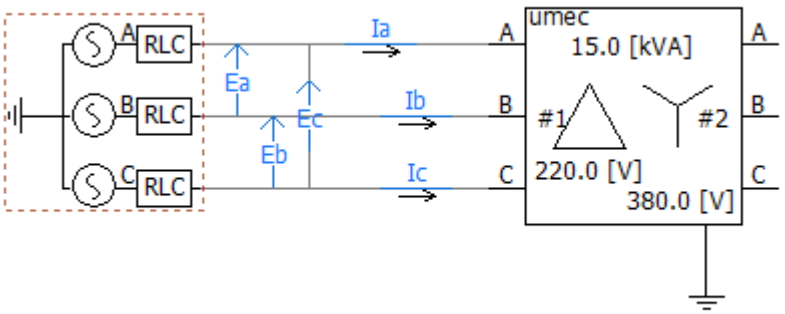

Figure 5.2: DY connection of the transformers

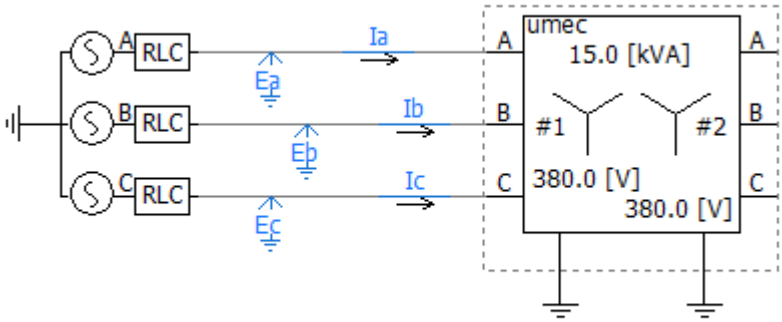

Figure 5.3: YY connection of the transformers

The knee point voltage was extracted from the magnetization curve using the IEC definition which states that, the knee point is defined as a point whereby a 10% increase in the excitation voltage causes the excitation current to increase by no more than 50%. The IEC knee was chosen to conservatively distinguish distortion caused by GIC from any possible distortion that would have otherwise been caused by ac excitation at a higher knee point. The corresponding current point to the knee point voltage on the magnetization curve is magnetizing current. This current was per unitized and would be used to characterise the dcGIC and acGIC injection. Due to core saturation susceptibility, the 3p5L was chosen to be the load transformer and was connected in YY. The 3p3L was chosen as the source transformer and was connected in delta-star configuration. The results are shown in Figures 5.4 and 5.5 show the phase A of the magnetization curves of the two transformers.

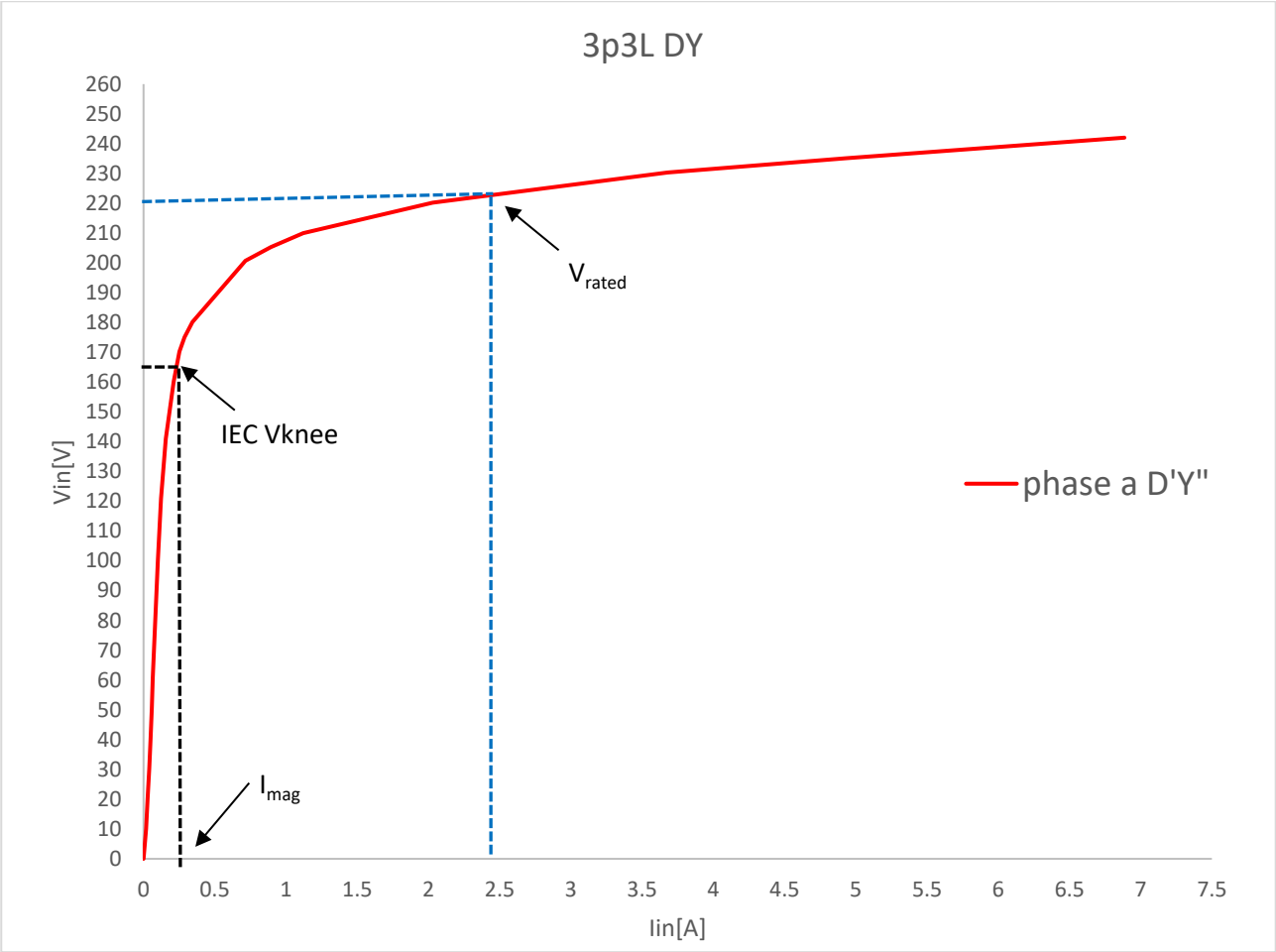

Figure 5.4: Phase A 3p3L magnetization curve showing IEC defined knee point and the Imag. The knee point is at 0.75pu below the rated voltage

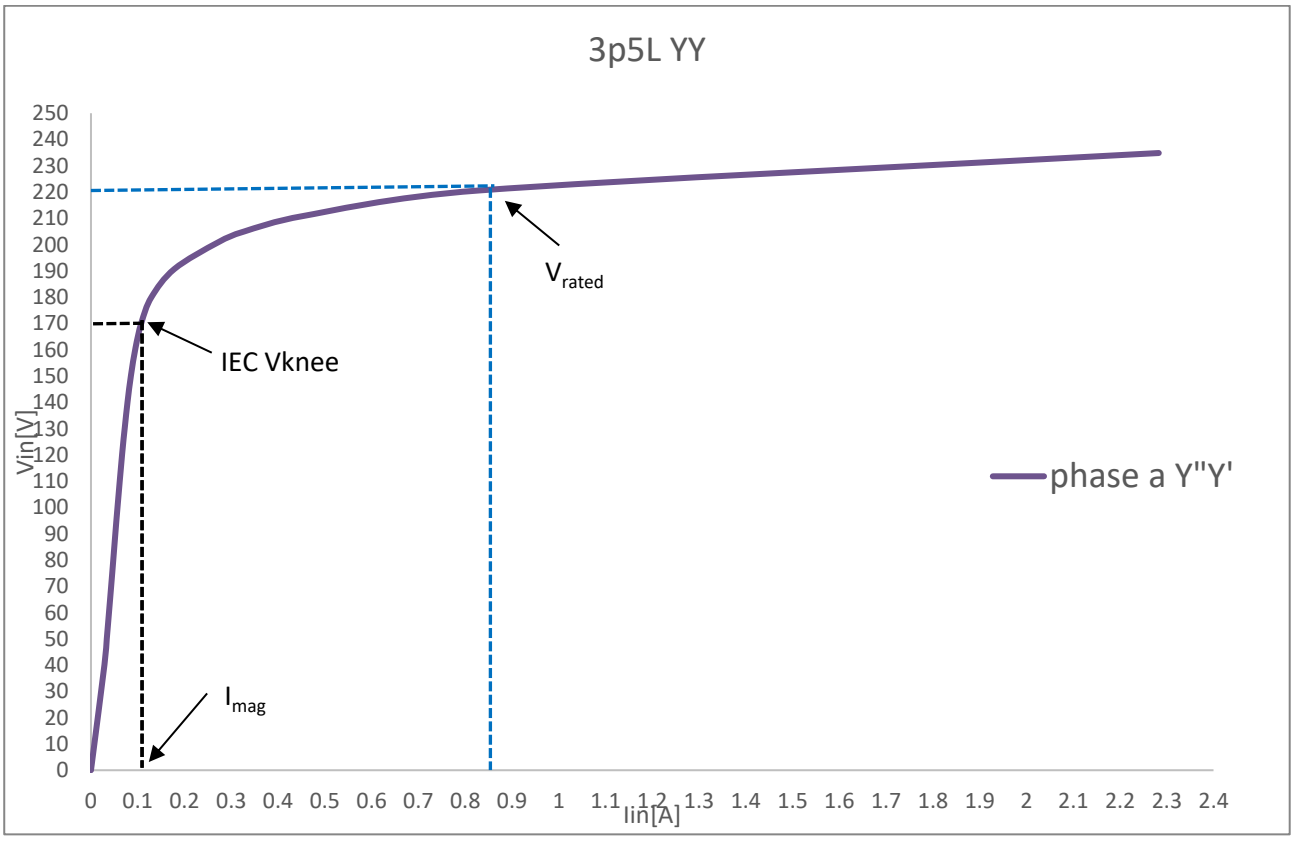

Figure 5.5: Phase A 3p5L magnetization curve showing IEC defined knee point and the Imag. The knee point is at 0.77pu below the rated voltage

The knee point calculations revealed that the 3p3L transformer saturated at a lower voltage of 165 V (line-to-neutral) compared to the 3p5L transformer at 170 V (line-to-neutral). From the magnetization curves of both the transformers, it is evident that the knee point voltage is lower than the rated voltage. The transformers enter into saturation region at a voltage lower than the rated voltage. Furthermore, the core joints of the transformer reduce the effective core cross-sectional area (csa) and create flux distortion, therefore the transformer reach saturation early [16]. The implication of this was that the transformers were derated to ensure that the operation of the transformers is not in saturation region before dcGIC or acGIC is introduced in the system. The new transformer ratings of the transformers are given in the following Table 5.2.

Table 5.2: Table showing new ratings of the transformers extracted from the no-load

Transformer	Voltage/ V	kVA Rating
3p3L, ΔY	165 V/286 V	11,3
3p5L, YY	294/294	11,6

5.1.2 Short Circuit Tests

The short circuit tests were conducted to determine the series parameters of the transformer. The parameters are important in the analysis of series voltage drop across the network. This test was conducted by short circuiting the secondary. These parameters are also entered on transformer models in summation software, together with open circuit parameters to accurately model the transformer response in simulation environment. The results of the short circuit tests are shown in the following Table 5.3 and Table 5.4 below.

Table 5.3: 3p3L short circuit tests results

	Phase A	Phase B	Phase C
Req[Ohm]	0.208	0.247	0.241
Zeq[Ohm]	0.244	0.261	0.264
Xeq[Ohm]	0.127	0.0855	0.107

Table 5.4: 3p5L short circuit tests results

	Phase A	Phase B	Phase C
Req[Ohm]	0.231	0.236	0.246
Zeq[Ohm]	0.252	0.251	0.265
Xeq[Ohm]	0.100	0.085	0.097

5.2 GIC Injection Circuit Setup

The circuits for both ac and dc injections were set up in the laboratory for testing. As a point of reference for the GIC level, the magnetization current of the 3p3L transformer was per unitized according to the no-load tests. This per unitized current (based on 1 phase) was then injected into the system on three levels:

- low GIC Injection: 1pu (0.302 A/ phase)
- Moderate GIC Injection: 3pu (0.906 A/phase)
- High GIC Injection: 6pu (2.718A/phase)

Simulations of the system on PSCAD were conducted to assess the extent to which triplen harmonics could be expected in the laboratory tests. The results would indicate whether any form of protection must be put in place to ensure the safety of the inverter and microcontroller. The current injection range was from a low injection of 0.302 A/phase (no-load exciting current for 3p3L) to an extreme case of 3 A/phase. The results showed that even for extreme GIC injection, the highest neutral current harmonic component is 370mA from dc injection and 327mA from ac injections. These currents were not high enough to cause any damage to the dc and ac injection circuitry based on the component's specifications. The simulation analysis concluded that the magnitude of triplen harmonics was not a serious threat to the circuit.

This conclusion was further verified in the laboratory when the full four bus network was connected and the voltage was varied. The purpose of this investigation was to record the neutral current of the system before any GIC. The system was connected at maximum load. The two transformer neutrals were connected and a current probe was clipped onto the connecting cable and was connected to an oscilloscope to monitor the neutral component. The results showed that even at a high load the highest component of triplen harmonics recorded was 167mA, which was within the acceptable current range for the components to be used in the experiment.

5.2.1 acGIC

The acGIC injection circuit described in chapter 3 was set up in the lab and was connected to the grounded neutrals of the transformer. An analysis of the neutral current under normal system conditions was conducted on PSCAD as mentioned in section 5.2. The analysis, done both on simulation and in the laboratory, concluded that the magnitude of triplen harmonics was not a serious threat to the circuit, even at maximum load. However, as a protective measure, the circuit-which consisted of an H bridge inverter, microcontroller and a dc power supply-was connected in series with a 200mH inductor. The micro-controller was used to control the switching sequence of the inverter. The switches were sized based on the maximum (peak) applied neutral current of 8.145 A, and neutral loop impedance of (0.668+j0.2) Ω. The dc power supply was used to power up the H-Bridge inverter. The laboratory setup of the injection circuit is shown in Figure 5.6

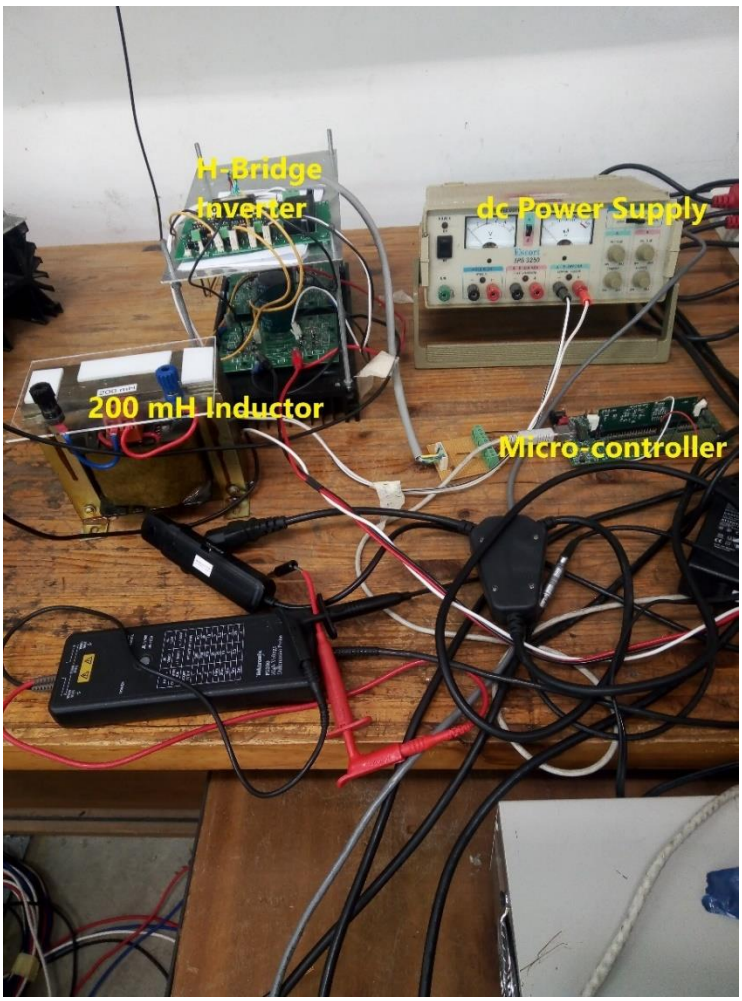

Figure 5.6: acGIC Injection Set-Up

5.2.2 dcGIC

To set up the dcGIC, a QPX 1200 SP Watt dc power supply was used to provide dcGIC for the analysis. The specifications of the power supply are given in Appendix A. The current was controlled by calculating the dc resistance based on the voltage and current measurements displayed on the power supply and adjusting the voltage to give the desired current output. A 200mH inductor was connected in series with the power supply as a protection from triplen harmonics and the dc current was injected into the source and load transformer neutrals. Figure 5.7 shows the dc power supply used in injecting dc into the transformer neutrals.

Figure 5.7: dc power supply used to dcGIC injection

5.3 Voltage Stability Assessments Tests

The set up and test procedure of the voltage stability are given in the following sections.

5.3.1 Test Set-Up

The full network set is shown in Figure 5.8.

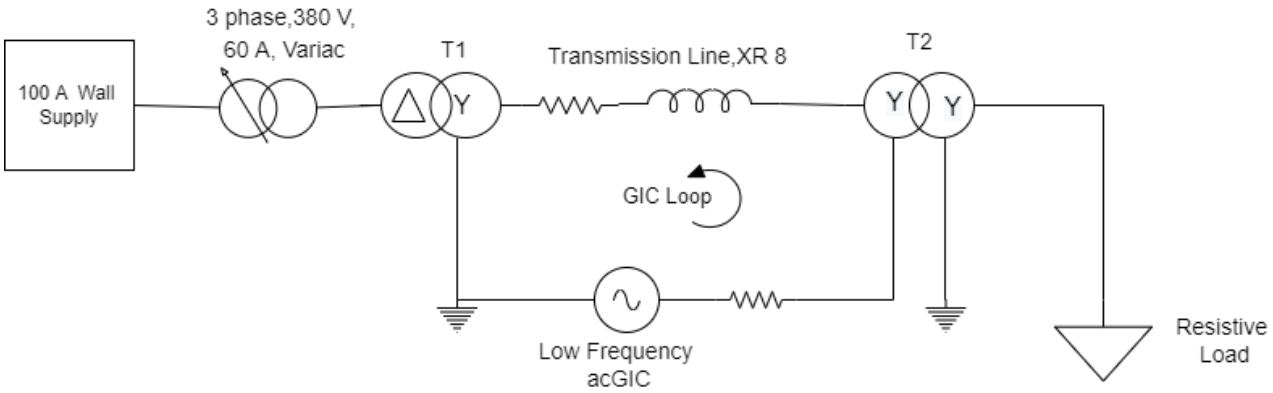

Figure 5.8: Laboratory Network Diagram: Laboratory Network Diagram

The apparatus of the experiment consists of the following:

- acGIC Circuit (10 mHz)
- 1 kW, 50-ohm single-phase resistors to provide a resistive load
- Three air-core inductors for non-saturable transmission line
- Two test transformers, one 3p3L and another 3p5L

The system voltage is controlled by a 3phase, 380 V,60 A, variac drawing the main supply from the wall and is connected to a 11.3 kVA, ΔY,165 V/286 V, three-phase three limb (3p3L), and a 11.6 kVA, YY,294 V/294 V, three-phase five limb (3p5L). Two Yokogawa Power Meters (YPMs) were used to take measurements at 3 busses in the test circuit. These locations were chosen because the equipment available only allowed a total of nine channels to be used, with each location using 3 channels. The YPM WT500 has 3 measurement channels while the YPM WT1800 has 6 channels. These two meters are synchronized using a bnc connector to ensure that every measurement is taken at the same instance across the network. The first three channels of the WT1800 were connected to primary side of the source transformer and measured and recorded the voltage, current, real power and both voltage and current harmonics at the supply. The other three channels were connected to primary side of the load transformer to monitor the same parameters as described above in the GIC loop. The WT500 was connected at the load to monitor voltage, active power, current and voltage and current harmonics.

5.3.2 Experimental Procedure

The resistors were each connected depending on the load level required at each point of the experiment. A frequency-dependent transmission line is emulated using a line resistance and an "air core" inductance specially fabricated to achieve a typical transmission XR ratio of 8. It is important to note that given the implications of the saturation study described in section 5.1.1, the transformer rating was adjusted and that influenced the final chosen loading percentages. The loading percentages were calculated based on the full load transformer rating (11.6 kVA) and the system operating voltage of 165 V and are as follow are shown in Table 5.5.

Table 5.5: Table showing available loading capacities

Loading Capacity (kVA)	Loading %
0	0
1.6	14
3.2	28
4.9	42
6.5	56
8.2	71

The loading capacities were chosen based on the availability of the load resistors. Ideally, the loading could be available to up to 100% of the full load. However, this is not possible in this experiment due to the availability of material and cost constraints. Furthermore, the power output further decreases due to a higher voltage drop and therefore loading the system higher than the specified maximum would not give the desired output and drive the system to voltage instability.

The transformer was loaded from 0% to 71% at no GIC, and the values of real power and voltage were recorded. These were used to generate the first PV curve to analyse the loadability of the system. The acGIC was introduced into the system. The GIC injection range was based on the saturation study which revealed at which GIC injection the transformers saturate. The procedure for obtaining the PV curve was repeated, with the only difference being that different PV curves were obtained for different GIC injection levels. The same procedure was repeated for dcGIC to analyse how the system responds to dc injection and that will be compared to the ac injection.

6. Simulation Protocol

PSCAD/EMDTC was the simulation software selected to do the transformer modelling and to simulate the subsequent voltage stability analysis tests performed in the laboratory. PSCAD/EMTDC simulation environment was chosen to simulate the power system due to the accuracy at which it computes transients. The purpose of the simulations was to compare the results obtained from the laboratory experiments with simulated data. In PSCAD, there are two transformer model options available: namely the classical model and the UMEC model. The differences in these models are discussed in the next sections and based on the differences, the best model which best fits this study will be chosen.

6.1 Classical Model

The classical model approach on PSCAD employs the equivalent circuit shown in Figure 6.1 in modelling a single-phase transformer with three limbs and a double wound centre limb.

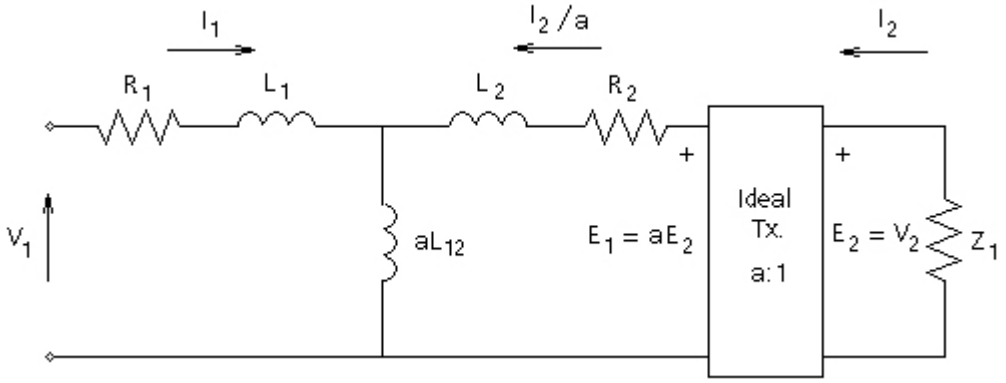

Figure 6.1: Equivalent circuit of the classical model on PSCAD

Table 6.1: Transformer parameter and the corresponding description

Parameter	Description	Unit
T_{MVA}	Transformer single-phase MVA	MVA
F	Base frequency	Hz
X_1	Leakage reactance	p.u of S_{base}
NLL	No-load losses	p.u of S_{base}
V_1	Primary winding voltage (RMS)	V
I_{m1}	Primary side magnetizing current [%]	% of I_{rated}
V_2	Secondary winding voltage (RMS)	kV
I_{m2}	Secondary side magnetizing current [%]	% of I_{rated}

Table 6.1 shows the description of the transformer data. The S_{base} is the MVA rating of the transformer. The no-load losses (NLL) and leakage reactance (X_1) are obtained from the open circuit and short circuit tests respectively. The secondary and primary magnetization currents are as a percentage of the primary base current shown in the following equations:

I_{m1} = x%*I_{base}(primary), I_{m2}=x%*I_{base}(secondary) (6.1)

where Ibase is given by:

I_{base}= S_{base}/V_{base} (6.2)

The core saturation characteristics in the model can be influenced by the three parameters:

- Air core reactance
- Magnetization current
- Knee voltage based on the rated voltage as 1 pu

The block showing how these parameters are entered in PSCAD is shown in Figure 6.2. Knee point voltage and magnetization current are readily available from the v-i curves obtained from open circuit tests. The air core reactance is estimated as twice the leakage reactance obtained from short circuit tests. The classical approach is useful in instances where there is limited transformer data and hence an approximation of the core characteristic is deployed. Even though more rigorous saturation models have been reported in the literature, the data is not available to make use of them; the saturation curve is rarely known beyond the knee point hence the classical model can be used for single-phase units with limited data.

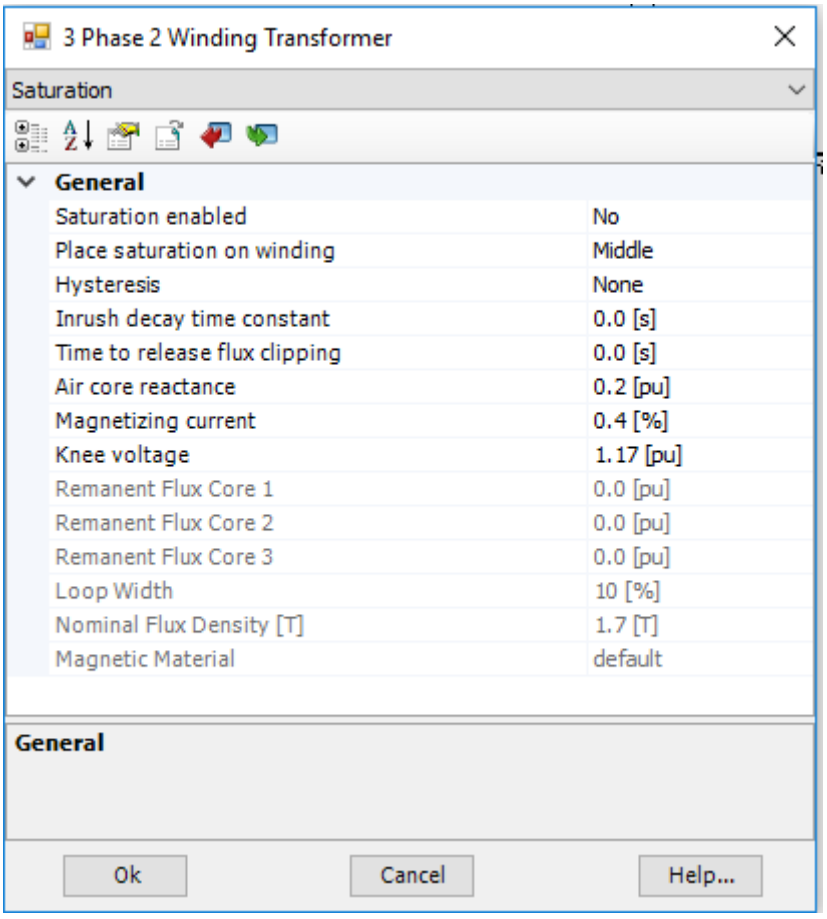

Figure 6.2: Saturation Properties for a 3phase 2 winding Transformer in PSCAD

6.2 UMEC Approach

The Unified Magnetic Equivalent Circuit (UMEC) transformer model is based on the core geometry. It differs from the classical approach in that it considers the magnetic coupling between windings of different phases in addition to coupling between windings of the same phase. In PSCAD, the three transformer core structures that can be represented using the UMEC approach are:

- Single-phase units with up to four windings
- Three-phase, three-limb(3p3L)
- Three-phase, five-limb(3p5L)

In the UMEC model, saturation is modelled differently in that non-linearity of the core is entered directly into the model as a piece-wise linear V-I curve. Figure 6.3 shows how these are the v-i parameters are entered into the simulation model.

From Figure 6.3, Point 5 – 1 pu voltage refers to the rated voltage of the transformer to be modelled. Based on the knee voltage of the classical model being estimated to be 1.17 pu, careful considerations need to be made for the UMEC when; a) defining the knee point voltage, and b) defining the model transformer's rated voltage. The classical model differs from the UMEC model in that instead of entering the v-i curve into the model, non-linearity is approximated based on knee point, the air core reactance, and the corresponding magnetization current. Based on the laboratory protocol, in which the modelling of inter-phase coupling is needed, the UMEC model will be used. The v-i curve generated from the laboratory open circuit test was entered into the software block shown in Figure 6.3 for both transformers to be used for the remaining tests.

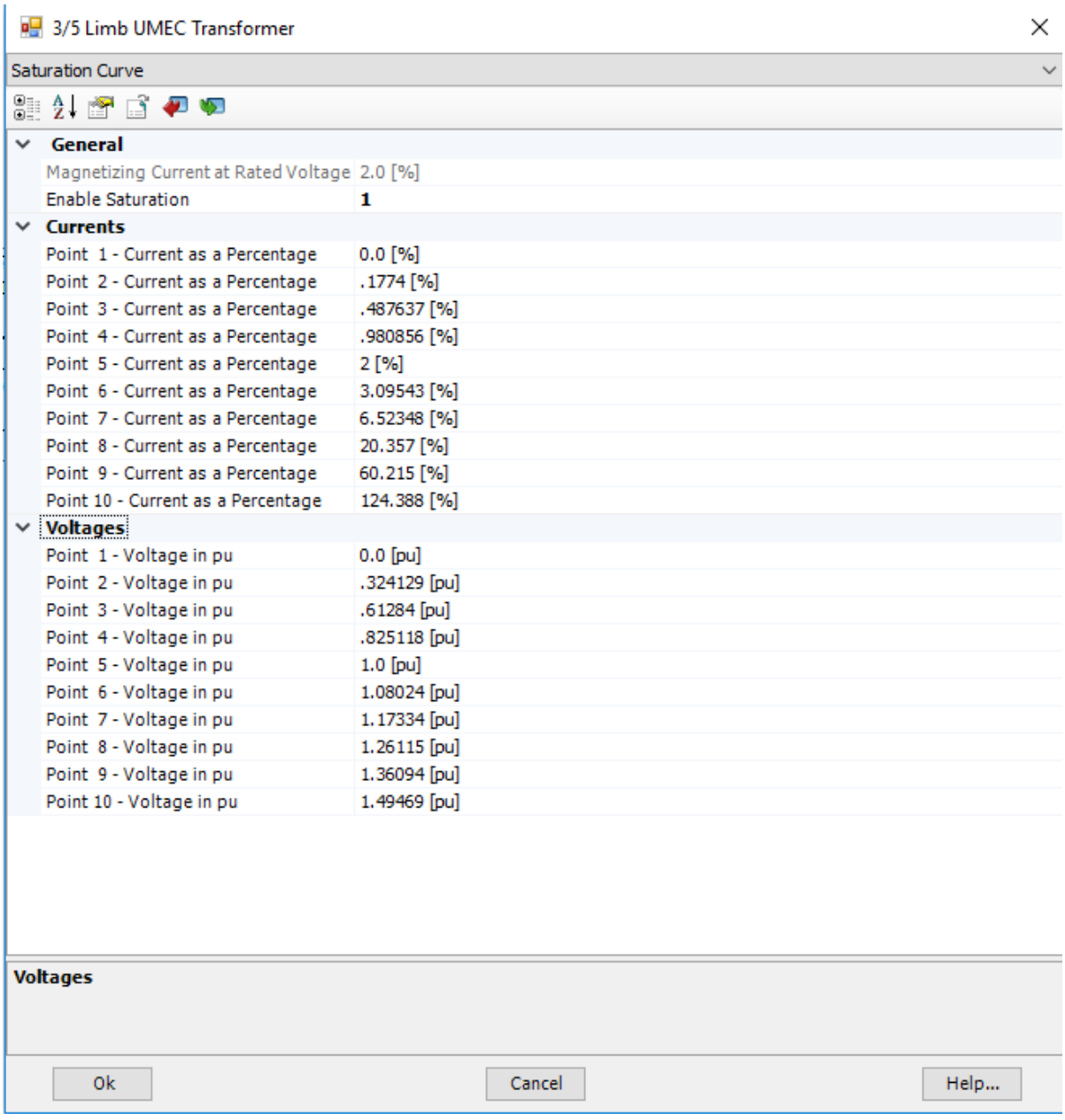

Figure 6.3: V-I parameters required by the PSCAD model

6.3 No Load Tests

The parametrized transformers were then subjected to no-load tests at similar conditions to the laboratory experiments. The v-i curve was generated and compared to the measured v-i curve. The knee transformers were also energized to the IEC knee and the corresponding average I_{mag} was recorded and compared to the laboratory measured average I_{mag}. Figure 6.4 and Figure 6.5 show the test set up of the open circuit tests on PSCAD.

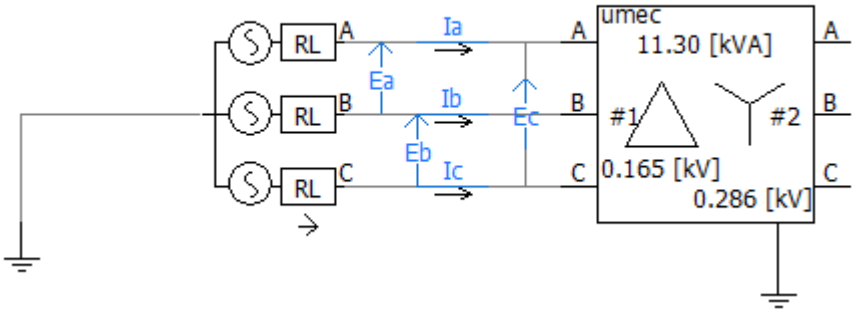

Figure 6.4: ΔY Configuration in 3p3L and 3p5L Test set-up

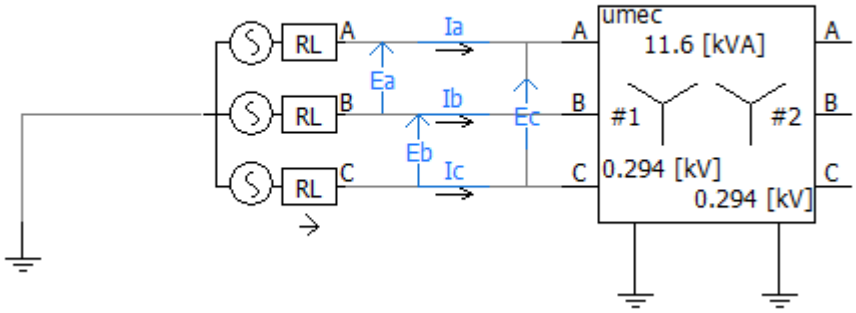

Figure 6.5: YY Configuration in 3p3L and 3p5L Test set-up

6.4 GIC Modelling on PSCAD

To replicate laboratory conditions on PSCAD regarding GIC representation, a single-phase voltage source was connected in series with the neutrals of the voltage source. This single-phase source can be connected as both a dc source and an ac source. To model dcGIC in the laboratory, a dc power supply was connected in series with the two transformer neutrals. The single-phase voltage source was used to model the dc power supply and a resistor was connected in series to control the current in the neutral. For acGIC analysis, the voltage source was connected as an ac source with a frequency of 10 mHz to model the laboratory conditions. The current was also controlled by the resistor connected in series with the voltage source. An ammeter was connected at the neutral to ensure that the desired current output is realised. Figure 6.6 shows how the parameters are entered on the voltage source model for both dcGIC and acGIC analysis.

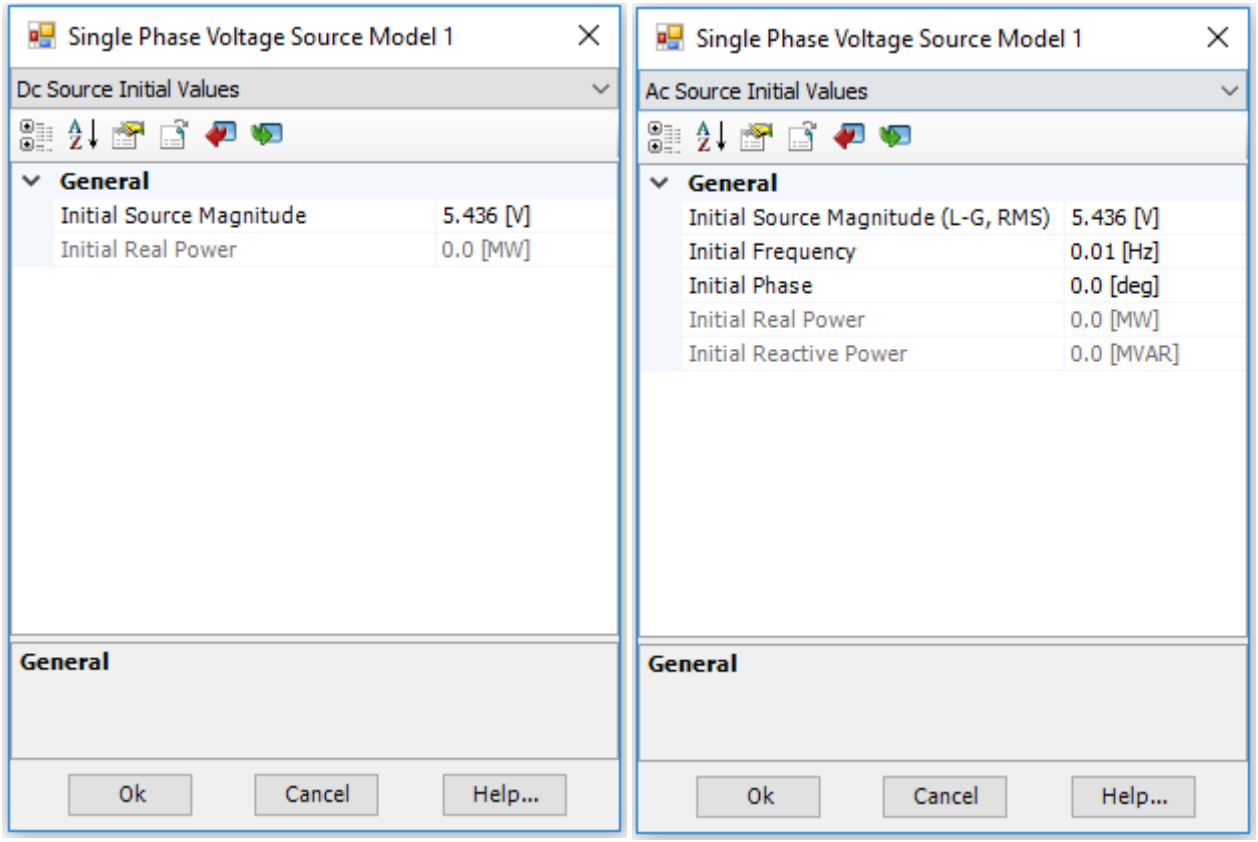

(a) (b)

Figure 6.6: PSCAD single phase voltage source used to model a) dcGIC and b) acGIC.

6.5 Voltage Stability Analysis

6.5.1 Test Network

For voltage stability analysis, a four-bus network was built on PSCAD and is shown in Figure 6.7

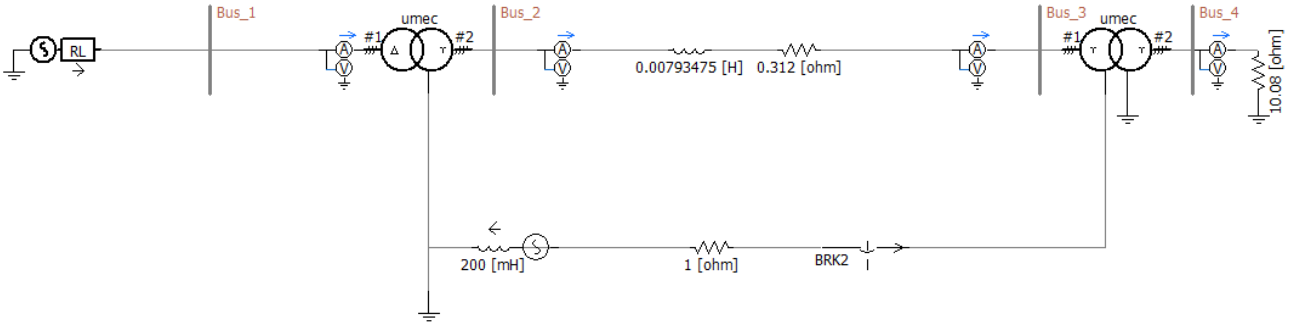

Figure 6.7: Four bus network built on PSCAD

Figure 6.7 shows 2 UMEC transformers; a 11.3 kVA, ΔY,165 V/286 V, three-phase three limb (3p3L) as the source transformer T1, and an 11.6 kVA, YY,294 V/294 V, three-phase five limb (3p5L) as the load transformer T2. The voltage was supplied by a 3-phase voltage source with a series RL and the RL parameters were obtained from the laboratory. The two transformer models were parameterized to match the physically performed no-load tests of the laboratory transformers. A resistor is connected to the load transformer to model a resistive load, as it is in the laboratory. The network also shows the two transformers' neutrals connected to model the GIC loop. A single-phase breaker is used to model the switch in the neutral (on time t=2 s to ensure that the system is in a steady state before dc or ac GIC).

6.5.2 Simulation Measurement Protocol

In the laboratory protocol, measurement was limited due to the availability of power analysers capable of taking measurements at all buses of the system. In the laboratory, only 9 channels were available to measure the voltage current, harmonics and power in the network. This meant that the bus 2 parameters could not be measured and hence limiting the amount of data available to analyse the system. However, there was no such limitation on PSCAD as the master library contained different kinds of measurement apparatus which could be used at any point in the system to take measurements. The available measuring apparatus on PSCAD are:

- Voltmeters
- Ammeters
- Power Meters
- Multimeters
- Fast Fourier Transform Block (FFT) for harmonics measurements

Some instantaneous and FFT readings measured online extracted from the measurement blocks and stored for further processing.

6.5.3 Simulation Procedure

The laboratory procedure described in chapter 3 was conducted in the PSCAD. The simulation was modelled over a period of 100s just as the laboratory protocol with measurements of current, voltage, harmonics and real power recorded for analysis. PV curve analysis and dynamic voltage change at the load due to the different GIC injections was investigated and compared to the laboratory results. To model the dc injection, a dc source was connected in series in the neutral loop. A resistor in series with the dc source was used to control the current supplied into the transformer neutrals. For ac injection, a 10mHz ac voltage source was connected in series with the neutral as shown in figure 6.7. The GIC injection was the same as the one described in the section 5.2. As a point of reference for the GIC level, the magnetization current of the 3p3L transformer was per unitized according to the laboratory no-load tests. This per unitized current (based on 1 phase) was then injected into the system on three levels:

- low GIC Injection: 1pu (0.302 A/ phase)
- Moderate GIC Injection: 3pu (0.906 A/phase)
- High GIC Injection: 6pu (2.718A/phase)

7. Results and Discussions

This chapter presents the results of the laboratory protocol and the simulation protocol done in PSCAD. The chapter first gives the results of the laboratory protocol in section 7.1 described in chapter 5 with the discussion of these results given at the end of the section. Section 7.2 describes the PSCAD simulation results of the protocol described in chapter 6. The results are discussed in detail under each section.

7.1 Laboratory Results and Discussions

The laboratory protocol described in chapter 5 was carried out and the results observed are presented in the following sections.

7.1.1 PV Curve Analysis

i. dcGIC Analysis

PV curves were conducted on the network for each dc injection and the results are shown in Figure 7.1.

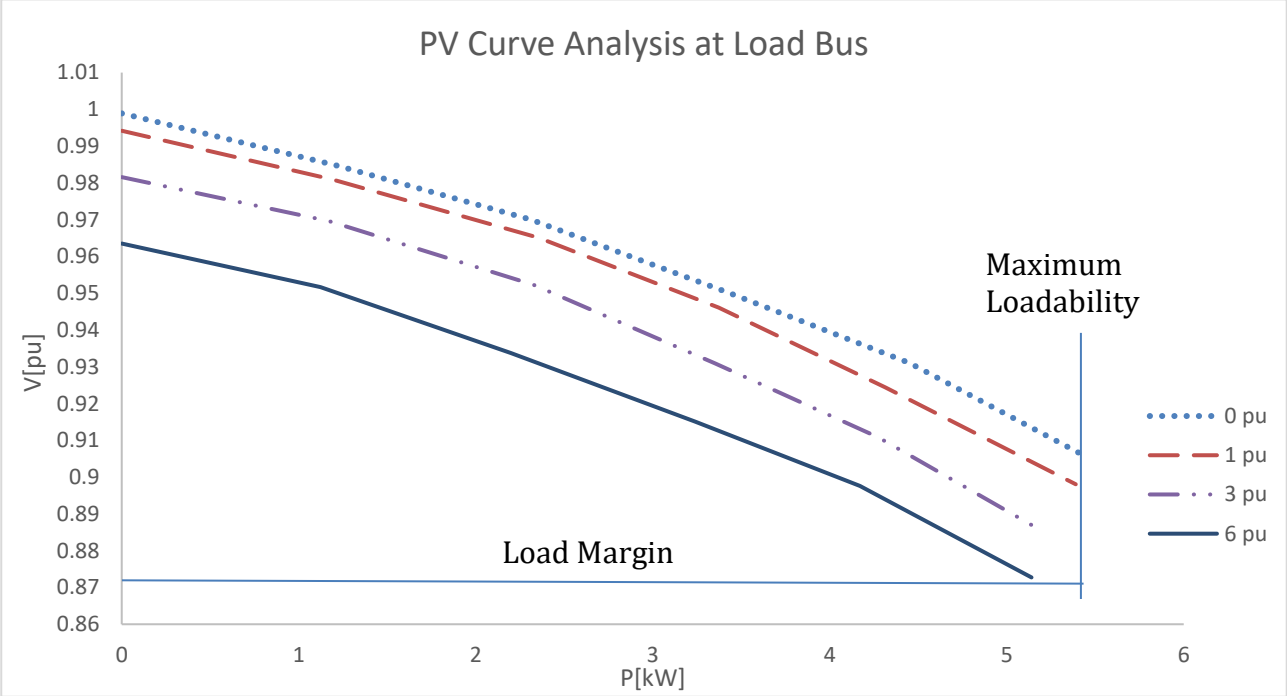

Figure 7.1: PV Curve Analysis when dcGIC is injected

Figure 7.1 shows the PV curve analysis at different GIC injections. The curves show a decrease in the load margin with increasing dc. This means that a system under dcGIC injection will reach the point of instability of the PV curve at a less power output than a system without dcGIC. The result of this is a reduction in the loadability of the system. Furthermore, there is a noticeable voltage drop at no load with increasing dcGIC. This is due to the distortion introduced into the system by dcGIC which in turn introduces losses and reduces the efficiency of delivery.

ii. acGIC Analysis

The PV curve analysis was conducted for the acGIC injection, and the results are shown in Figures 7.2 to 7.5. The PV curves were taken at a certain point of the acGIC cycle namely: peak (90 Degrees), zero crossing and 45 degrees. This was to capture the PV curve at different points of the 10 mHz acGIC cycle to show how the loadability of the systems changes as the magnitude of the GIC varies. This gives an insight into the changes that occur in the system during a GMD event where a multi frequency multi-amplitude GIC flows into the power system.

Peak

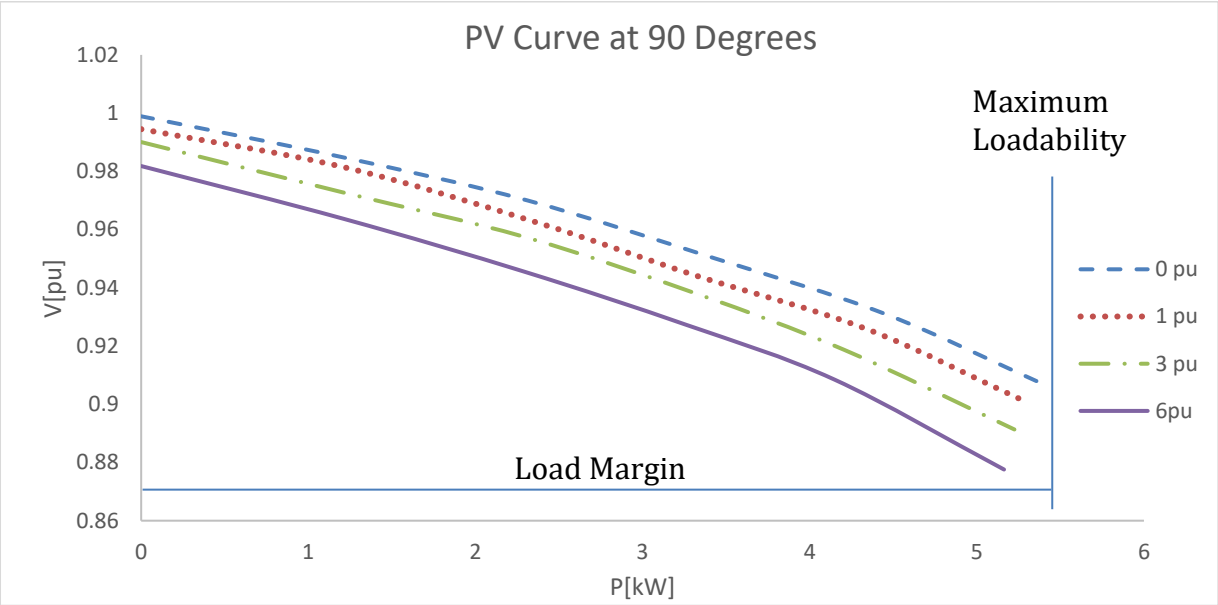

Figure 7.2: PV curve analysis conducted at the peak (90 Degrees) of the acGIC cycle

45 Degree Crossing

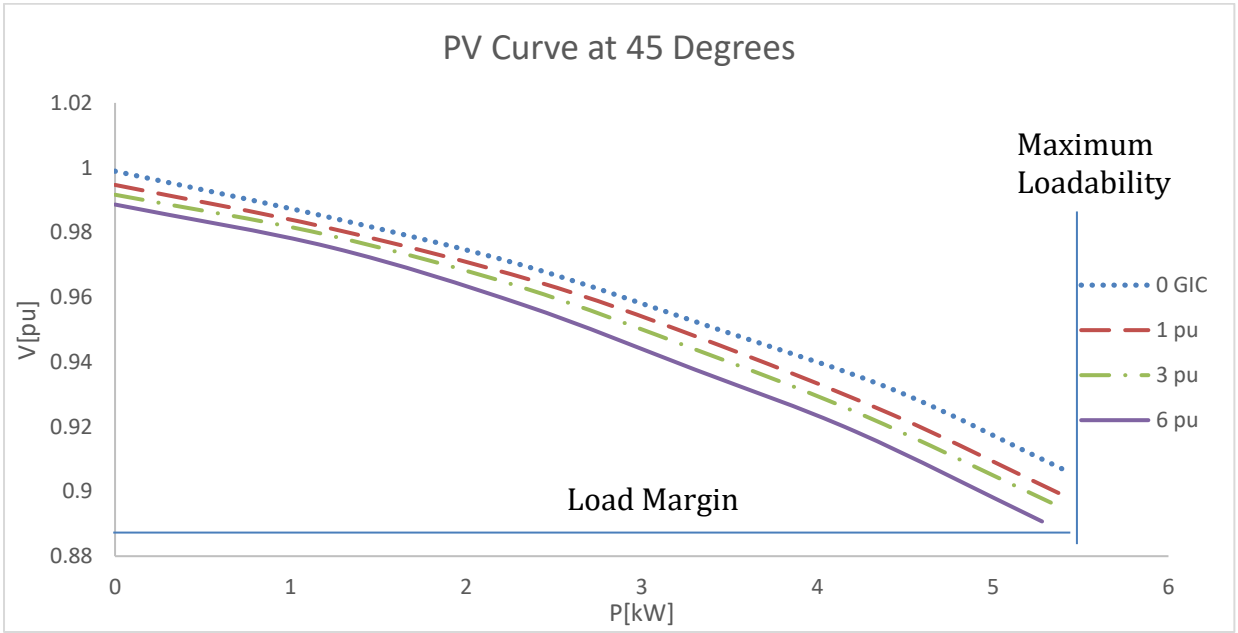

Figure 7.3: PV curve analysis of the system conducted at the 45-degree crossing of the acGIC cycle

Zero Crossing

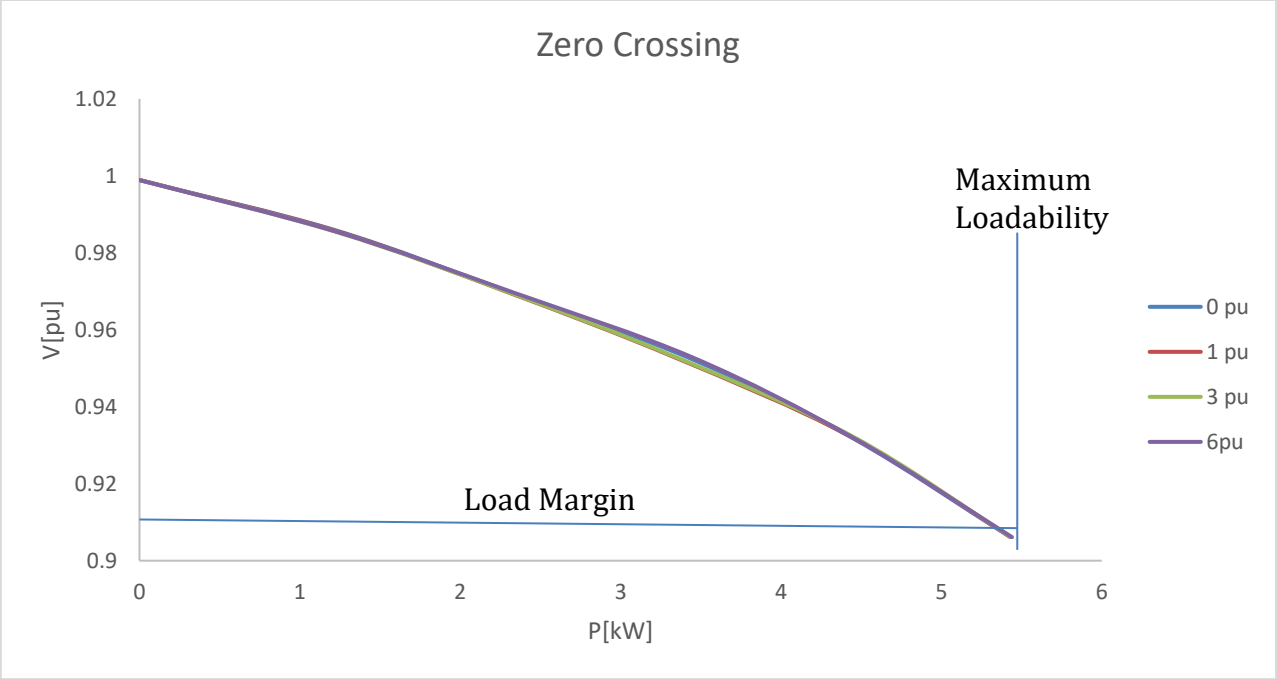

Figure 7.4: PV curve analysis conducted at zero crossing of the acGIC cycle

Intra-cycle change in loadability with 6pu Analysis

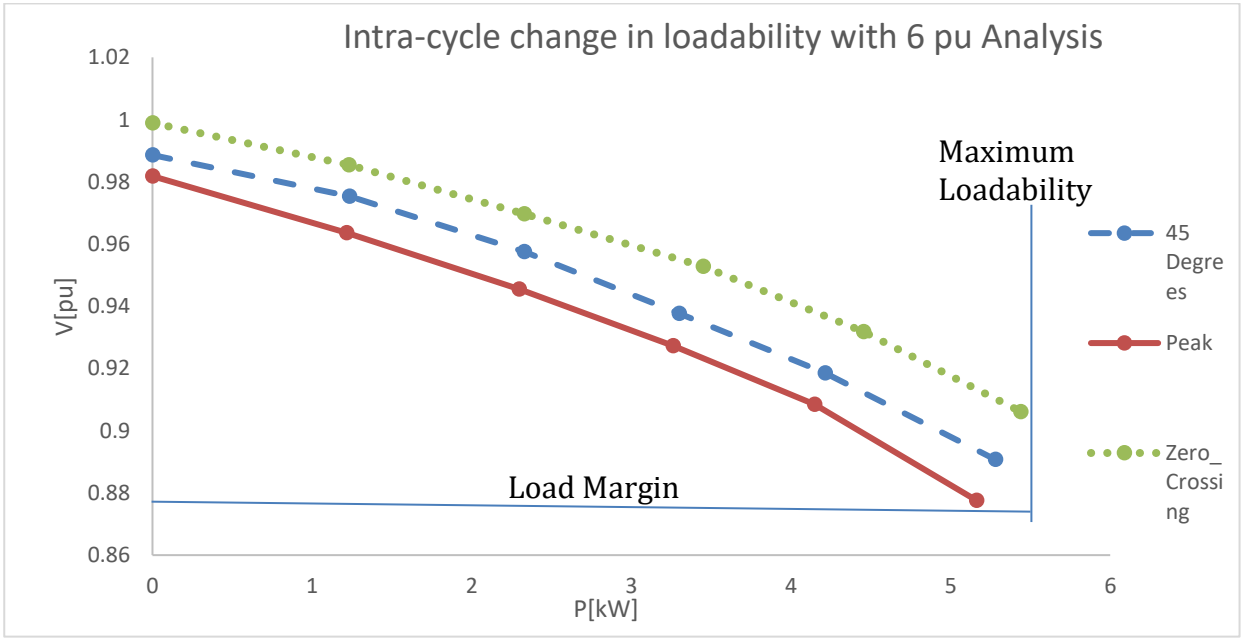

Figure 7.5: PV Curves of the 6pu for acGIC analysis

The results from Figure 7.2 to Figure 7.5 shows PV curve analysis conducted at 3 selected points over 1 cycle of the acGIC(100s). Figure 7.5 particularly shows an analysis of the curves at maximum acGIC injection level where the effects of GIC flow in the network are more pronounced. The results show that there is a larger voltage drop and a larger decrease in loadability from peak to zero crossing. This is due to the decrease in the magnitude of the GIC flowing in the system as the snapshots are taken at different points of the acGIC cycle. The loadability and voltage drop are both impacted by the acGIC magnitude flowing at the time of analysis and so as the acGIC cycle decreases in magnitude from peak

to 45 degrees, the effects of the GIC are less pronounced. The analysis conducted at zero crossing shows no change for all injection which was expected because this the point where the GIC current being injected has a magnitude of zero and so at the point the system is under normal operating conditions.

The implications of these results show that PV curve analysis conducted on systems under GIC influence depends on the magnitude of GIC flowing at the time the network parameters are recorded for analysis. This is important as a real GIC is a multi-amplitude, multi frequency signal and steady- state analysis at different points may present computational challenges particularly on a large data set. These results show that analysis to evaluate the GIC effects on loadability of the power system depends only on the maximum value of the GIC flowing at the time.

iii. ***Discussion***

The results show that the effects of voltage drop and load margin decrease are more severe in the dcGIC investigation compared to the acGIC section. For instance, when comparing the peak acGIC analysis with the dcGIC case at 6pu injection, both the maximum power output and voltage due to GIC are 1.167 % and 0.34 % lower for the dcGIC compared to acGIC. It is important to note that in both acGIC and dcGIC PV curve analysis, the PV curves do not all start at 1pu voltage at no load, which is unusual for PV curve analysis. This is due to two reasons. Firstly, the distortion due to the GIC flow into the system introduces losses and reduce the efficiency of delivery at the load [73]. The second reason is that according to Chisepo *et al.* [74], transformer part wave saturation experienced by transformers as aresult of GIC flow causes a drop in the instantaneous inductance of the transformer. This results in an increase in the Q drawn by the transformer thereby leading to a voltage drop at no load shown by the PV curves.

7.1.2 Bus 4 Voltage Analysis

The bus voltage was monitored using YPM WT500 at the load and readings over 1 cycle of acGIC (100s). This voltage was plotted for four cases, which are:

- 1pu-Minimum Loading
- 1pu-Maximum Loading
- 6pu-Minimum Loading
- 6pu-Maximum Loading

The readings for both dcGIC and acGIC analysis were taken over 100s (which is a full cylcle of acGIC) to enable comparison of the readings obtained between the two GIC injection modules. The plots showing the results of the volage response are given in the following sections. These plots are to give insight to the differences in the bus voltage response in acGIC compared to dcGIC.

i. Minimum Loading, Minimum GIC (GIC=1pu)

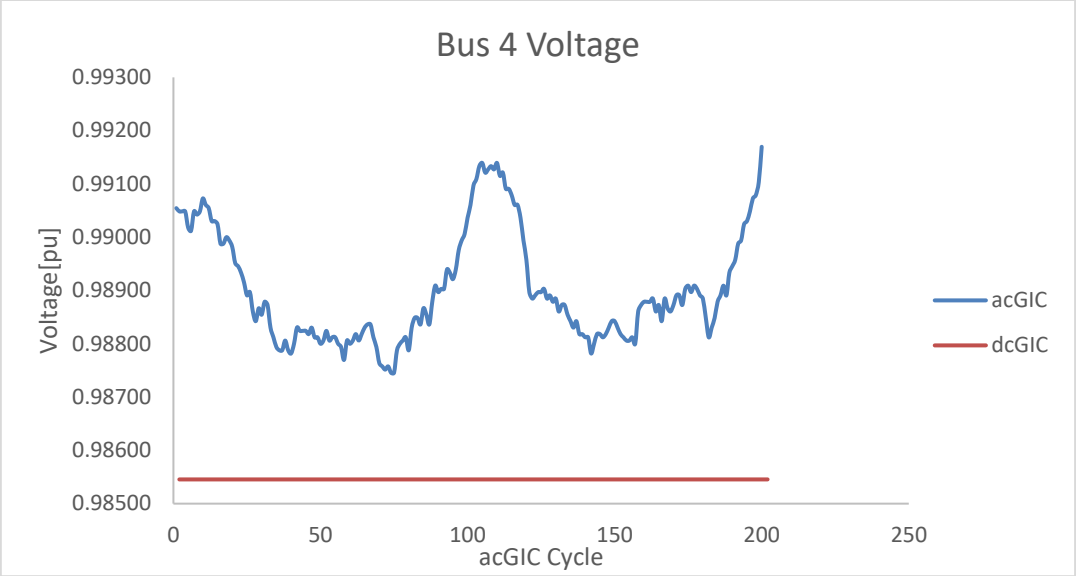

Figure 7.6: Graph showing how the load voltage varies during the 100s acGIC cycle with results obtained from acGIC and dcGIC of 1pu at light loading conditions.

Figure 7.6 shows the voltage at the load under both acGIC and dcGIC conditions. The dcGIC throughout the 100s shows a constant response at 0.985 pu which is expected for constant current injection. The voltage shows a varying response with respect to the acGIC, varying from 0.992 pu (zero-crossing) to 0.9875 pu (peak). The voltage drop during the acGIC cycle is with a 0.454% range. The results also show that the impact on the voltage of GIC is more severe in the acGIC model compared to the dcGIC.

ii. Maximum Loading, Minimum GIC (GIC=1pu)

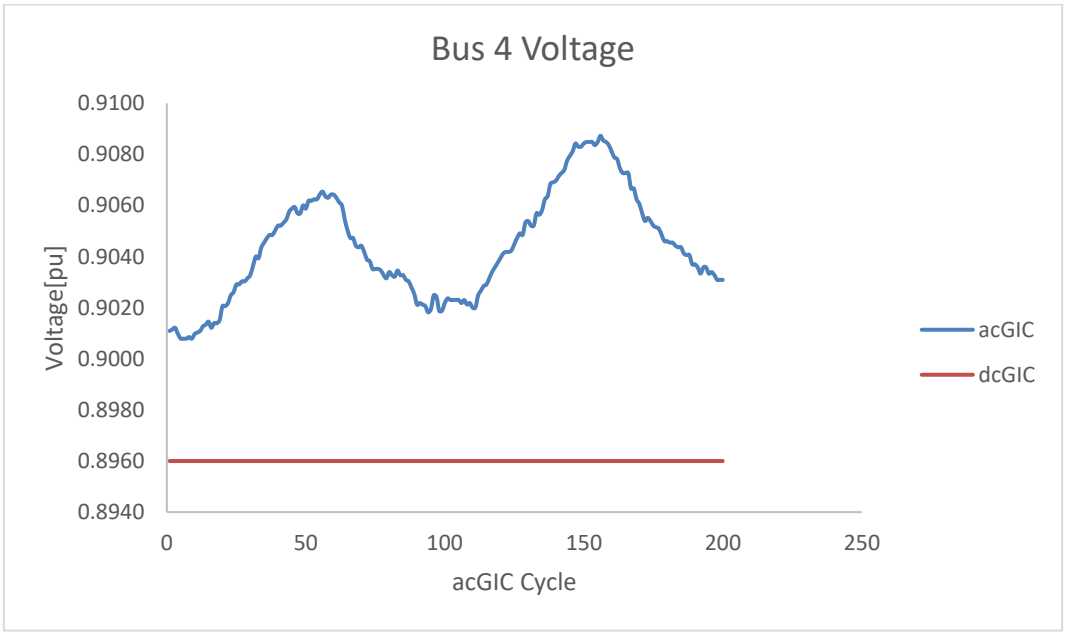

Figure 7.7: Graph showing how the load voltage varies during the 100s acGIC cycle with results obtained from acGIC and dcGIC of 1pu at heavy loading conditions.

Figure 7.7 shows the voltage variation over the 100s for both dcGIC and acGIC injections. The dcGIC shows a constant response of 0.896 as expected from a constant current injection. The acGIC voltage varies from 0.9085 (zero crossing) to 0.9008(peak). The acGIC voltage drop varies within a 0.454% range.

iii. ***Minimum Load, Maximum GIC (GIC =6pu)***

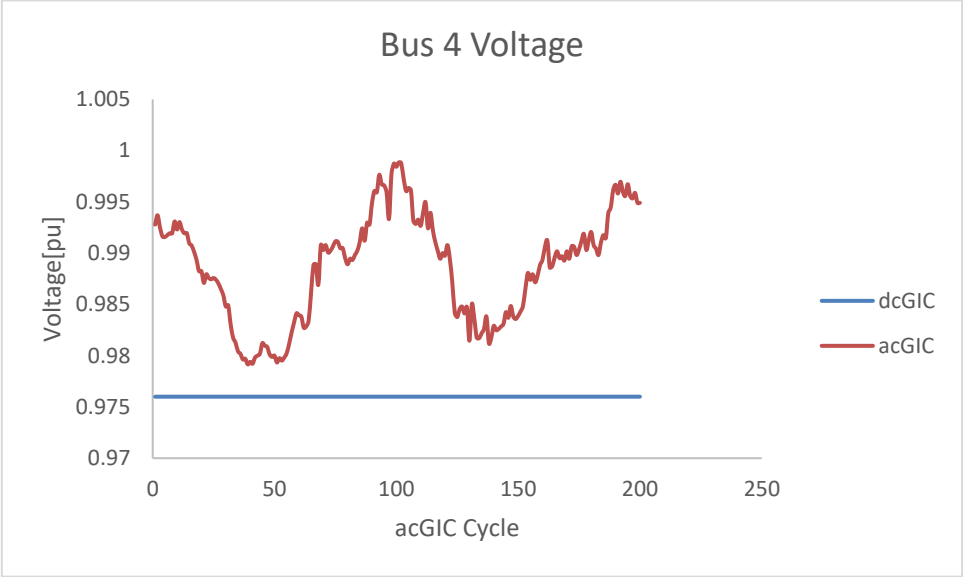

Figure 7.8: Graph showing how the load voltage varies during the 100s acGIC cycle with results obtained from acGIC and dcGIC of 6pu at light loading conditions.

Figure 7.8 shows a similar trend in the voltage response due to both dcGIC and acGIC as observed in Figure 7.6 and 7.7. The voltage for the lightly loaded system under dcGIC injection drops by 1.0% as the GIC increases from 1 pu to 6pu. The voltage drop range when the system is under acGIC injection is 2%, which is higher compared to the 1pu case. These results show that an increase in GIC injected in the system resulted in an increased voltage drop for the same loading conditions.

iv. ***Maximum Load, Maximum GIC (GIC =6pu)***

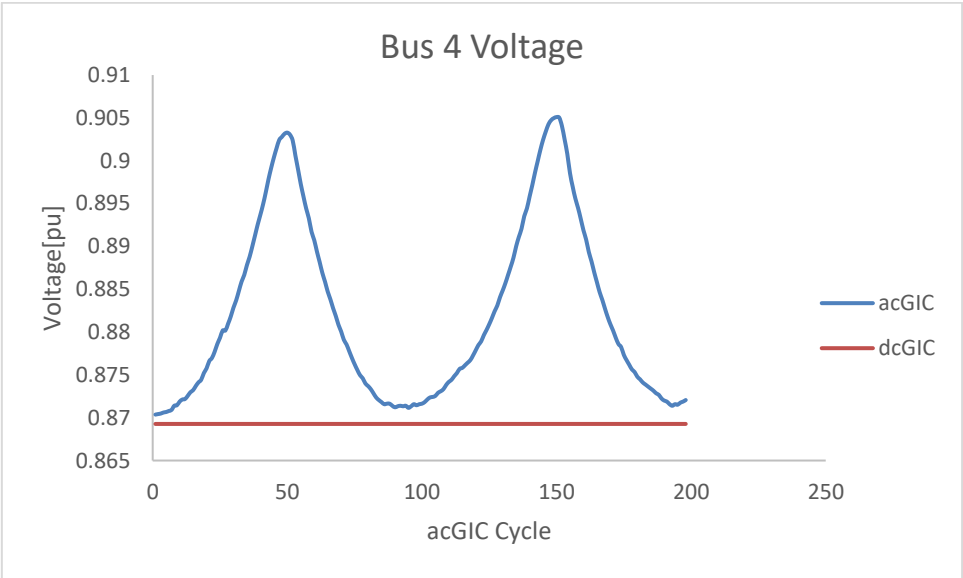

Figure 7.9: Graph showing how the load voltage varies during the 100s acGIC cycle with results obtained from acGIC and dcGIC of 6pu at heavy loading conditions.

Figure 7.9 shows the variation of the voltage response during one cycle of the acGIC signal. The voltage drop is within a 3% range, which is an increase of 2.5% as a result of the GIC increase from 1pu to 6pu. The voltage under dcGIC injection decreased by 3% as dcGIC was increased from 1pu to 6pu load conditions.

v. Discussion

The results showed that the heavily loaded system was more prone to a voltage drop due to GIC compared to a lightly loaded system. Load curtailment has been suggested as a mitigation strategy in literature [75] during a GMD event to counter a voltage collapse and the results from both acGIC and dcGIC injection analysis corroborate this argument. The dcGIC model, just as in the PV curve analysis, resulted in a more adverse impact on the system in all loading and GIC conditions. The voltage during acGIC injection varied with respect to the acGIC flowing at a time in the system. The effects on the voltage were more severe at peak of the acGIC cycle and as the magnitude of the acGIC decreases, the effects voltage decrease.

7.1.3 Harmonic Analysis

Harmonics were investigated in both Bus 3 (Transmission line) and Bus 4 (Load Bus) to observe the effect of the GIC on the harmonics in the system. The measurements were made for both voltage and current harmonics up to the 15th order. The investigation was made for phase A of both buses 3 and 4 because the system is relatively balanced, and therefore a response obtained from one of the three phases can be used to draw sound conclusions on the system response. To show this balance between the phases, a no-load case of harmonics measured at Bus 3 was plotted. This plot was for the dcGIC injection of 1pu and this is shown in Figure 7.10 and Figure 7.11.

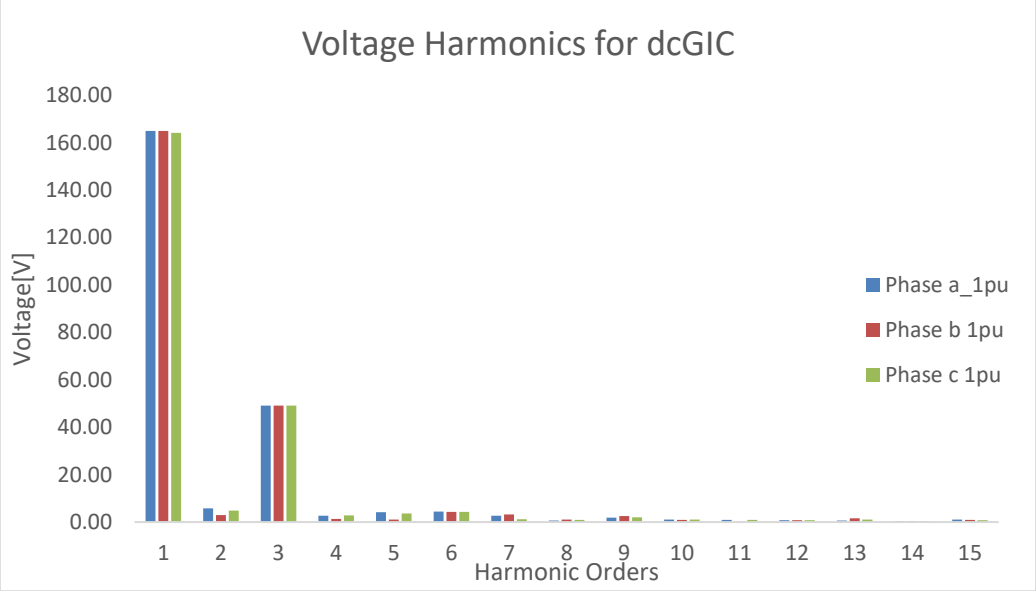

Figure 7.10: Phase A, B and C Voltage Harmonics at Bus 3 for a No Load Case

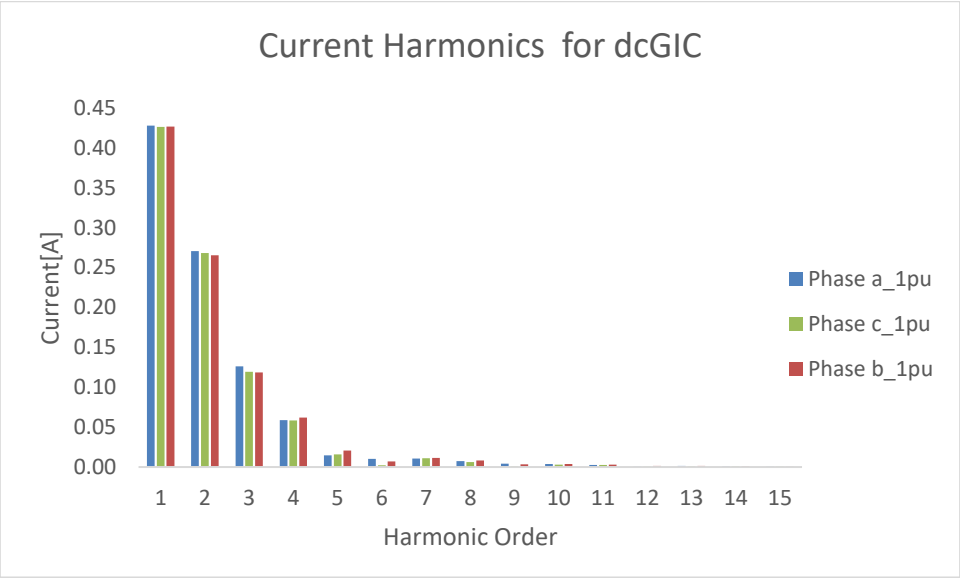

Figure 7.11: Phase A, B and C Current Harmonics at Bus 3 for a No Load Case

Harmonic spectra analysis made on bus 3 to show how each of the harmonic orders vary with increasing GIC. Furthermore, THD analysis was conducted at the load bus and was recorded over a full acGIC cycle (100s) for both acGIC and dcGIC analysis.

i. ***Bus 3 Harmonic Analysis***

Harmonic measurement at Bus 3 was made for the following test cases:

- No Load
- Minimum Load (Lightly Loaded System)
- Maximum Load (Heavily Loaded System)

The results show the generation of harmonics due to GIC and how it differs for each injection. The acGIC analysis was conducted at three points: peak (90 degrees), 45 degrees and zero crossing. The analysis is to show how each harmonic component changes as the acGIC varies from peak to zero crossing. The dcGIC results are also shown for each case and compared with the acGIC results. A comparison between the peak and dcGIC for the heavily loaded system is presented. The comparison for other loading cases can be found in Appendix 10.3

No Load Analysis

Harmonic Spectral Analysis-dcGIC

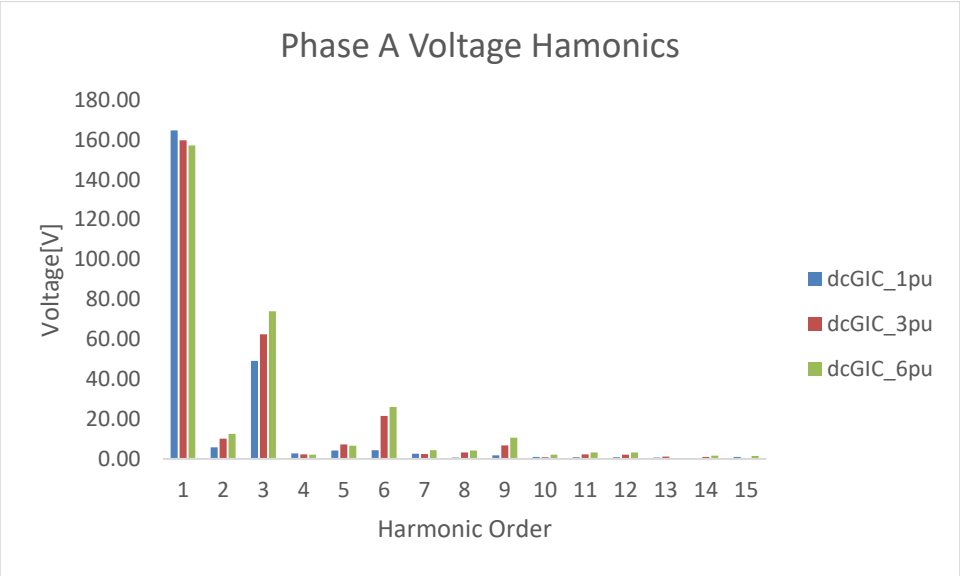

Figure 7.12: Voltage Harmonic showing different levels of GICs at no load.

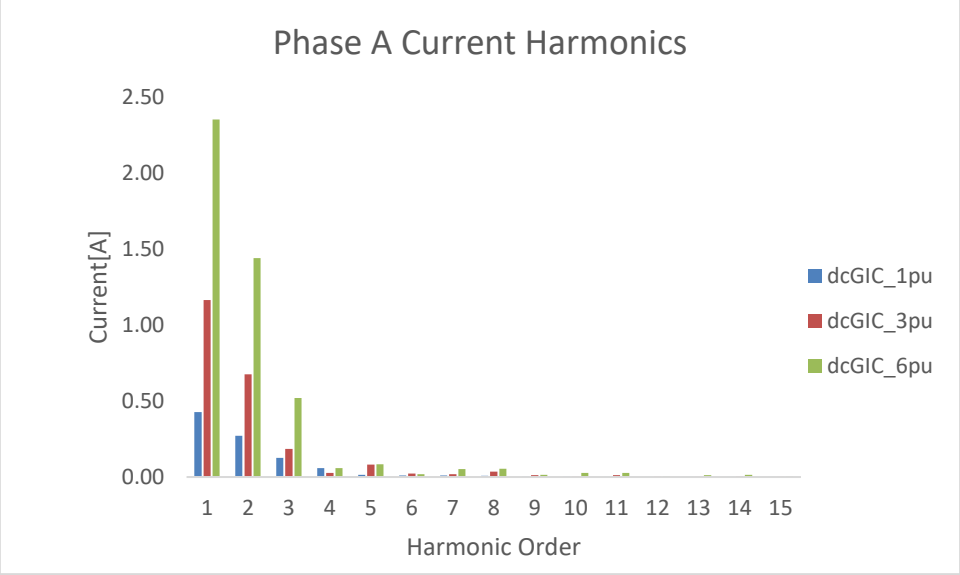

Figure 7.13: Current Harmonics at different levels of GICs at no load

Figure 7.12 and Figure 7.13 show the bus 3 harmonics at no load. The voltage and current harmonic magnitudes increase with increasing GIC as has been reported in literature [76],[77]. The voltage harmonic spectrum shows a high presence of triplen harmonics and a small presence of even order harmonics. The current harmonic spectrum also shows an increase in harmonic magnitude with increasing dcGIC. The results show that the 2nd order harmonic has the highest magnitude (after the fundamental) followed by the 3rd harmonic. This is in agreement with a finding by Chisepo [44] in which no load tests showed that the current harmonics increased according to this following expression:

$$H^{2nd} > H^{3rd} > \ldots\ldots H^{th} \tag{7.1}$$

Where H^{th} is the magnitude of the highest harmonic order.

Harmonic Spectra for No Load Case-acGIC

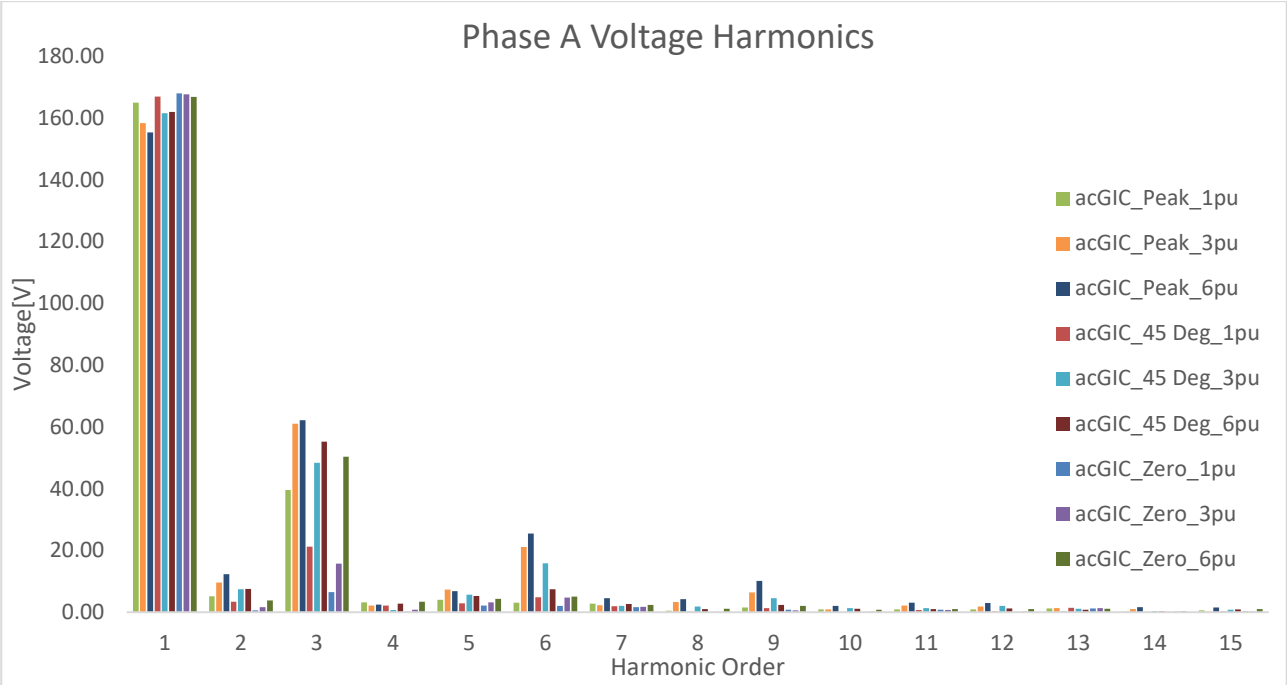

Figure 7.14 :Voltage harmonic spectra with increasing acGIC measured at different points of the acGIC cycle

Figure 7.14 shows the result of the voltage harmonic spectrum at no-load conditions as acGIC flows in the system. The results show that there is an increase in the magnitude of the triplen harmonics generated as the acGIC increases from 1 pu to 6pu. The variations of the harmonic orders as throughout the acGIC cycle show that harmonic orders are the highest at peak magnitude and are the lowest at zero crossing. This shows that during the acGIC cycle the harmonic magnitude varies directly proportional with current magnitude flowing in the transformer at that instance.

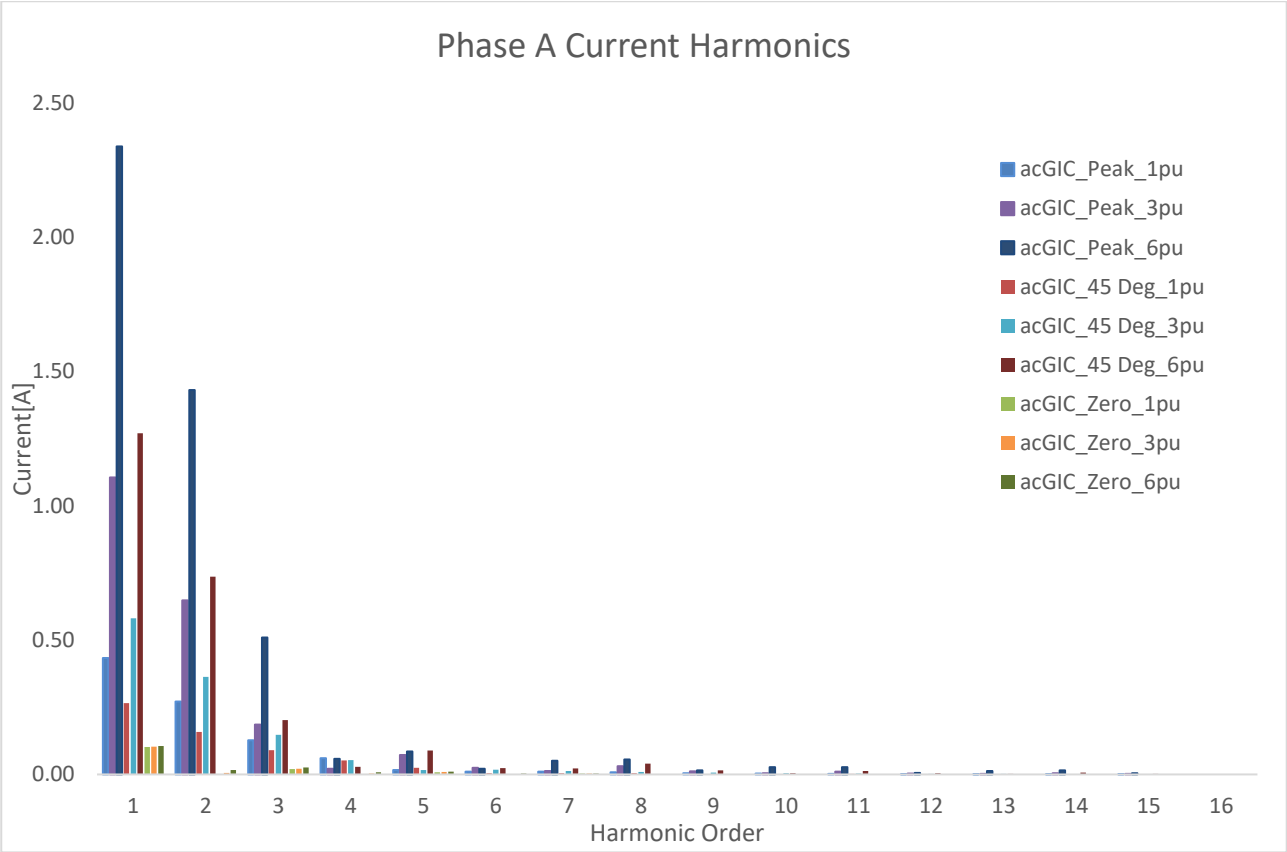

Figure 7.15: Current Harmonics measured at different points of the acGIC cycle at the load

Figure 7.15 shows the current harmonics at different acGIC injections at no load. The results show that the largest components are generated at peak acGIC, followed by the 45 degrees crossing point and lastly the zero crossing. The harmonics follow the same trend shown in Figure 7.13 in which the 2nd order harmonic has the largest magnitude, followed by the 3rd harmonic and others.

Minimum Load (Lightly Loaded System)

Harmonic Spectra for a Lightly Loaded System-dcGIC

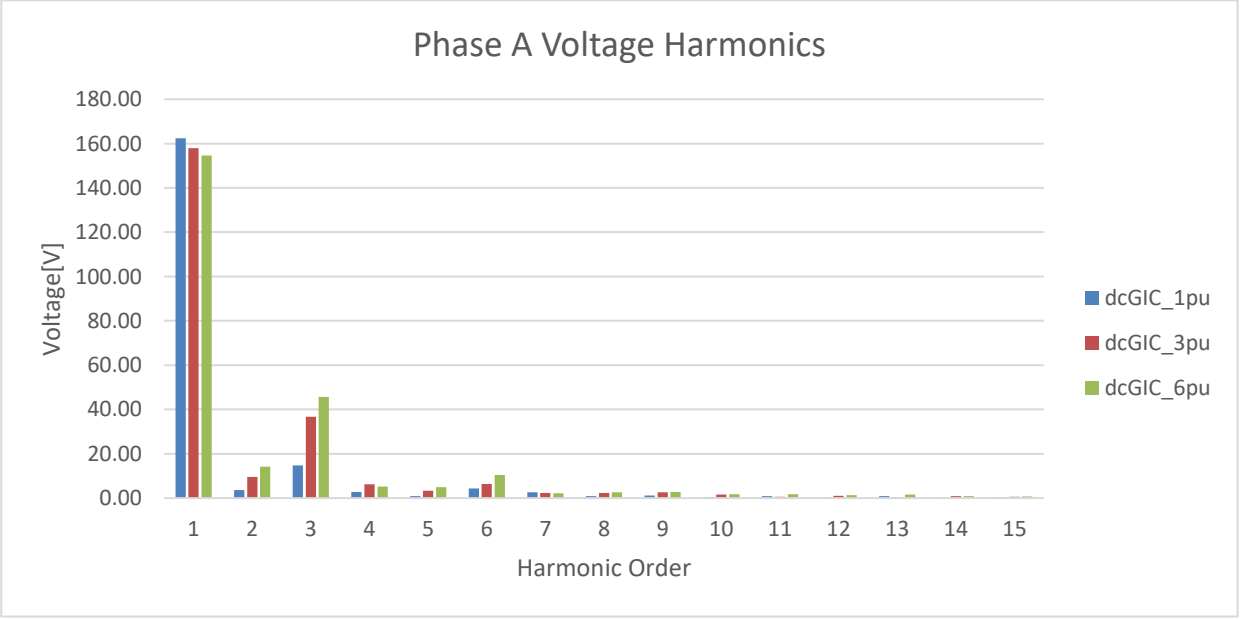

Figure 7.16: Voltage harmonic spectrum at light loading conditions under dcGIC injections

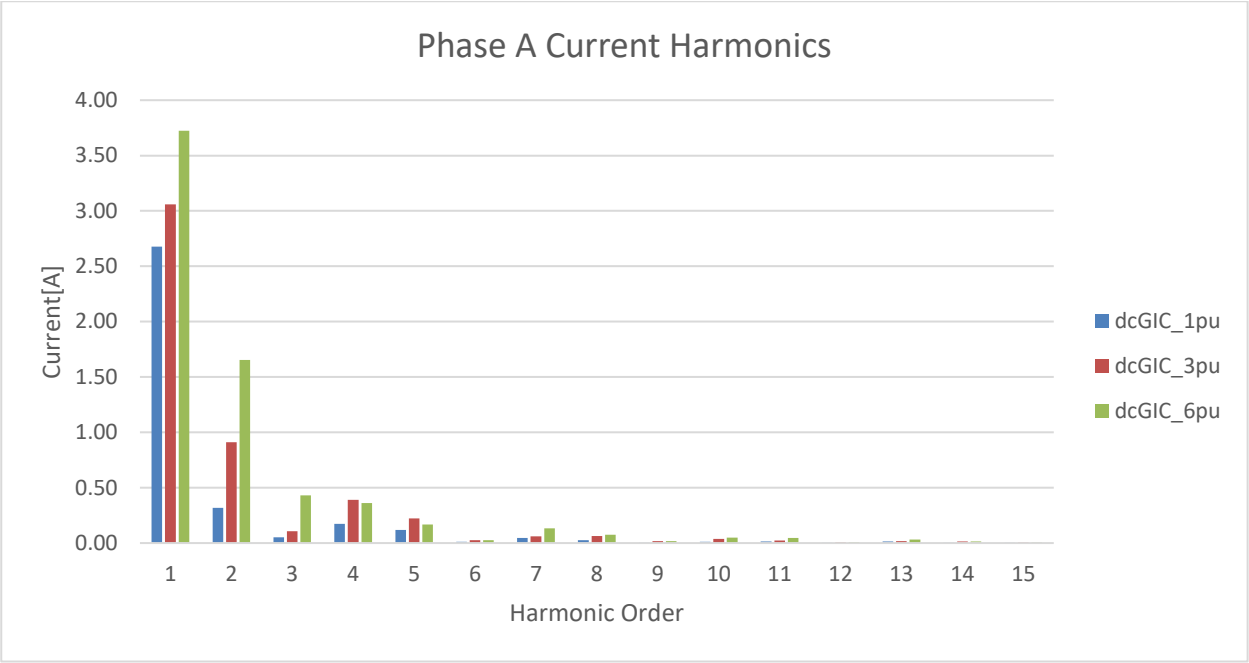

Figure 7.17: Current harmonic at light loading conditions under dcGIC injections

Figure 7.16 and Figure 7.17 show that the same trend is observed as in no-load conditions the nature of the spectrum. The amount of voltage distortion observed from the spectrum has slightly decreased from the no-load condition. The current spectrum distortion has slightly decreased as the presence of harmonics beyond the 8th harmonic is negligible compared to the no-load case, despite a slight increase in the current magnitude for the 2nd and 4th order harmonics.

Harmonic Spectra for a Lightly Loaded System with acGIC

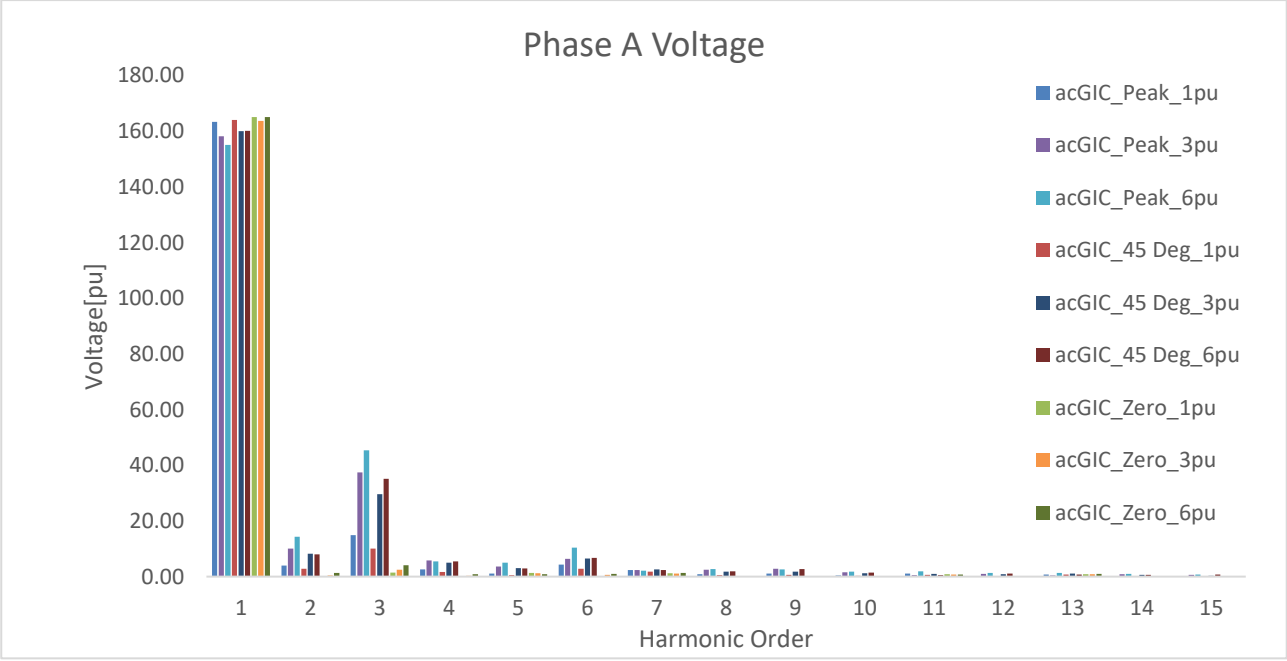

Figure 7.18: Voltage harmonic spectrum at light loading conditions under acGIC injection

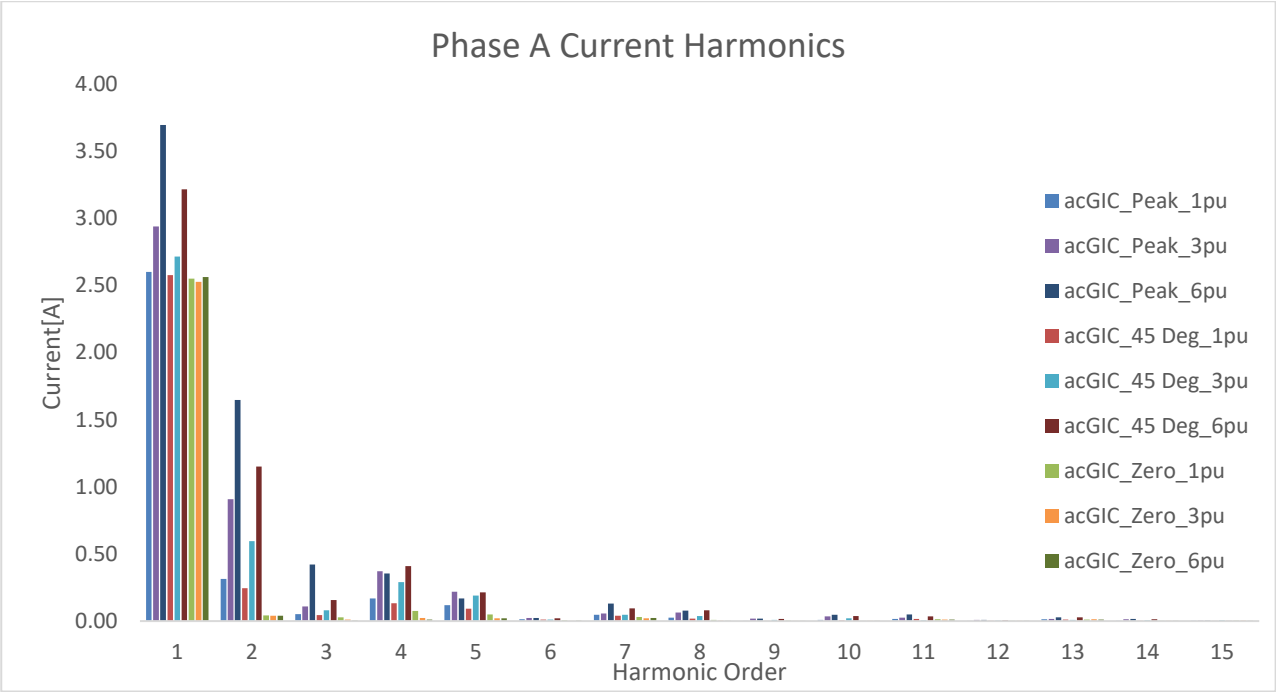

Figure 7.19: Current harmonic spectrum at light loading conditions under acGIC injection

Figures 7.18 and 7.19 show a similar trend in the spectrum as observed in the no load case in that the highest amount of distortion is observed at the peak value of the acGIC cycle. However, the level of harmonic distortion in the voltage spectrum decreased in the lightly loaded case compared to the no load case. The current spectrum shows a slightly decreased level of distortion compared to the no load case, however, there is a slight increase in the magnitude of the 2nd and 4th order harmonics.

Maximum Load (Heavily Loaded System)

Harmonic Spectral Analysis -dcGIC

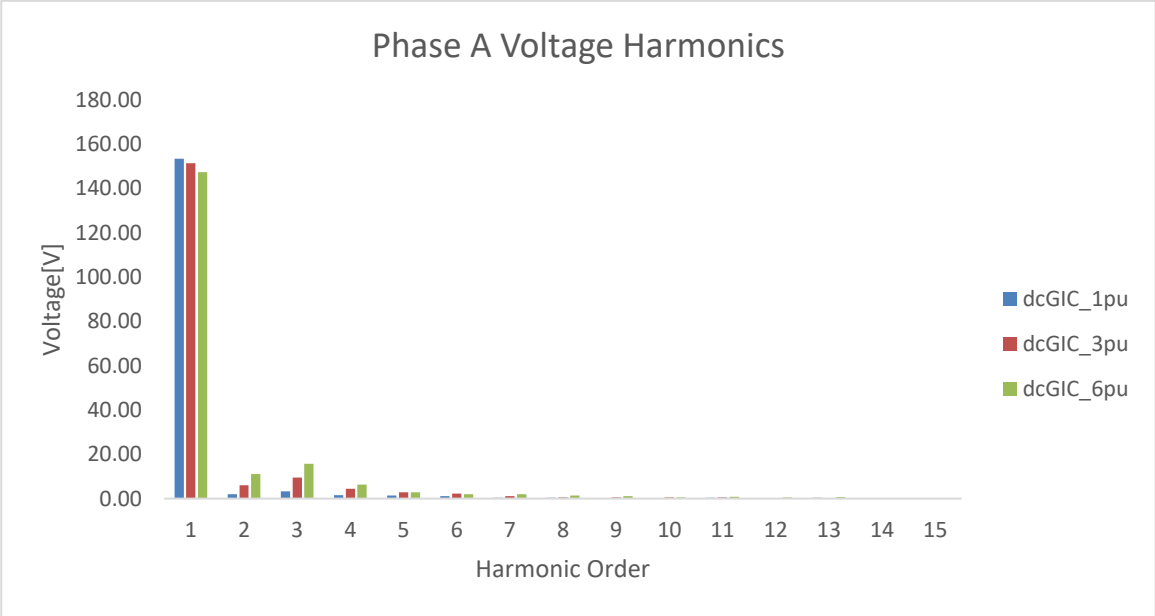

Figure 7.20: Voltage harmonic spectrum at heavy loading conditions under dcGIC injection

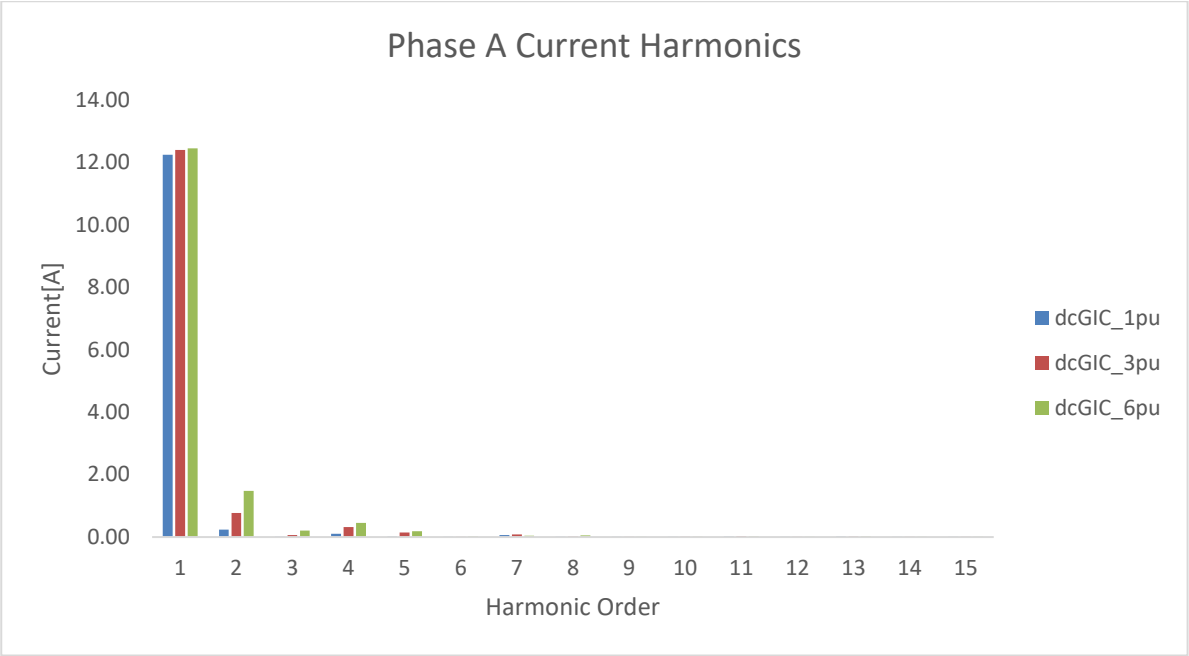

Figure 7.21: Current harmonic spectrum at heavy loading conditions under dcGIC

Figures 7.20 and 7.21 show that the loading significantly decreases the distortion of both the current and voltage harmonic spectrum. The voltage spectrum shows that there is insignificant harmonic components generated beyond the 9th order. The current spectrum in Figure 7.21 shows that their components generated are insignificant beyond the 6th harmonic.

Harmonic Spectra Analysis-acGIC

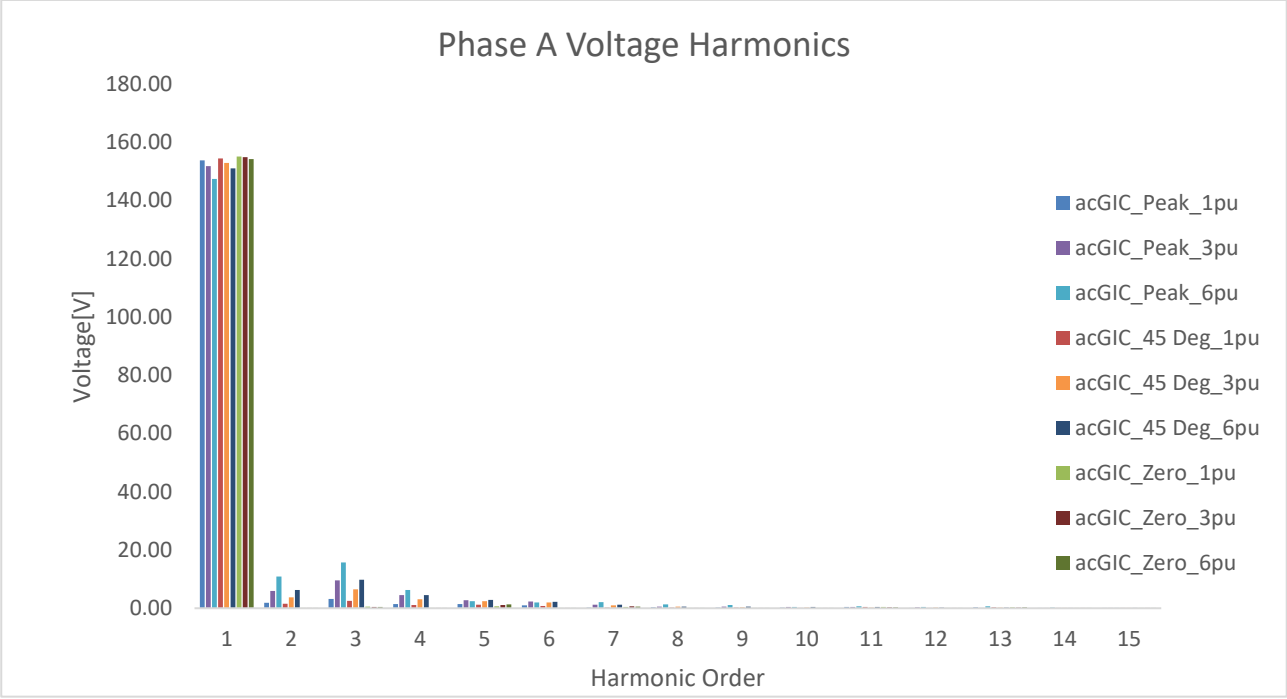

Figure 7.22: Voltage harmonic spectrum at heavy loading conditions under acGIC

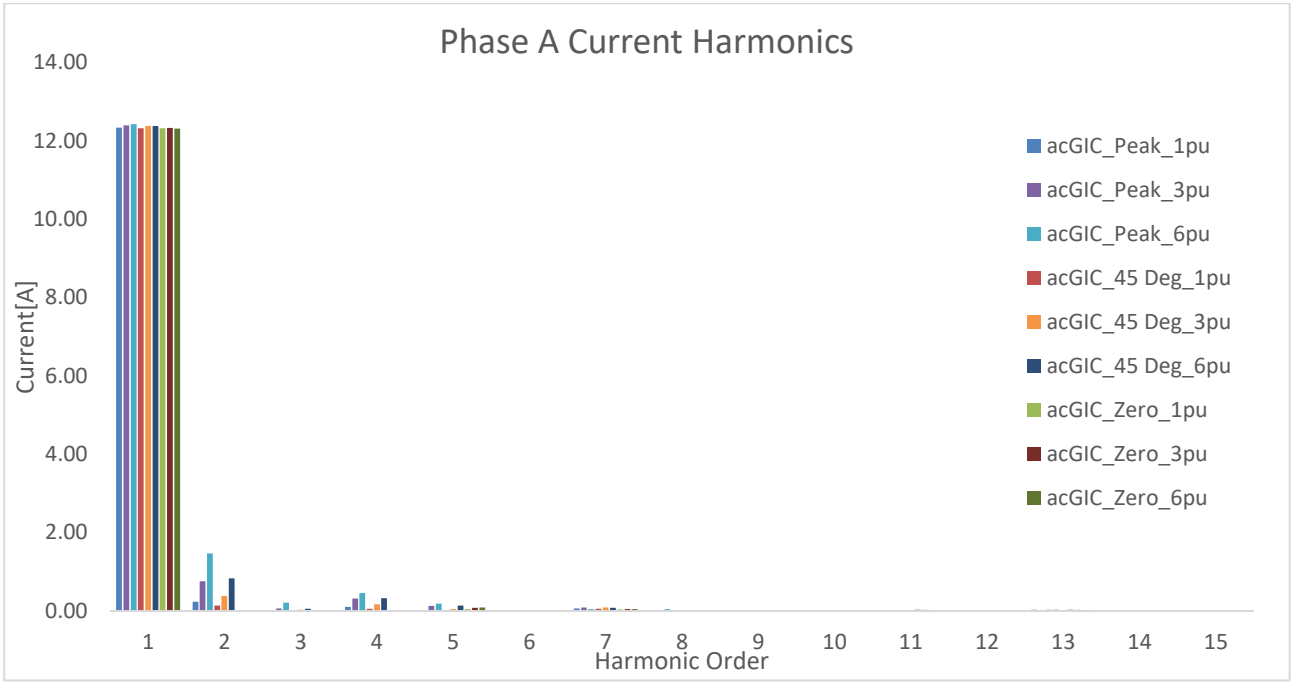

Figure 7.23: Current harmonic spectrum for a heavily loading condition under acGIC

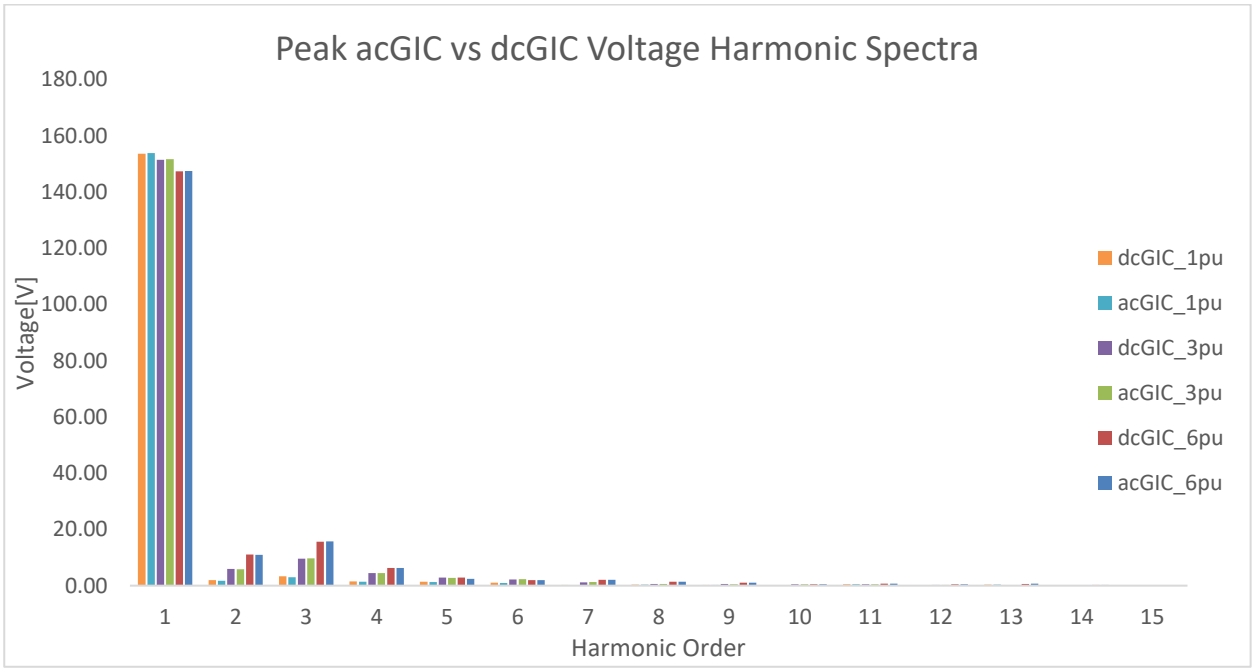

Figure 7.24: Comparison of the Peak acGIC vs dcGIC voltage harmonic spectra for a heavily loaded system

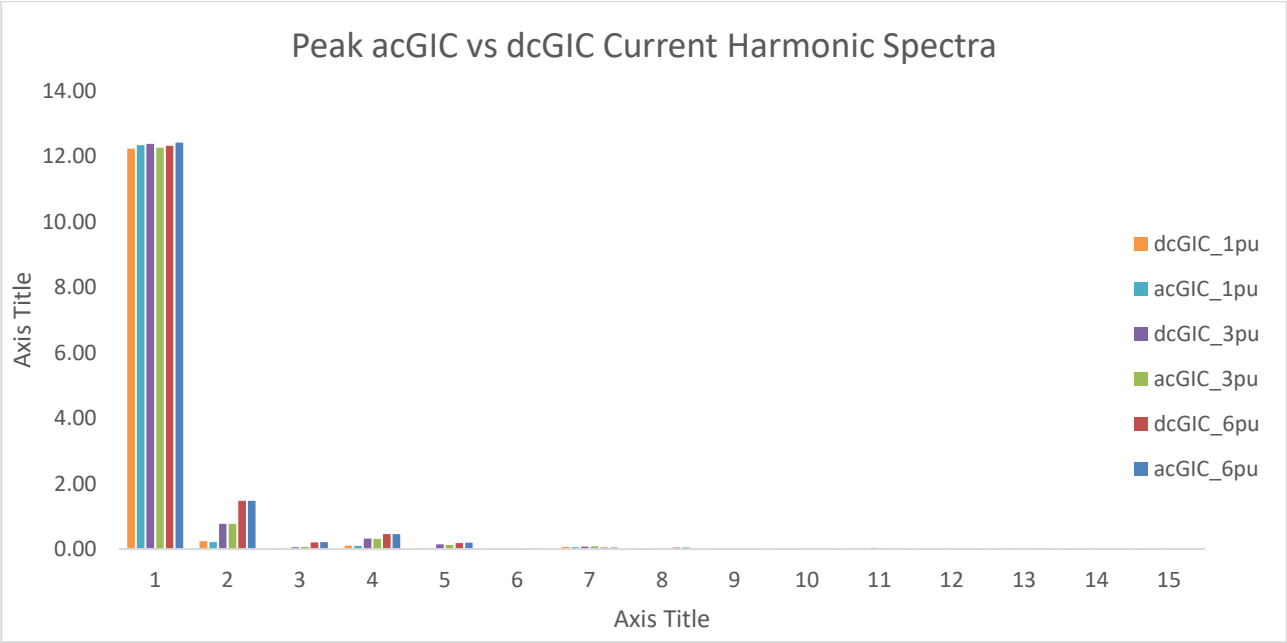

Figure 7.25: Comparison of the peak acGIC vs dcGIC current harmonic spectra for a heavily loaded system

As observed in the dcGIC injection for a heavily loaded system, Figures 7.20 and 7.25 show a significant decrease in the level of distortion in both voltage and current compared to the light load conditions observed in earlier analysis.

The implication of these results shows that, an increase in GIC flowing in the transmission line leads to an increase in harmonic distortion in the system. The results showed once again that the dcGIC model was the worst-case scenario with higher magnitudes of even and harmonic orders observed compared to the peak analysis of acGIC. PV curve analysis and Bus 4 voltage analysis carried in previous sections showed that the dcGIC model has more adverse effects on the system compared to acGIC.

Furthermore, it is important to note that, acGIC at peak and dcGIC have nearly equal components being generated by the system as evidenced by Figure 7.24 and Figure 7.25. There is no significant difference, and this shows that at peak injection of acGIC, the power system responds as though a dcGIC of peak magnitude is flowing in the system. This was observed in the previous sections with slight differences in magnitude. The network response to acGIC varies between peak and zero crossing with the harmonics generated varying according to the signal in real time.

ii. Bus 4 THD Analysis

The voltage and current THD was monitored and recorded at the load bus. Given that an analysis has been conducted for the transmission line, the THD at the load was of keen interest. The recording was made over a cycle of a 100s to obtain the variation of THD over a full acGIC cycle. The THD was monitored for dcGIC over 100s as well and the plots show both dcGIC and acGIC plotted on the same graph to observe the effect of GIC on THD in real time. The analysis was conducted for 4 test cases, namely:

- Minimum Load, Minimum GIC
- Maximum Load, Minimum GIC
- Minimum Load, Maximum GIC
- Maximum Load, Maximum GIC

The effect of loading, not just GIC was taken into consideration and was included in these test cases. The readings were not taken from the same starting point on the acGIC cycle e.g from peak for all cases as some were taken from peak or zero crossing point.

Minimum Load, Minimum GIC(GIC=1pu)

The following show the voltage and current THD at light loading conditions at 1pu GIC injection.

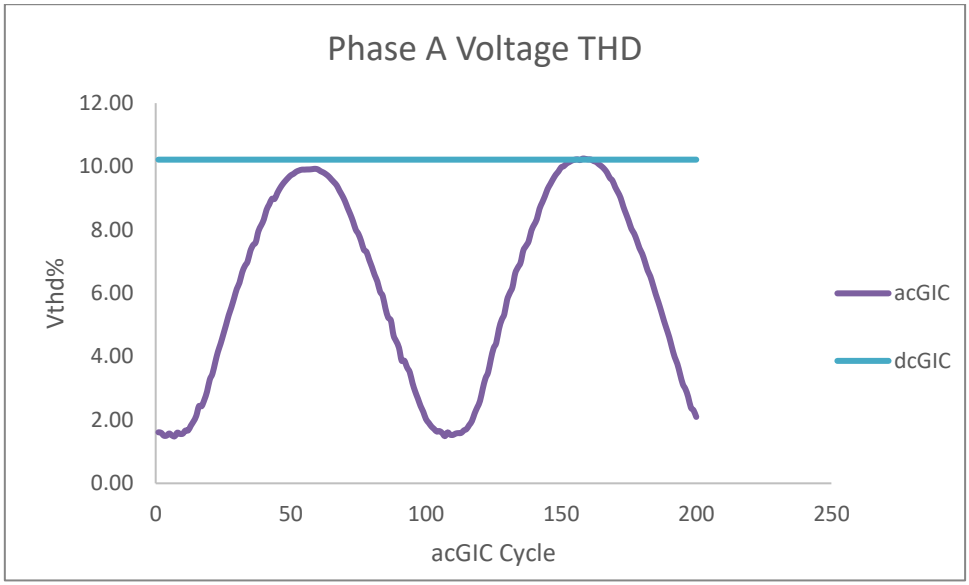

Figure 7.26: Variation of the voltage THD throughout a 100s acGIC cycle in the system under dcGIC and acGIC injections at minimum loading

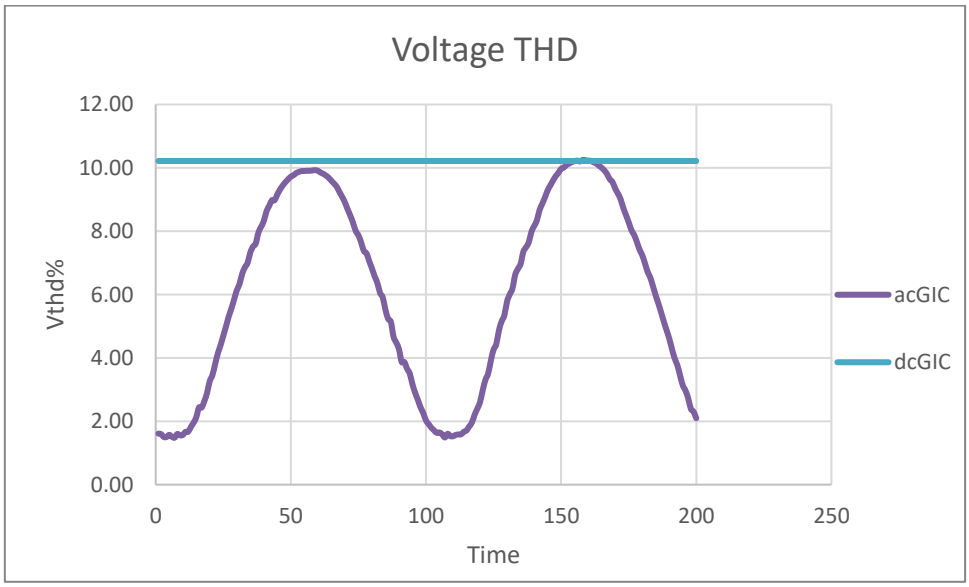

Figure 7.27: Variation of the current THD throughout a 100s acGIC cycle in the system under dcGIC and acGIC injections at minimum loading

Figure 7.26 and Figure 7.27 show a variation of the voltage and current THD with the acGIC cycle. The results show that the THD due to dcGIC injection has a constant response as expected from a constant current. However, the THD resulting from an acGIC injection shows a varying response according to the magnitude of current flowing, with the highest magnitude occurring at peak and the lowest occurring at the zero crossing.

Maximum Load, Minimum GIC(GIC=1pu)

The following show the voltage and current THD at heavy loading conditions at 1pu GIC injection.

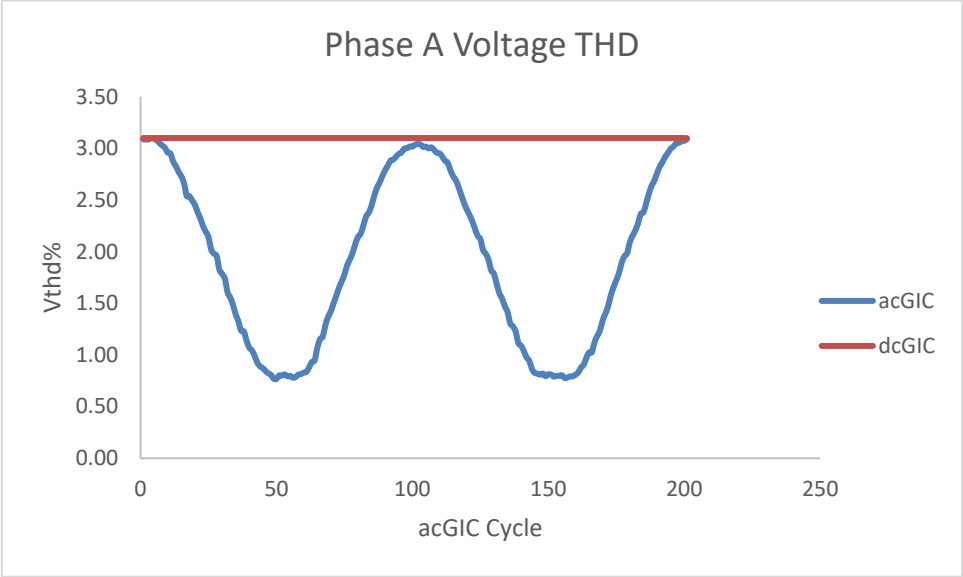

Figure 7.28: Variation of the voltage current THD throughout a 100s acGIC the system under dcGIC and acGIC injections at maximum loading

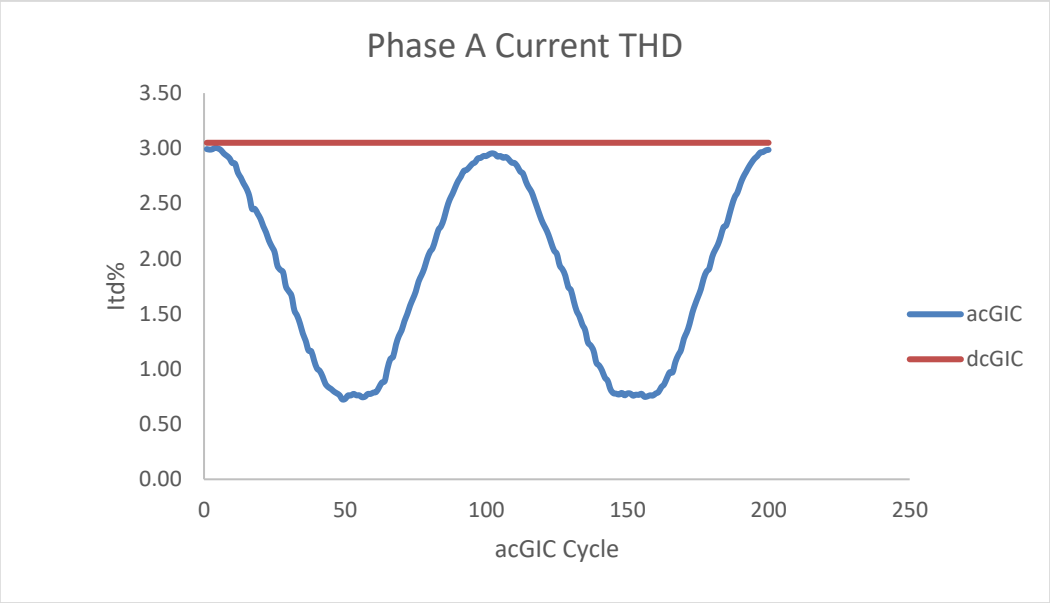

Figure 7.29: Variation of the current THD at minimum load throughout an acGIC cycle for a system under dcGIC and acGIC injection

Figures 7.28 to Figure 7.29 show the variation of the voltage and current THD for a heavily loaded system at minimum GIC. The response follows a similar trend to the one observed in Figures 7.26 and 7.27, with the major difference being that the value of both voltage and current THD has significantly decreased compared to the lightly loaded case at the same GIC injection. This decrease is attributed to the increase of the fundamental component relative to other higher harmonic components which become negligible at heavy loading as evidenced by the harmonic spectra in section 7.1.3.

Minimum Load, Maximum GIC(GIC=1pu)

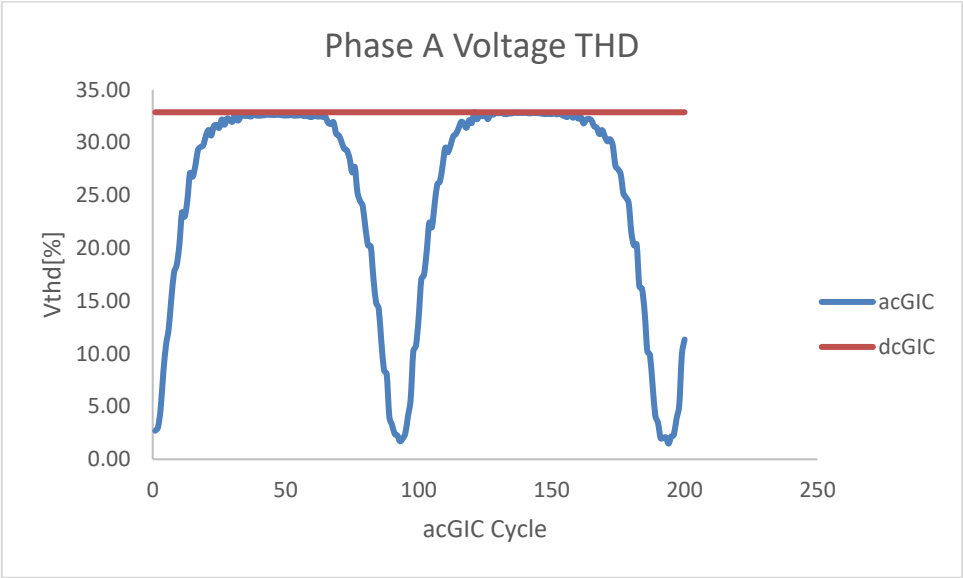

Figure 7.30: Variation of the voltage THD at minimum load throughout an acGIC cycle for a system under dcGIC and acGIC injection

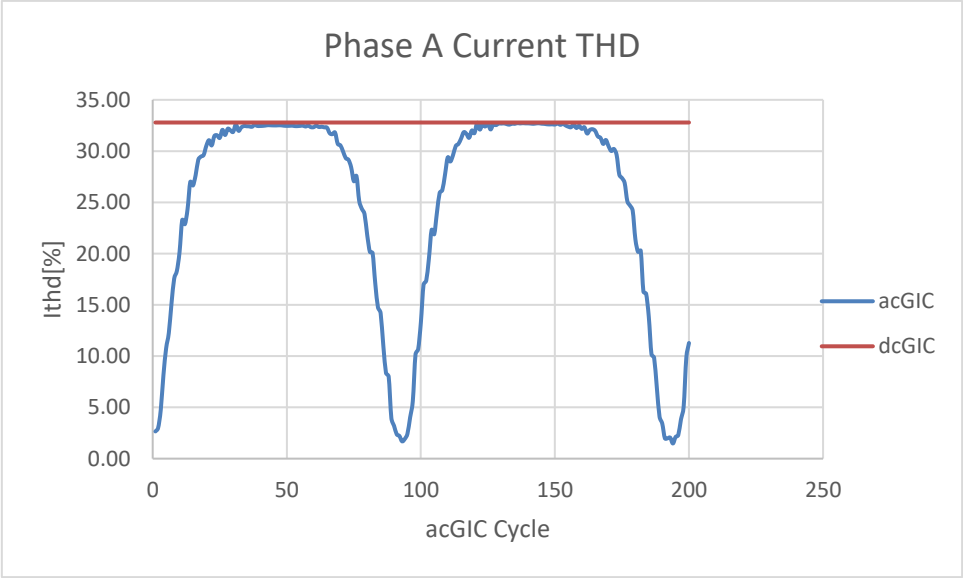

Figure 7.31: Variation of the current THD at minimum load and maximum GIC throughout an acGIC cycle for a system under dcGIC and acGIC injection

Figures 7.26 and 7.27 show that the voltage and current THD have significantly increased when the GIC increased from 1 pu to 6 pu at the same loading level. The voltage and current THD due to the acGIC injection appear to flatten out at peak before decreasing as it approaches the zero crossing. The voltage and current THD due to dcGIC increases from 10.22% to 32.87% and 10.21% to 32.79% respectively as the GIC increases.

Maximum Load, Maximum GIC(GIC=6pu)

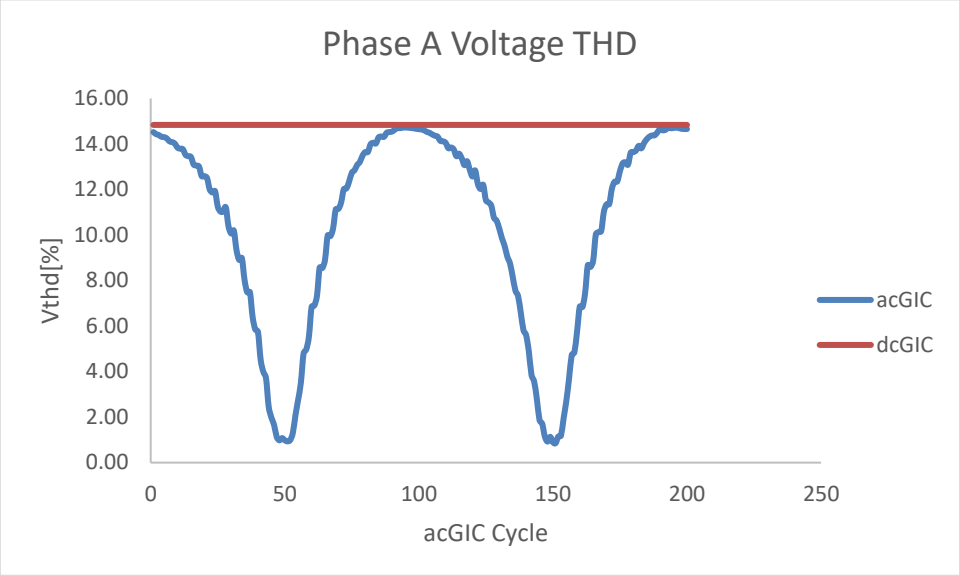

Figure 7.32: Variation of the voltage THD at maximum load and maximum GIC throughout an acGIC cycle for a system under dcGIC and acGIC injection

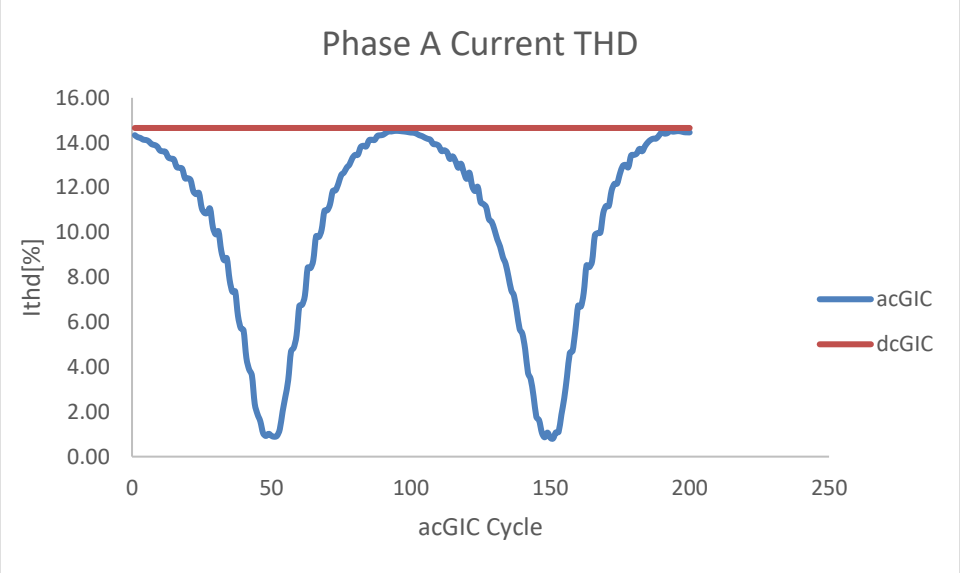

Figure 7.33: Variation of the current THD at maximum load and maximum GIC throughout an acGIC cycle for a system under dcGIC and acGIC injection

Figure 7.28 and 7.29 show variation of current and voltage THD at maximum load under dcGIC and acGIC injections. The results show that the voltage and current THD due to dcGIC increases from 3.2% to 14.84% and 3.05% to 14.66% respectively as GIC increases.

iii. ***Discussion***

The results show that an increase in GIC results in an increase in harmonics distortion in the transmission line and at the load. From literature, an increase in GIC results in an increase in the harmonics generated in the system. The Hydro-Quebec grid collapse was caused by the tripping of SVCs and relays due to increased harmonics in the system as a result of GIC flow [78]. The results also show that loading has a direct impact on the harmonic distortion. The THD and the harmonic spectra results showed that an increase in the loading significantly reduced the distortion experienced by the system. The THD is a ratio of all harmonic components to the fundamental component and the spectral analysis

showed that at heavy loads higher components become negligible. This means that the fundamental components increase relative to the higher order components and the THD value is reduced.

The differences in the system response due to acGIC and dcGIC were also observed in the results from the spectral analysis to the THD analysis at the load. The response due dcGIC was constant and with the acGIC giving a varying response with respect to the signal. The voltage and current harmonic response from dcGIC were around 0.6 % to 1% greater than the peak acGIC response in both spectral analysis and THD analysis. Given that a real GIC is not a constant current signal, the results imply that harmonic generation in a power system is also not constant, however, is dependent on the magnitude of the current at a particular instance in the Geomagnetic storm.

7.1.4 Reactive Power Analysis

From literature, it has been known that the flow of GICs increases the conventional reactive power drawn by the power system. This analysis was made at Bus 3 which is within the GIC loop. Given that the load connected at Bus 4 is a purely resistive load, there was no reactive power measurements taken and so reactive power analysis was conducted at Bus 3 to see the impact on the transformer and transmission line.

According to Overbye *et al* [19], the reactive power loss in the transformer is directly proportional to the GIC according to the following relationship:

$$Q_{Loss} = V_{pu} K I_{GIC} \tag{7.2}$$

Where, Q_{Loss} is the reactive power loss, K has units MVars/Amp and I_{GIC} is the GIC current flowing and V_{pu} is the per unit voltage. The effect at light loads and heavy loads were investigated, and the phase A results are given below.

Lightly Loaded System

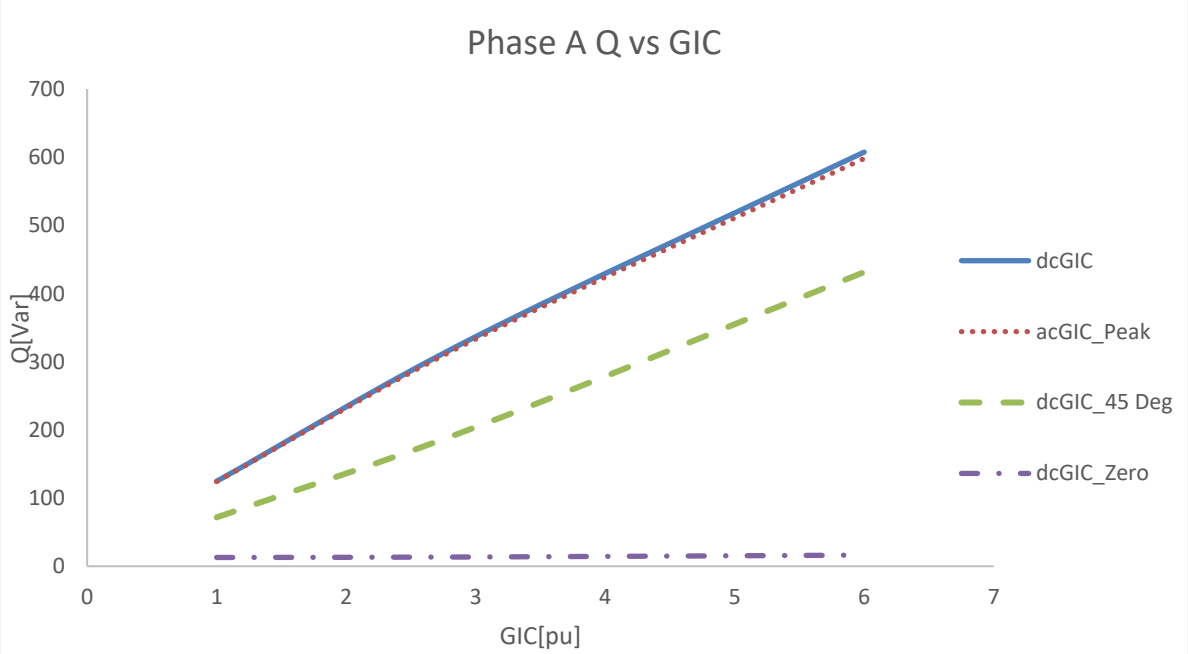

Figure 7.34: Variation of reactive power with GIC under dcGIC and acGIC injections for a lightly loaded system

Heavily Loaded System

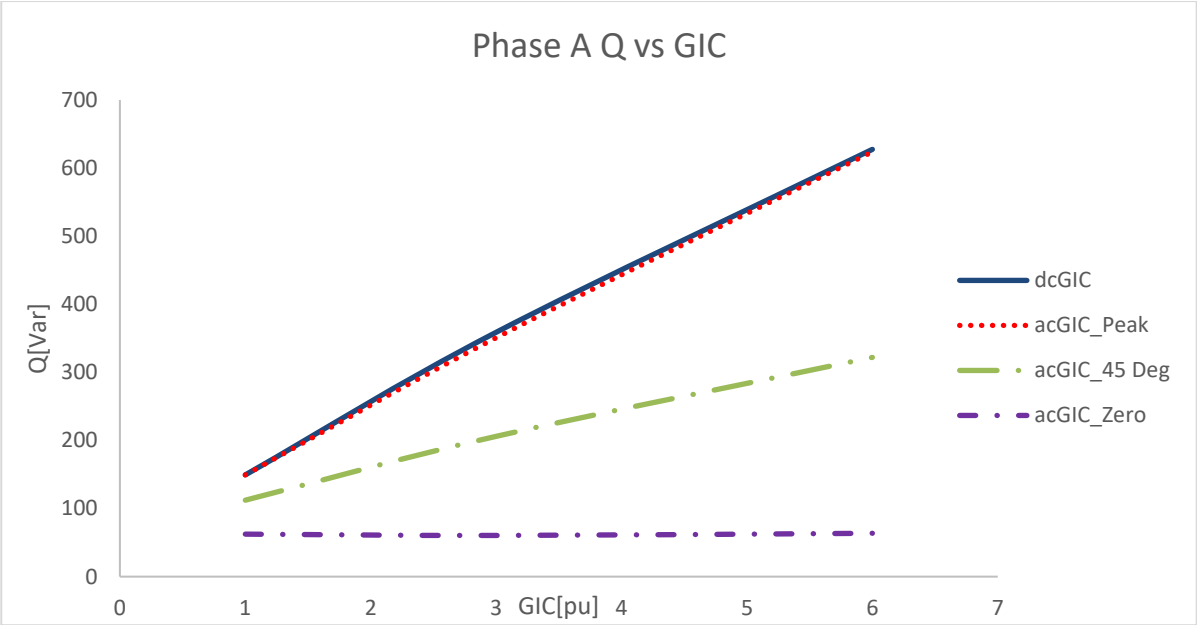

Figure 7.35: Variation of reactive power with GIC under dcGIC and acGIC injections for a heavily loaded system

The results in Figure 7.30 and Figure 7.31 show that the reactive power at bus 3 increases linearly with increasing GIC, an observation in agreement with the literature [79]. There is a small increase in the reactive power drawn as loading increases which are due to the increase in current flowing in the system. The results also show that the reactive power response of the power system, like the harmonics and voltage, also varies with acGIC. The reactive power drawn is at maximum at peak and decreases as the acGIC magnitude drops from peak to zero crossing. The dcGIC response shows a slightly higher value than the peak value which has been a consistent observation with other parameters like bus voltage and harmonics.

7.1.5 Laboratory Results Discussion

The results in the laboratory presented two different system responses to acGIC injection and dcGIC injection. From the bus voltage analysis to the reactive power analysis, the response of the system varied with respect to acGIC cycle, with the most severe effects occurring at the peak of the acGIC cycle.

The PV curve analysis showed that the increase in the flow of GICs in the system results in a reduction in the loadability of the system. This was true for both acGIC and dcGIC injections. The results showed that for PV curve analysis to be carried out effectively on a varying signal, only the maximum magnitude is needed as it will give the most severe response and will enable effective mitigation methods. It will also reduce the need to evaluate the PV curve at different points as the point that has a more severe impact on the system is the highest amplitude.

The bus voltage analysis showed that an increase in the GIC flowing in the system resulted in a decrease in the bus voltage. The power system experienced a larger voltage drop under dcGIC analysis than in acGIC analysis. Under acGIC conditions, the voltage signal varied with the acGIC signal, with more impact occurring at the peak and less at the zero-crossing. The results also revealed that there is a larger voltage

drop in a heavily loaded system than a lightly loaded system and hence a heavier loaded network had adverse effects of GICs on the voltage.

The harmonic analysis showed that an increase in the GIC flowing in the system results in an increase in the harmonic distortion in the system. This has been established in the literature and has been validated by the laboratory results. The results showed that the harmonics varied with varying acGIC flowing in the system, with the level of observed distortion decreasing as the magnitude decreased from peak to the zero-crossing. The system response due to dcGIC showed a constant response expected from a non-varying injection.

Reactive power analysis also showed that there is a linear increase in the reactive with increasing GIC flowing in the system. The increase in the reactive power was evident in both acGIC and dcGIC models and the increase is in a former linear relation. The loading had a small impact on the reactive power increase, with the GIC being the greatest contributing factor. The reactive power varied with the magnitude of the acGIC, with the highest reactive power being drawn at peak and the lowest at the zero crossing. The impact of dcGIC injection on the reactive power was slightly more than the peak of the acGIC injection.

In all the different investigations carried out in this laboratory protocol, the main difference in the power system's response to dcGIC and acGIC was that the effects of the GICs were more severe in the dcGIC model than the acGIC model. These results imply that the dcGIC injection in the laboratory presents the worst-case scenario or the "prospective GIC case [47]" compared to the ever-changing acGIC. The system response due to dcGIC is constantly at the prospective GIC case whereas under acGIC, the very-low-frequency conditions in real-time are constantly changing, never reaching the prospective GIC.

One key outcome from the laboratory analysis is that the results produced from acGIC measured at peak were comparable to the dcGIC analysis. This validated the model of the acGIC given that there was no prior existing benchmark to compare existing results with as opposed to dcGIC.

7.2 Simulation Results and Discussion

The results of simulation protocol are presented in the section 7.2.1 to 7.2.4

7.2.1 No Load Test

The no load tests were conducted on the PSCAD transformer models and were compared with the laboratory no load tests. This was to confirm that the PSCAD transformers were matched with the laboratory transformers to enable proper comparison of simulation and laboratory results.

The no load tests with the parametrized transformers were conducted to investigate the degree to which the simulation and laboratory models are the same. Table 7.1 and 7.2 shows both no load simulation and laboratory test results for the 3p3L and the 3p5L respectively.

Table 7.1: Table showing the different magnetization currents for the 3p3L obtained from both laboratory and simulation environment

	3p3L			Average
	Imag_a/A	Imag_b/A	Imag_b/A	Imag/A
Laboratory	0.3020	0.2875	0.3665	0.3189
Simulation	0.3576	0.2226	0.3596	0.3133

Table 7.2: Table showing the different magnetization currents for the 3p5L obtained from both laboratory and simulation environment

	3p5L			Average
	Imag_a/A	Imag_b/A	Imag_c/A	Imag/A
Laboratory	0.1077	0.1172	0.1165	0.1138
Simulation	0.0975	0.1323	0.1015	0.1104

The results from both the transformers show that the simulation and laboratory environments agree with each other. The slight differences in the average values for both the 3p5L and 3p3L may be due to the UMEC model being slightly different to the laboratory model despite the O.C and S.C parameters entered. These results show that the transformer and laboratory models have been successfully matched based on the preliminary tests and the entered results.

7.2.2 PV Curve Analysis

The PSCAD model in the four-bus system shown in chapter 6 and PV curve analysis with both acGIC and dcGIC was conducted on the network. For the acGIC injection analysis, snapshots of the system parameters will be taken during the simulation at peak, 45 degrees and zero crossing to plot the PV curve.

i. dcGIC Analysis

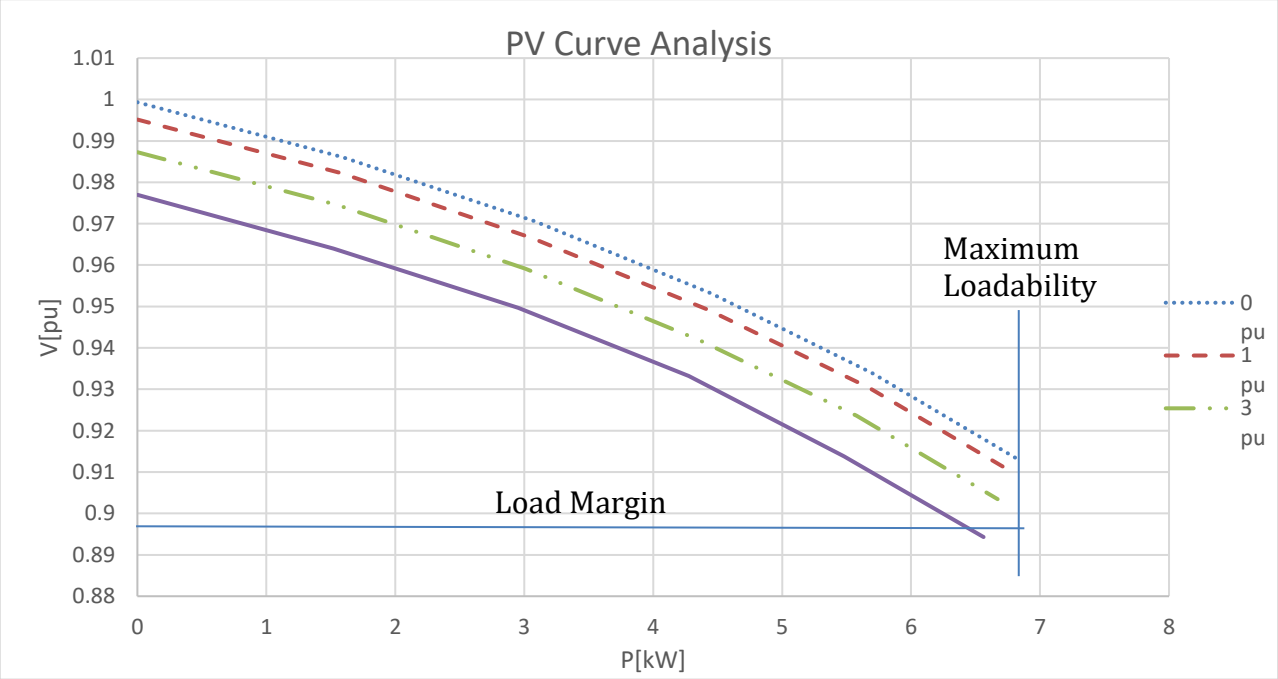

Figure 7.36: PV curve analysis of a network under dcGIC conditions

Figure 7.36 shows the PV curve analysis under dcGIC. The curve shows that as the GIC injection increases, the load margin decreases due reduced power output at the load for the same loading configuration. This implies that the loadability of the power system is decreased with increasing dcGIC flow in the power system. There is a noticeable voltage drop at no load with increasing GIC which is a result of distortion introduced by GIC which causes losses.

ii. acGIC Analysis

Peak Voltage

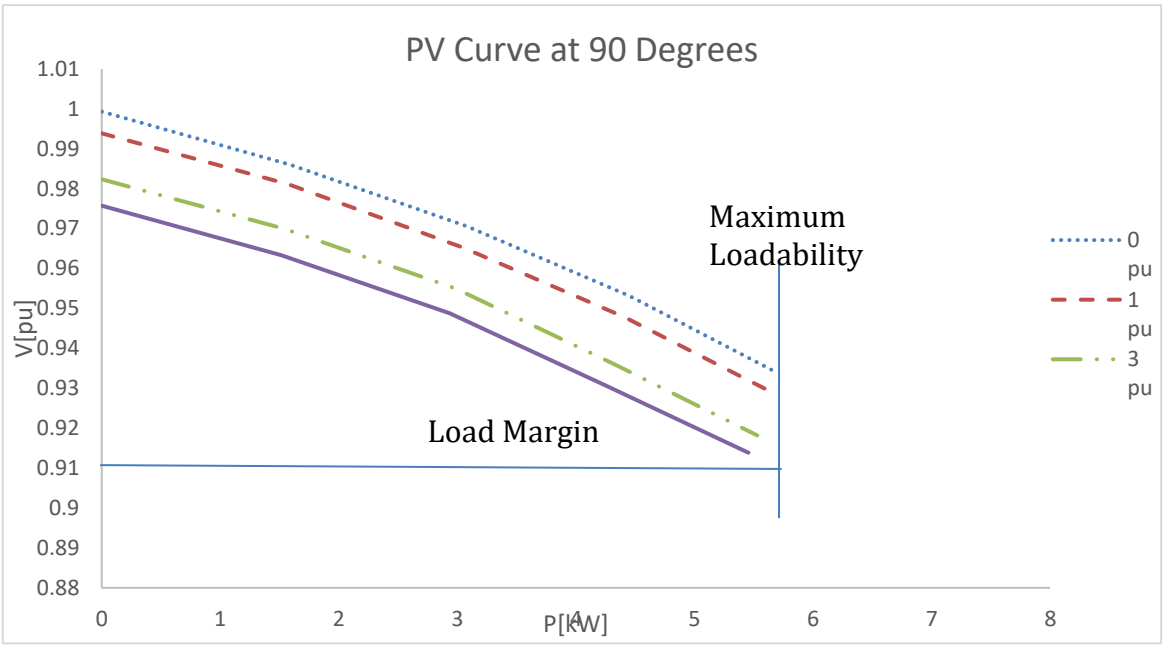

Figure 7.37: PV curve analysis conducted at the peak of the acGIC cycle

45 Degrees Crossing

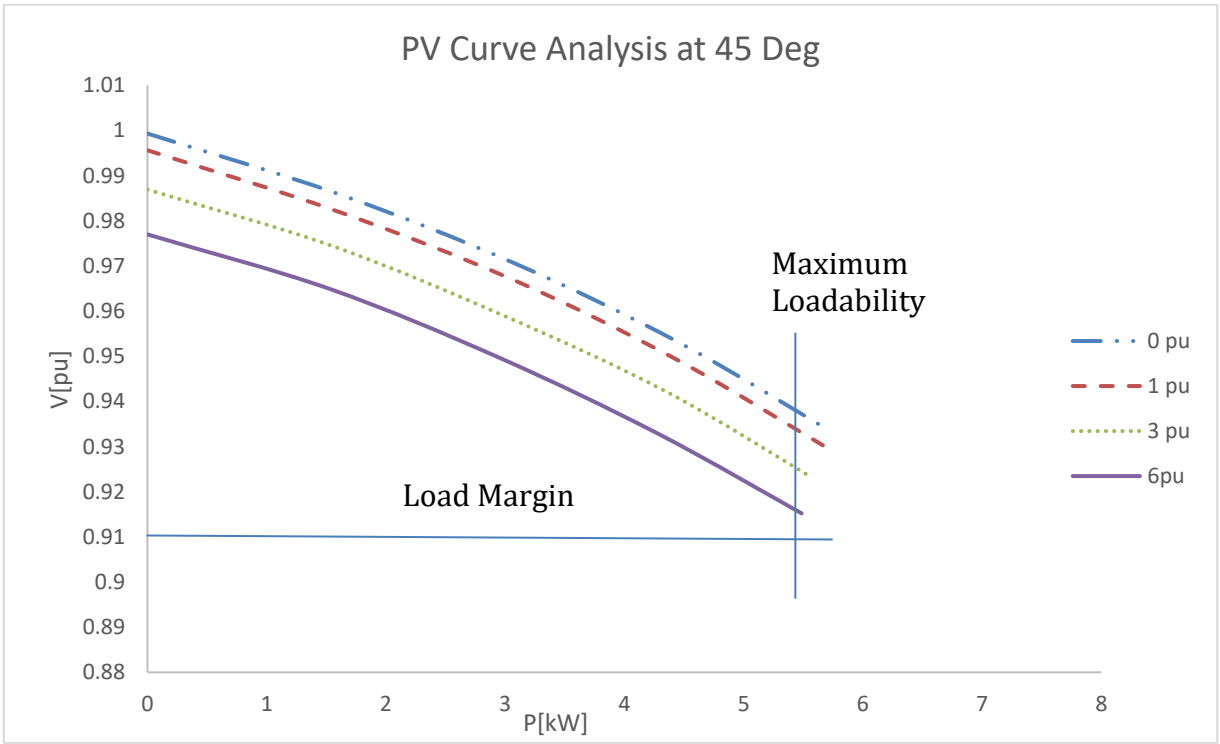

Figure 7.38: PV curve analysis of the system conducted at the 45-degree crossing of the acGIC cycle

Zero Crossing

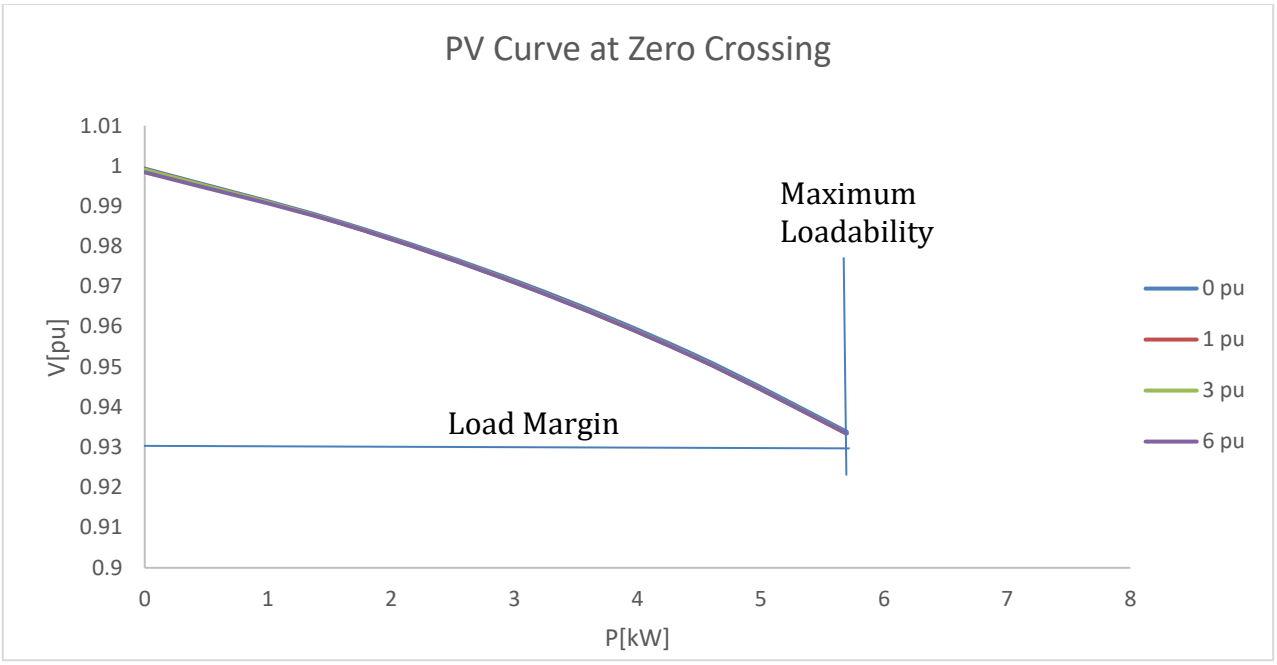

Figure 7.39: PV curve analysis conducted at zero crossing of the acGIC cycle

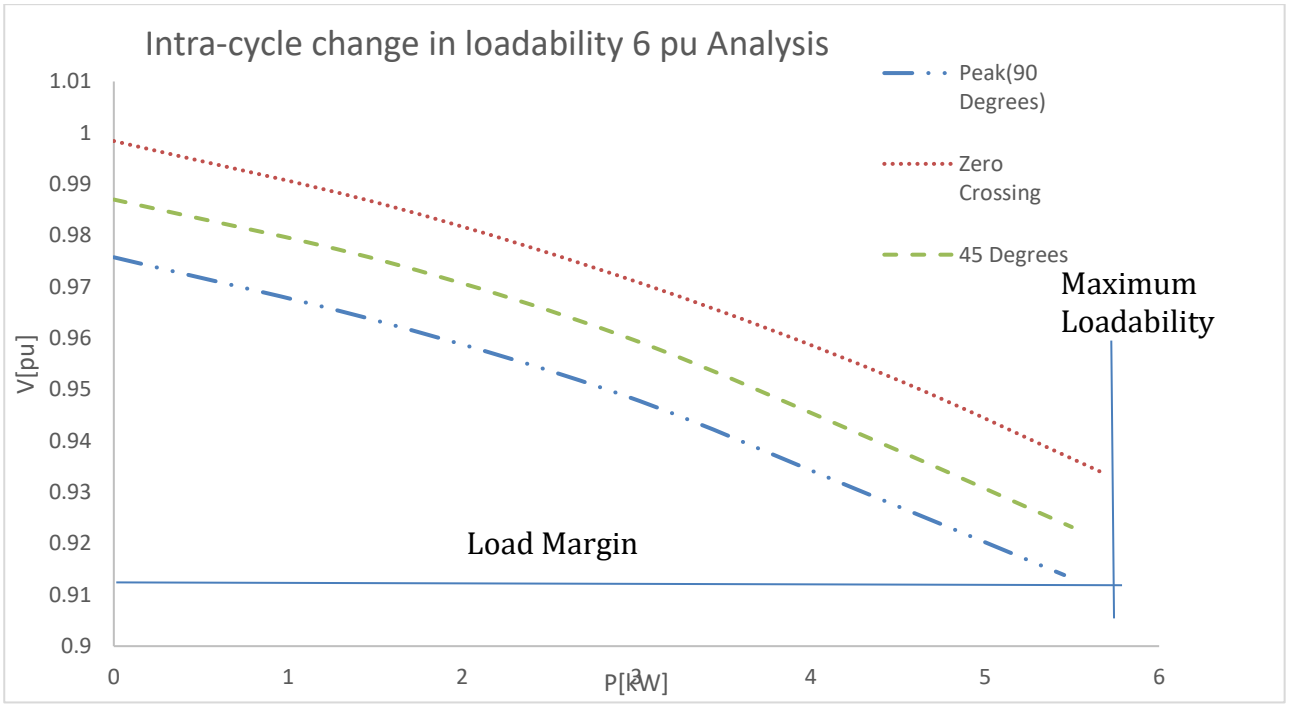

Figure 7.40: 6pu Analysis of the PV curves for acGIC

Figure 7.37 to 7.40 shows the variation of the PV curve at different points of the acGIC cycle. The results show that the impacts of the GIC flow are severe at peak of the acGIC and reduce as the acGIC moves from peak to zero crossing. The effect on the loadability on the power system decreases as themagnitude of the acGIC flowing in the system decreases throughout the cycle. At zero crossing of the acGIC cycle, the PV curves show no change because the magnitude of current being injected into the transformers is zero and the system experiences no asymmetric excitation.

7.2.3 Bus 4 Voltage Analysis

i. Minimum Load, Minimum GIC(GIC=1pu)

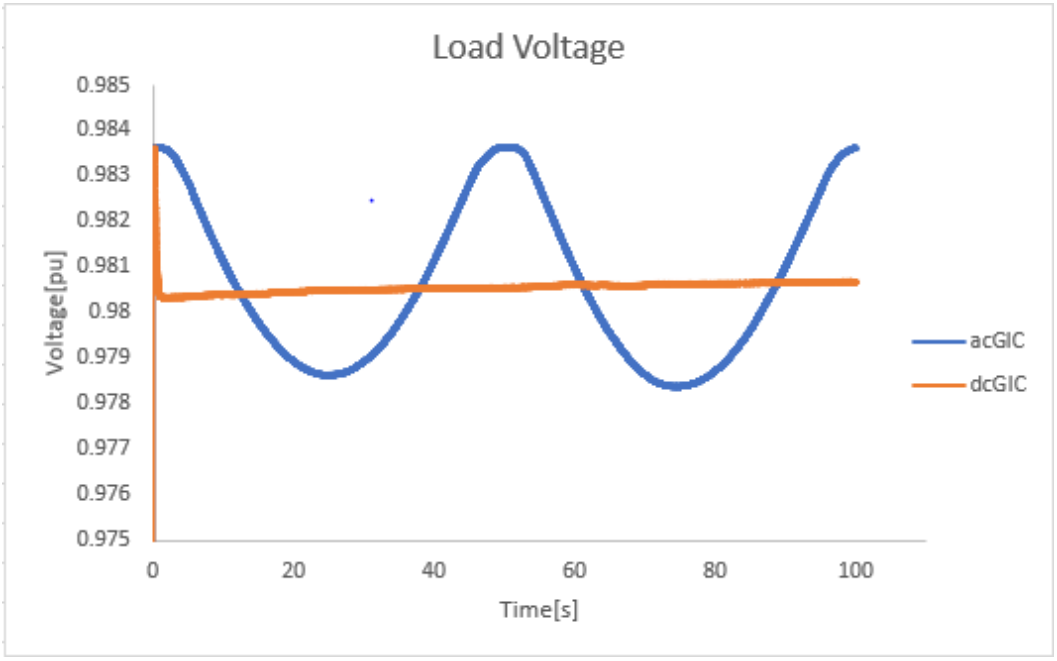

Figure 7.41: Graph showing how the load voltage varies during the 100s acGIC cycle with results obtained from acGIC and dcGIC of 1pu at light loading conditions

ii. Maximum Load, Minimum GIC(GIC=1pu)

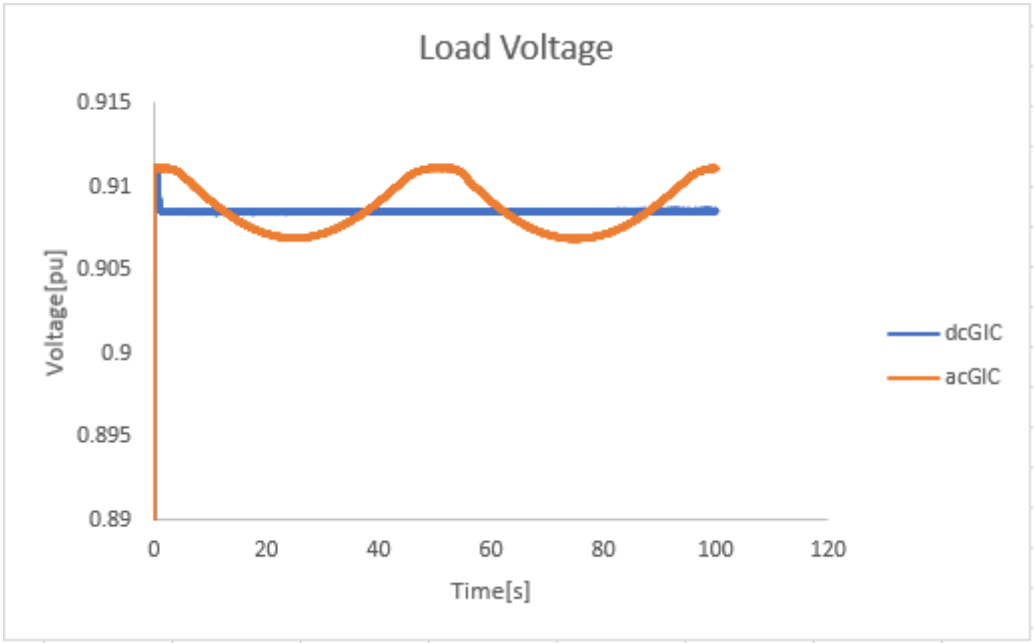

Figure 7.42: Graph showing how the load voltage varies during the 100s acGIC cycle with results obtained from acGIC and dcGIC of 1pu at heavy loading conditions

Figure 7.41 and Figure 7.42 show the results of the bus voltage variation at the load due to both acGIC and dcGIC at different loading conditions. The voltage varies with respect to the magnitude of the current flowing at the time, with dcGIC giving a constant voltage response and the acGIC giving a voltage response varying according to the current signal. The results show that at minimum load and maximum load the voltage due to acGIC reaches voltage similar to dcGIC periodically, an observation also made by [80] in a similar investigation. The acGIC appears to have a more severe impact on the system compared to the dc GIC for the two loading conditions.

iii. ***Minimum load, High GIC(GIC=6pu)***

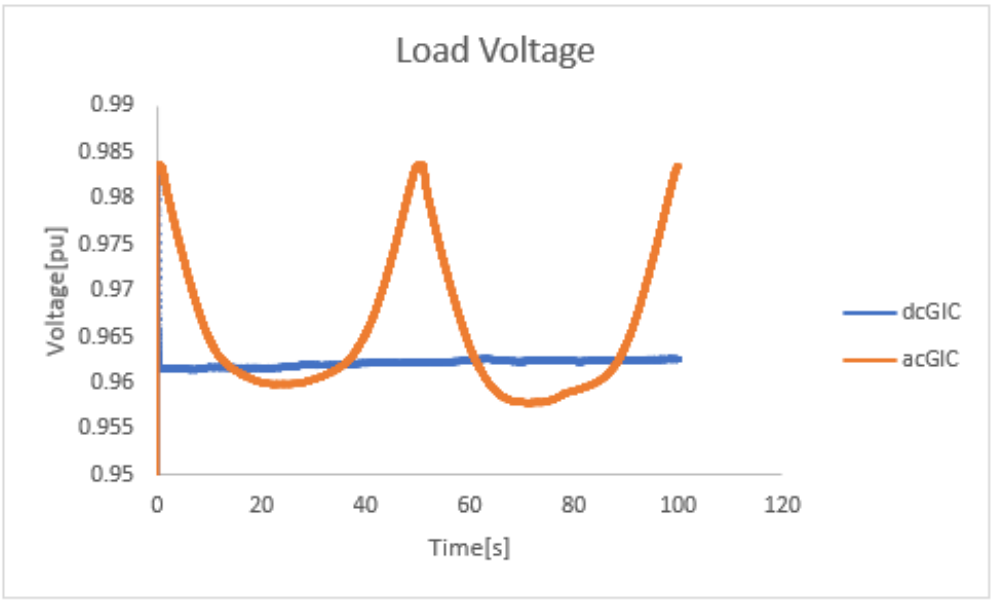

Figure 7.43: Graph showing how the load voltage varies during the 100s acGIC cycle with results obtained from acGIC and dcGIC of 6pu at light loading conditions.

iv. ***Maximum Load, High GIC(GIC=6pu)***

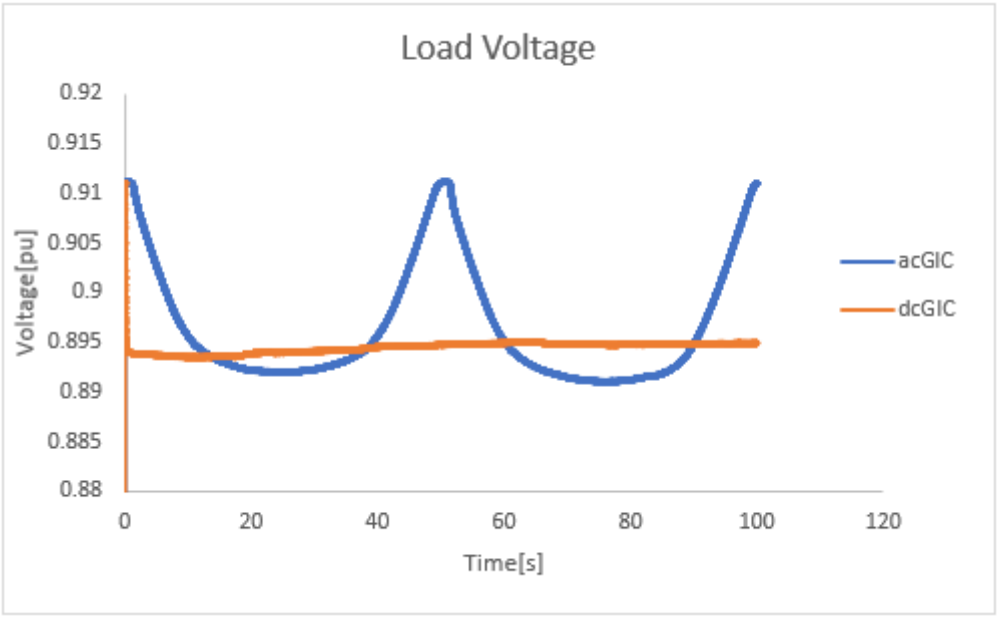

Figure 7.44: Graph showing how the load voltage varies during the 100s acGIC cycle with results obtained from acGIC and dcGIC of 6pu at light loading conditions.

Figures 7.43 and 7.44 show that in both loading conditions, the voltage decreased as the GIC increased. The acGIC injection had a more serious effect on the voltage at peak compared to the dcGIC injection. The voltage response due to acGIC in both loading conditions varies according to the magnitude of the acGIC flowing at a certain instance. Figures 7.41 to Figure 7.44 showed that the voltage drop range due acGIC was slightly more in the lightly loaded system compared to the heavily loaded systems. In all test cases, it was evident that the response of the power system voltage due to GIC was severely impacted by the acGIC injection compared to the dcGIC regardless of the load conditions.

7.2.4 *Reactive Power Analysis*

The following shows the variation of the GIC

i. *Lightly Loaded System*

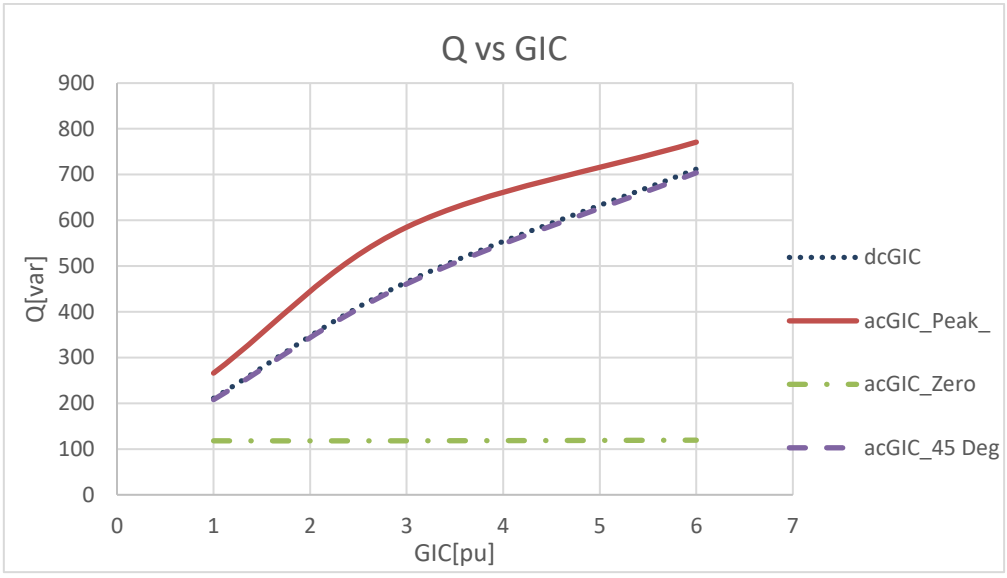

Figure 7.45: Variation of reactive power under acGIC and dcGIC injection at lightly loaded conditions

ii. *Heavily Loaded*

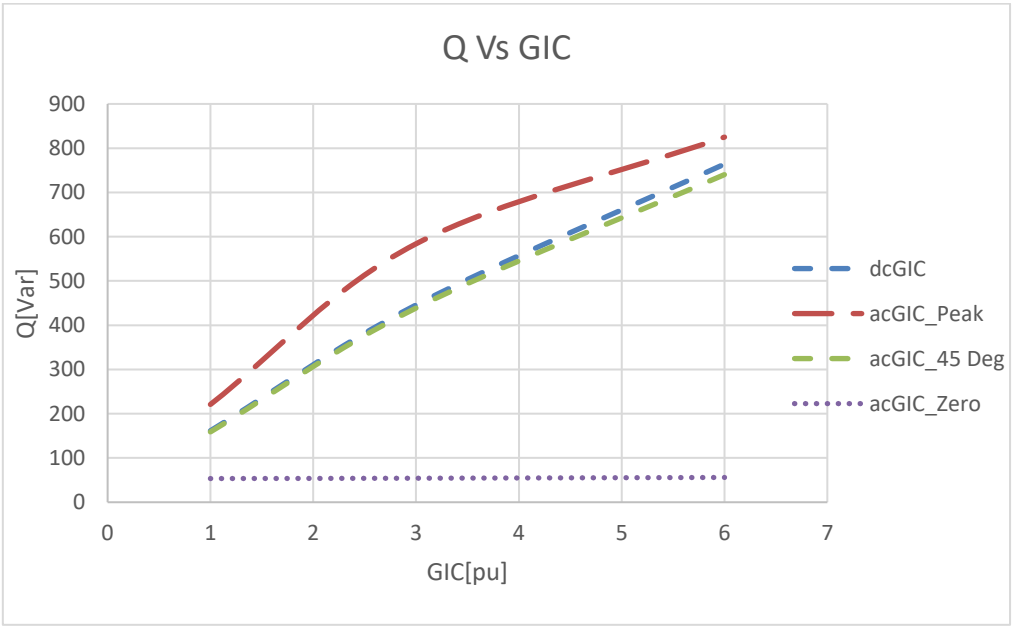

Figure 7.46: Variation of reactive power under acGIC and dcGIC injection at lightly loaded conditions

Figure 7.45 and Figure 7.46 show the reactive power variation with different GIC injections. The results show that an increase in the GIC injection increases the reactive power drawn by the transformers, as reported in literature [81]. The acGIC injection resulted had the most impact at the peak magnitude. The dcGIC injection resulted in a response similar to the 45-degree crossing of the acGIC cycle. This result was consistent in both lightly loaded and heavily systems, however, the heavily loaded system had slightly larger reactive power values than the lightly loaded system. This due to the increased current being drawn by the load increasing the reactive power losses in the system.

7.2.5 Simulation Results Discussion

The no load tests showed that the laboratory and simulation transformers had been successfully matched with very small differences in the magnetization currents. This successful parametrization is ensured that adequate comparison to draw a conclusion can be taken out.

The PV curve analysis was undertaken when the system showed that under dcGIC injection, the system loadability decreased with increasing GIC. The acGIC results also showed that the loadability decreased with increasing GIC depending on which part of the acGIC cycle the analysis was taken. The results showed the effect of GIC on the system decreased as the amplitude of the acGIC decreased from peak to zero crossing. The implication of this result showed at PV curve analysis is dependent on the magnitude of current flowing in the transformer neutrals at the instance a snapshot of the system parameters is taken regardless of the injection methodology used.

The bus voltage analysis showed that the acGIC injection had a more severe impact on the bus voltage than the dcGIC injection. The results also showed that the system lightly loaded was subject to more volt drop due to the acGIC compared to the heavily loaded system.

The reactive power analysis results showed that the acGIC injection resulted in a large value of reactive power drawn by the transformer than dcGIC. The results obtained from dcGIC analysis were almost the same in the magnitude of reactive power as the results obtained from the acGIC analysis taken at 45-degrees of the acGIC cycle.

The results show that the effects on the power system due to the use of acGIC as a GIC representative are more severe compared to the results using dcGIC. This was seen in the PV analysis, bus voltage analysis and reactive power analysis. The acGIC results in a response that varies in real with the magnitude of current flowing in the transformer neutral, whereas the dcGIC give a constant response.

7.3 Laboratory and Simulation Results Discussion

The results obtained from the laboratory and simulation protocols provided some important insight into to the GIC phenomena. To enable proper comparison in both the simulation and laboratory protocols, the transformers had to be matched using data obtained from O.C and S.C tests conducted in the laboratory. As reported earlier in section 7.2.1, the magnetization currents for the transformers in both simulation and laboratory environments agreed indicating that the transformers had been successfully matched.

The PV curve analysis from both the simulation and laboratory showed a similar response. The analysis due to both dcGIC and acGIC in both laboratory and simulation showed that an increase in GIC flow resulted in the decrease in loadability. The loadability decrease drives the network into voltage instability. In acGIC analysis, both laboratory and simulation results showed a varying loadability response. The difference however is that the real power output at the load was between 21%-23% higher in the simulation than the laboratory for all the GIC levels. This was due to the increased losses experienced in the laboratory compared to the simulation. This increased loss is due to factors like voltage drops along connecting wires used in the laboratory and the laboratory transformer response to asymmetric excitation. These losses in the laboratory resulted in a lower voltage output and thereby power output according to $P=\frac{V^2}{R}$. This difference in output was also observed in the acGIC analysis.

The load voltage simulation and laboratory environments showed similar response to both acGIC and dcGIC injection. The voltage due to acGIC in both laboratory and simulation varied with varying GIC, with the minimum voltage occurring at peak, and maximum voltage occurring at zero crossing. The dcGIC remained constant throughout the 100s period as expected from a constant GIC model. The reactive power analysis also showed a similar response in both simulation and laboratory environments. The reactive power varied linearly with GIC in both acGIC and dcGIC. In the acGIC analysis, the reactive power was varying from peak to zero crossing, with the peak being the linear graph with the highest gradient and the zero crossing being low gradient graph.

However, in the simulation analysis the acGIC results showed a more severe response in the bus 4 voltage and reactive power analysis compared to dcGIC. This is different from the laboratory results which showed that the dc injection is a worst-case scenario and has more severe impact on the network. This difference can be attributed to the response to asymmetric excitation of the UMEC transformer model on PSCAD. This is despite sufficient input of parameters in the models to match the transformer models in the simulation environment. An explanation to this phenomena was conducted by Zirka *et al.* [82] in which he found inaccuracies in the UMEC model. The analysis found that for transformers with concentric windings, any design the model of separate leakage inductances (which the UMEC model) is incorrect and provides inaccurate predictions when the core approaches saturation. Given that core saturation is a crucial part of this analysis, this finding is very important because it explains why the models show almost similar O.C results to laboratory analysis, yet during saturation due to GIC inaccurate results differing from the laboratory results are realised. The implication of this results is that more investigation into UMEC models needs to be done to further enhance accurate simulation and laboratory comparison and analysis.

8. Conclusions

The research carried out in this dissertation aimed to investigate the need for a non-zero frequency (Hertz) current representation of GIC to better understand the real time effects of GICs on the voltage stability of power systems. The study presented a novel design of an acGIC injection module which was used as GIC representation and was compared with the conventional dcGIC representation of GIC. The protocol involved the design of transmission line, load rig and the acGIC injection circuit. Magnetization characteristics were used to characterize the transformers and used to select adequate dcGIC and acGIC injection levels. This chapter presents discussions of the results given in chapter 6 and chapter 7. The research questions are then answered and lastly the validity of the hypothesis is presented.

8.1 Magnetization Characteristics

The magnetization characteristic of the transformer, obtained through no-load tests, revealed that the transformers reach saturation at voltages below their nameplate rating. These results implied that the transformer had to be de-rated before the full voltage stability protocol tests commenced. This de-rating was done to ensure any saturation experienced by the transformer was only to asymmetric excitation. The magnetization curves obtained were then evaluated to find a knee point voltage which would be the operating voltage of the power system. The IEC 61689-2-2012 knee point (even though it is originally intended for current transformers) was chosen to, conservatively, distinguish distortion caused by GIC from any possible distortion that would have otherwise been caused by an ac excitation at a higher knee point.

8.2 PV Curve Analysis

PV curve analysis carried out in the laboratory showed that the corroboration with literature that GICs reduce the loadability of the system. The most significant finding this study showed was that the PV curve analysis in real GIC analysis only must be performed at the highest recorded amplitude in order to give the maximum effect of GIC on loadability. Due to the varying nature of real GIC, only at peak are the effects on the system more pronounced and it makes more sense to evaluate the PV curve at peak, hence reducing unnecessary computation. Snapshots of the system response at any point other than the peak in the GIC storm will not give a true picture of the vulnerability of the load bus during a GMD.

8.3 Bus 4 Voltage Analysis

The Bus 4 voltage analysis showed variation of voltage with different GIC injection models at different loads. The results showed that their voltage response fluctuates with acGIC as opposed to a constant response shown in dcGIC model. Voltage fluctuations due to GIC which occurred in Hydro Quebec in 1989 has been reported in literature [83],[84] and the results of the acGIC results showed fluctuating voltage response. The acGIC injection, though being a first approximation of real GIC, showed a more representative voltage response compared to the dcGIC. The acGIC results presented a more accurate picture of the various voltage change experienced during a GMD and further revealed that the dcGIC case is a worst case scenario, constantly at prospective GIC [47].

8.4 Harmonics Analysis

The results obtained from harmonic analysis showed that an increase in the GIC regardless the nature of GIC injected resulted in an increase in the distortion measured in the system. The acGIC harmonic analysis showed that the THD fluctuates according to the acGIC signal, with peak injection yielding a higher THD value. The results also highlighted the significance of loading on the harmonic distortion in

the system due to both acGIC and dcGIC. The heavily loaded system experienced a lower distortion compared to the lightly loaded system because of the dominant resistive loading component of current. Even though these results agreed with literature analysis only done using dcGIC, the acGIC results showed consistent results with literature when measurements were taken at peak.

8.5 Reactive Power Analysis

The reactive power analysis showed that regardless of what injection the system is subjected to, there reactive power drawn by the transformers increases with increasing GIC. The GIC injection showed that the reactive power varied with time and was fluctuating according to the acGIC cycle. These results seem to agree with the certain observations made in literature about observed reactive power swings and fluctuations [3],[39]. The dcGIC injection results in a real a linear relationship between reactive and with increasing GIC (as long as the power supply can continue to supply vars [85]), whereas the acGIC also showed a linear relationship however only for peak and zero-crossing points.

8.6 Load Modelling Analysis

The load used in this research was a resistive load to model unity power factor conditions. In practice however, loads are more complex and dynamic, and this had been taken into account to fully validate the protocol. The load models as shown in literature are constant current, constant power and constant impedance. The load model used in this experiment was a constant impedance model with an impedance factor (or power factor) of 1. The role of the resistive load was to capture the maximum effect of GICs on the power system voltage stability as described in section 4.3. However, to further validate the observed results, tests were run on different power factors in PSCAD on more realistic loads and the results were compared with unity power factor conditions. The tests were conducted on a lightly loaded system and a heavily loaded system at 1pu and 6pu dcGIC. The results showed that even though there were slight deviations in voltage-which were expected given the decreased power factor-the system response is virtually the same with respect to GIC flow in the system. A resistive load was enough to draw the conclusions drawn in this dissertation. The results of the load voltages are shown in Appendix 10.4.

8.7 Answers to Research Question

A summary of answers to the research questions formulated in Chapter 1 are presented below:

a) How can GIC be emulated in the laboratory?

In literature, dc has been used as a representative of GIC in laboratory studies. The dc was either supplied through a battery or a dc power supply. In the instance where a battery is used to model GIC in the laboratory, the current was controlled through resistors connected in series with the battery.

b) What is a typical frequency for GIC and how can it have emulated in the laboratory?

In the initial stages of the investigation, it was thought that GIC is a single frequency and hence only one frequency signal is adequate. However, after thorough research through literature, it was discovered that a real GIC is a multi-frequency, multi amplitude signal, with high power components below 50 Hz. Therefore, as a first approximation of the real GIC signal, a 10 mHz ac signal was designed in the laboratory to model a representative emulation of GIC.

c) How can the power systems' real time response to acGIC be assessed?

Literature did not provide a methodology on the assessment of power systems response to acGIC in the laboratory. In this study, the assessment of power system response with acGIC was done by logging measurements of the power system parameters in real time using Yokogawa Power Analyzer. This was done at different injections levels of acGIC injections. From the results three points of interest were noted on along the acGIC cycle, which are:

- Peak
- 45 degrees
- Zero crossing

These points were chosen to obtain parameters at crucial points along the acGIC curve for analysis. These parameters measured at these points revealed how the system responds as the magnitude of the acGIC injection varies from zero crossing to 45 degrees to peak current.

d) How is the voltage stability of the power system impacted as a result of dcGIC compared to acGIC

The voltage stability assessment in this study was accomplished using PV curve analysis. It had been established from the literature that through PV curve analysis the flow of GICs reduces the loadablity of the system. However, this had been limited to dcGIC analysis. This study showed that the load margin varies in real-time with acGIC depending on the magnitude of the current flowing. Under acGIC analysis, the tendency of the power system to reach the point of voltage instability varies with varying acGIC magnitude. At peak acGIC, the power system has a higher tendency of reaching the point of instability as seen by the decrease in the load margin. This effect on the load margin decreases as the current magnitude reduces and at zero crossing, the system is virtually under no GIC influence.

This is different from dcGIC in that with dcGIC, a worst-case scenario of the voltage stability assessment is presented. Given that the current injection is a constant, there is no variation in the loadability of the system and by extension the tendency of the load bus to experience voltage instability. Therefore, given that real GIC is a multi-frequency, multi amplitude signal acGIC gives a more realistic picture of how the system behaves due to real GIC through the variations and fluctuations in systems, particularly, the voltage and real power at the load.

8.8 Validity of the Hypothesis

In chapter 1, an introduction to this study presented along with the background and objectives led to the formulation of the following hypothesis:

"**The design and implementation of a laboratory protocol to represent GIC as a non-zero Hz current can be used to better understand the real-time effects of GICs on the voltage stability of power system**"

The results presented in chapter 7 along with the discussions and conclusions which improves the understanding of real-time effects of GICs on voltage stability prove that the hypothesis is valid. This research lays the foundation for a more representative emulation of GIC in the laboratory and simulation domain to further improve the understanding of GIC effects on the voltage stability of power systems.

9. List of References

[1] T. S. Molinski, “Why utilities respect geomagnetically induced currents,” 2002. [Online]. Available: www.elsevier.com/locate/jastp.

[2] S. A. Mousavi, G. Engdahl, and E. Agheb, “Investigation of GIC effects on core losses in single phase power transformers,” *Arch. Electr. Eng.*, vol. 60, no. 1, pp. 35–47, 2011, doi: 10.2478/v10171-011-0004-9.

[3] S. Mkhonta, T. T. Murwira, D. T. O. Oyedokun, K. A. Folly and C. T. Gaunt, "Investigation of Transformer Reactive Power and Temperature Increases Under DC," 2018 IEEE PES/IAS PowerAfrica, 2018, pp. 595-600, doi: 10.1109/PowerAfrica.2018.8520998

[4] S. Lu and Y. Liu, “FEM analysis of DC saturation to assess transformer susceptibility to geomagnetically induced currents,” *IEEE Trans. Power Deliv.*, vol. 8, no. 3, pp. 1367–1376, 1993, doi: 10.1109/61.252663.

[5] O. A. and A. P. Risto Pirjola, Ari Viljanen, “Power And Pipelines (Ground Systems),” 1990.

[6] L. Bolduc, “GIC observations and studies in the Hydro-Québec power system,” *J. Atmos. Solar-Terrestrial Phys.*, vol. 64, no. 16, pp. 1793–1802, Nov. 2002, doi: 10.1016/S1364-6826(02)00128-1.

[7] V. D. Kappenman, J. G., Albertson, “Bracing for the geomagnetic storms,” *IEEE Spectr.*, p. 368, 1990.

[8] L. G. Mănescu and D. Ruşinaru, “Loss based performance index for the reactive power control,” *Proc. Int. Conf. Optim. Electr. Electron. Equipment, OPTIM*, pp. 307–312, 2012, doi: 10.1109/OPTIM.2012.6231932.

[9] J. Yao, M. Liu, C. Li, and Q. Li, “Harmonics and reactive power of power transformers with DC bias,” *Asia-Pacific Power Energy Eng. Conf. APPEEC*, pp. 10–13, 2010, doi: 10.1109/APPEEC.2010.5449369.

[10] M. K. Jukan, A. Jukan, and A. Toki, “Identification and Assessment of Key Risks and Power Quality Issues in Liberalized Electricity Markets in Europe,” June, 2011.

[11] A. F. M. Nor, M. Sulaiman, A. F. A. Kadir, and R. Omar, “Classifications of voltage stability margin (VSM) and load power margin (LPM) using probabilistic neural network (PNN),” *ARPN J. Eng. Appl. Sci.*, vol. 12, no. 19, pp. 5591–5596, 2017.

[12] S. B. Bhaladhare, A. S. Telang, and P. P. Bedekar, “P-V , Q-V Curve – A Novel Approach for Voltage Stability Analysis,” *Natl. Conf. Innov. Paradig. Eng. Technol.*, pp. 31–35, 2013.

[13] P. Sauer, “Reactive power and voltage control issues in electric power systems,” *... Math. Restructured Electr. Power Syst.*, vol. Chapter 2, pp. 11–24, 2005, doi: 10.1007/0-387-23471-3_2.

[14] M. Wu and P. Rastgoufard, "The application of reactive power control equipment in power system stability and security performance enhancement," IEEE Power Engineering Society General Meeting, 2004., 2004, pp. 2114-2119 Vol.2, doi: 10.1109/PES.2004.1373256

[15] P. R. Price, “Geomagneticaily Induced Current Effects on Transformers,” *IEEE Power Eng. Rev.*, vol. 22, no. 6, p. 62, 2002, doi: 10.1109/MPER.2002.4312311.

[16] L. D. Borrill, H. K. Chisepo, and C. T. Gaunt, “Importance of core joints in GIC/dc studies with scaled

down laboratory transformers," *Int. J. Electr. Power Energy Syst.*, vol. 120, no. January, p. 105974, 2020, doi: 10.1016/j.ijepes.2020.105974.

[17] H. K. Chisepo, C. T. Gaunt, L. D. Borrill, and B. C. Za, "Measurement and FEM analysis of DC/GIC effects on transformer magnetization parameters," 2019.

[18] S. Tigere, L. Phaphathisa, K. A. Folly, D. T. O. Oyedokun and C. T. Gaunt, "Power System Voltage Stability in the Presence of GIC-Like Currents," 2018 IEEE PES/IAS PowerAfrica, 2018, pp. 567-572, doi: 10.1109/PowerAfrica.2018.8521066

[19] T. J. Overbye, K. S. Shetye, Y. Z. Hughes, and J. D. Weber, "Preliminary consideration of voltage stability impacts of geomagnetically induced currents," *IEEE Power Energy Soc. Gen. Meet.*, no. March, 2013, doi: 10.1109/PESMG.2013.6673068.

[20] D. Oyedokun, M. Heyns, P. Cilliers, and C. T. Gaunt, "Frequency components of geomagnetically induced currents for power system modelling," *2020 Int. SAUPEC/RobMech/PRASA Conf. SAUPEC/RobMech/PRASA2020*,2020,doi:10.1109/SAUPEC/RobMech/PRASA48453.2020.9041021.

[21] D. H. Boteler, "Assessment of geomagnetic hazard to power systems in Canada," *Nat. Hazards*, vol. 23, no. 2–3, pp. 101–120, 2001, doi: 10.1023/A:1011194414259.

[22] C. M. Ngwira and A. A. Pulkkinen, "An Overview of Science Challenges Pertaining to Our Understanding of Extreme Geomagnetically Induced Currents," *Extrem. Events Geosp.*, pp. 187–208, 2018, doi: 10.1016/B978-0-12-812700-1.00008-X.

[23] R. Caraballo, "Geomagnetically induced currents in Uruguay: Sensitivity to modelling parameters," *Adv. Sp. Res.*, vol. 58, no. 10, pp. 2067–2075, 2016, doi: 10.1016/j.asr.2016.03.006.

[24] M. Heindl *et al.*, "Investigation Of GIC Related Effects On Power Dc- Load Source TUT," 2011.

[25] R. Pirjola, "Effects of space weather on high-latitude ground systems," *Adv. Sp. Res.*, vol. 36, no. 12, pp. 2231–2240, 2005, doi: 10.1016/j.asr.2003.04.074.

[26] C. T. Gaunt and G. Coetzee, "Transformer failures in regions incorrectly considered to have low GIC-risk," *2007 IEEE Lausanne POWERTECH, Proc.*, pp. 807–812, 2007, doi: 10.1109/PCT.2007.4538419.

[27] X. Qian, H. Tian, Y. Yin, Y. Li, M. Liu, and Z. Jiang, "Geomagnetic Storms' Influence on Intercity Railway Track Circuit," *Urban Rail Transit*, vol. 2, no. 2, pp. 85–91, 2016, doi: 10.1007/s40864-016-0040-2.

[28] Z. M. K. Abda, N. F. Ab Aziz, Mohd Zainal Abidin Ab Kadir, and Z. A. Rhazali, "A review of geomagnetically induced current effects on electrical power system: Principles and theory," *IEEE Access*, vol. 8, November, pp. 200237–200258, 2020, doi: 10.1109/ACCESS.2020.3034347.

[29] L. Bolduc, "GIC observations and studies in the Hydro-Québec power system," *J. Atmos. Solar-Terrestrial Phys.*, vol. 64, no. 16, pp. 1793–1802, 2002, doi: 10.1016/S1364-6826(02)00128-1.

[30] A. Pulkkinen, S. Lindahl, A. Viljanen, and R. Pirjola, "Geomagnetic storm of 29–31 October 2003: Geomagnetically induced currents and their relation to problems in the Swedish high‐voltage power transmission system," 2005, doi: 10.1029/2004SW000123.

[31] S. A. Mousavi, C. Carrander, and G. Engdahl, "Comprehensive Study on Magnetization Current Harmonics of Power Transformers due to GICs," 2013.

[32] J. Kappenman, S. F. Ave, and E. Suite, "Geomagnetic Storms and Their Impacts on the U.S. Power

Grid," no. 805, p. 197, 2010.

[33] A. A. Hussein and M. H. Ali, "Mitigation of adverse effects of gics on transformers using look-up table controlled ground resistance," *Proc. IEEE Power Eng. Soc. Transm. Distrib. Conf.*, vol. 2016-July, 2016, doi: 10.1109/TDC.2016.7519935.

[34] J. G. Kappenman Member IEEE Minnesota Power, L. Co Duluth, M. V D Albertson Senior Member IEEE, and N. Mohan Member IEEE, "Current Transformer And Relay Performance In The Presence Of Geomagnetically-Induced Currents," 1981.

[35] R. Girgis and K. Vedante, "Effects of GIC on power transformers and power systems," *Proc. IEEE Power Eng. Soc. Transm. Distrib. Conf.*, pp. 1–8, 2012, doi: 10.1109/TDC.2012.6281595.

[36] M. Lahtinen and J. Elovaara, "GIC occurrences and GIC test for 400 kV system transformer," *IEEE Trans. Power Deliv.*, vol. 17, no. 2, pp. 555–561, 2002, doi: 10.1109/61.997938.

[37] A. Rezaei-Zare, L. Marti, A. Narang, and A. Yan, "Analysis of three-phase transformer response due to GIC using an advanced duality-based model," *IEEE Trans. Power Deliv.*, vol. 31, no. 5, pp. 2342–2350, 2016, doi: 10.1109/TPWRD.2015.2505499.

[38] "IEEE Transactions on Power Delivery, Vol. 9, No. 2, April 1994," vol. 9, no. 2, 1994.

[39] J. Koen and T. Gaunt, "Geomagnetically induced currents in the Southern African electricity transmission network," 2003 IEEE Bologna Power Tech Conference Proceedings,, 2003, pp. 7 pp. Vol.1-, doi: 10.1109/PTC.2003.1304165.

[40] M. A. Clilverd *et al.*, "Geomagnetically Induced Currents and Harmonic Distortion: High Time Resolution Case Studies," *Sp. Weather*, vol. 18, no. 10, 2020, doi: 10.1029/2020SW002594.

[41] "NERC_1989-Quebec-Disturbance_Report.pdf."

[42] L. Gérin-Lajoie, S. Guillon, J. Mahseredjian, and O. Saad, "Impact of transformer saturation from GIC on power system voltage regulation," *IEEE Int. Conf. Power Syst. Transients*, May 2014, 2013.

[43] L. Kang, B. He, P. Yang, and X. Dong, "Analysis on the Impact of Geomagnetic Storm on Reactive Power and Voltage in Extrahigh Voltage Power Grid," *E3S Web Conf.*, vol. 118, pp. 4–7, 2019, doi: 10.1051/e3sconf/201911802049.

[44] K. S. Shetye and T. J. Overbye, "Parametric steady-state voltage stability assessment of power systems using benchmark scenarios of geomagnetic disturbances," *2015 IEEE Power Energy Conf. Illinois, PECI 2015*, 2015, doi: 10.1109/PECI.2015.7064886.

[45] H. Chisepo, "The Response of Transformers to Geomagnetically Induced-like Currents," 2014.

[46] A. Rezaei-Zare, "Behavior of single-phase transformers under geomagnetically induced current conditions," *IEEE Trans. Power Deliv.*, vol. 29, no. 2, pp. 916–925, 2014, doi: 10.1109/TPWRD.2013.2281516.

[47] D. T. O. Oyedokun, "Geomagnetically Induced Currents (GIC) in Large Power Systems Including Transformer Time Response," 2015.

[48] M. Chakravorty and S. Patra, "Voltage stability analysis using conventional methods," *Int. Conf. Signal Process. Commun. Power Embed. Syst. SCOPES 2016 - Proc.*, pp. 496–501, 2017, doi: 10.1109/SCOPES.2016.7955879.

[49] N. Hatziargyriou *et al.*, "Definition and Classification of Power System Stability - Revisited & Extended," *IEEE Trans. Power Syst.*, vol. 36, no. 4, pp. 3271–3281, 2021, doi: 10.1109/TPWRS.2020.3041774.

[50] S. Kundur, Prabha, Paserba , John, Vitet, “Overview on Definition and Classification of Power System Stability On Beharfof IEEE/ClGRE Joint Task Force on Stahilia Terms and Definitions,” pp. 1–4, 2003.

[51] A. Singhal and V. Ajjarapu, “Long-term voltage stability assessment of an integrated transmission distribution system,” *2017 North Am. Power Symp. NAPS 2017*, 2017, doi: 10.1109/NAPS.2017.8107402.

[52] W. Freitas, J. C. M. Vieira, L. C. P. Da Silva, C. M. Affonso, and A. Morelato, “Long-term voltage stability of distribution systems with induction generators,” *2005 IEEE Power Eng. Soc. Gen. Meet.*, vol. 3, no. 1, pp. 2910–2913, 2005, doi: 10.1109/pes.2005.1489419.

[53] E. Munkhchuluun, L. Meegahapola, and A. Vahidnia, “Long-term voltage stability with large-scale solar-photovoltaic (PV) generation,” *Int. J. Electr. Power Energy Syst.*, vol. 117, no. November 2019, p. 105663, 2020, doi: 10.1016/j.ijepes.2019.105663.

[54] M. J. Hossain, H. R. Pota, and V. Ugrinovskii, *Short and Long-Term Dynamic Voltage Instability*, vol. 41, no. 2. IFAC, 2008.

[55] N. Hosseinzadeh, A. Aziz, A. Mahmud, A. Gargoom, and M. Rabbani, “Voltage stability of power systems with renewable-energy inverter-based generators: A review,” *Electron.*, vol. 10, no. 2, pp. 1–27, 2021, doi: 10.3390/electronics10020115.

[56] S. S. Refaat, H. Abu-Rub, A. P. Sanfilippo, and A. Mohamed, “Impact of grid-tied large-scale photovoltaic system on dynamic voltage stability of electric power grids,” *IET Renew. Power Gener.*, vol. 12, no. 2, pp. 157–164, 2018, doi: 10.1049/iet-rpg.2017.0219.

[57] N. Nikpour, “Dynamic And Static Voltage Stability Analysis Of Distribution Systems In The Presence Of Distributed Generation,” 2016.

[58] I. This and C. Line, “Chapter-Viii Voltage Stability Analysis With Upfc- Pv Curve,” pp. 119–126.

[59] S. Chakrabarti, “Notes on Power System Voltage Stability,” *Dept. EE, IIT, Kanpur http// …*, pp. 1–16, 2010.

[60] C. Reis, A. Andrade, and F. P. Maciel, “Voltage stability analysis of electrical power system,” *2009 Int. Conf. Power Eng. Energy Electr. Drives*, vol. 0, pp. 244–248, 2009, doi: 10.1109/Powereng.2009.4915211.

[61] H. Mostafa, “Voltage Stability and Power Flow Studies of Distribution System Voltage Stability and Power Flow Studies of Distribution System,” no. July, 2018.

[62] N. Parsai, “PV curve –Approach for Voltage Stability Analysis,” vol. 4, no. 2, pp. 46–52, 2015.

[63] M. Parihar, M. K. Bhaskar, D. Bohra, and D. Sarvate, “PV- Curve Analysis of 3 Bus Power System using,” vol. 6, no. 5, pp. 201–205, 2017.

[64] T. Aziz, T. K. Saha, and N. Mithulananthan, “Distributed generators placement for loadability enhancement based on reactive power margin,” *2010 9th Int. Power Energy Conf. IPEC 2010*, April 2014, pp. 740–745, 2010, doi: 10.1109/IPECON.2010.5697023.

[65] A. O. Muhammed and M. Rawa, “A systematic PVQV-curves approach for investigating the impact of solar photovoltaic-generator in power system using powerworld simulator,” *Energies*, vol. 13, no. 10, 2020, doi: 10.3390/en13102662.

[66] W. Chandrasena, P. G. McLaren, U. D. Annakkage, and R. P. Jayasinghe, “Modeling GIC effects on power systems: The need to model magnetic status of transformers,” *2003 IEEE Bol. PowerTech - Conf. Proc.*, vol. 2, pp. 981–986, 2003, doi: 10.1109/PTC.2003.1304679.

[67] M. J. Heyns, S. I. Lotz, and C. T. Gaunt, “Geomagnetic Pulsations Driving Geomagnetically Induced Currents,” *Sp. Weather*, vol. 19, no. 2, 2021, doi: 10.1029/2020SW002557.

[68] P. Jankee, “Synchronous generator and excitation system response to GIC,” December, 2020.

[69] W. Chandrasena, P. G. McLaren, U. D. Annakkage, and R. P. Jayasinghe, “An improved low-frequency transformer model for use in GIC studies,” *IEEE Trans. Power Deliv.*, vol. 19, no. 2, pp. 643–651, 2004, doi: 10.1109/TPWRD.2004.824429.

[70] J. L. Willems, “The IEEE Standard 1459: What and why?,” *AMPS 2010 - 2010 IEEE Int. Conf. Appl. Meas. Power Syst. Proc.*, no. August, pp. 41–46, 2010, doi: 10.1109/AMPS.2010.5609324.

[71] H. Chisepo, “Measurements and finite element modelling of transformer flux with dc and power frequency curren,” 2019.

[72] “IEC61869-2-2012.pdf.”

[73] N. S. Sithebe and D. T. O. Oyedokun, “Impact of GICs on the Voltage Stability Margin of Power Systems,” *IEEE AFRICON Conf.*, vol. 2019-Septe, 2019, doi: 10.1109/AFRICON46755.2019.9133807.

[74] H. K. Chisepo, C. T. Gaunt, and L. D. Borrill, “Measurement and FEM analysis of DC/GIC effects on transformer magnetization parameters,” *2019 IEEE Milan PowerTech, PowerTech 2019*, no. September, 2019, doi: 10.1109/PTC.2019.8810423.

[75] T. R. Hutchins and T. J. Overbye, “The effect of geomagnetic disturbances on the electric grid and appropriate mitigation strategies,” *NAPS 2011 - 43rd North Am. Power Symp.*, pp. 1–5, 2011, doi: 10.1109/NAPS.2011.6025162.

[76] V. N. Rajput, D. H. Boteler, N. Rana, M. Saiyed, S. Anjana, and M. Shah, “Insight into impact of geomagnetically induced currents on power systems: Overview, challenges and mitigation,” *Electr. Power Syst. Res.*, vol. 192, November 2020, 2021, doi: 10.1016/j.epsr.2020.106927.

[77] W. Chandrasena, P. G. McLaren, U. D. Annakkage, and R. P. Jayasinghe, “Modeling GIC effects on power systems: The need to model magnetic status of transformers,” *2003 IEEE Bol. PowerTech - Conf. Proc.*, vol. 2, no. July, pp. 981–986, 2003, doi: 10.1109/PTC.2003.1304679.

[78] H. Kirkham, Y. Makarov, J. Dagle, J. DeSteese, M. Elizondo, and R. Diao, “Geomagnetic Storms and Long-Term Impacts on Power Systems,” December, 2011, [Online]. Available: http://www.pnnl.gov/main/publications/external/technical_reports/PNNL-21033.pdf.

[79] J. Berge, R. K. Varma, and L. Marti, “Laboratory validation of the relationship between Geomagnetically Induced Current (GIC) and transformer absorbed reactive power,” *2011 IEEE Electr. Power Energy Conf. EPEC 2011*, vol. 9, pp. 491–495, 2011, doi: 10.1109/EPEC.2011.6070251.

[80] P. Jankee, H. Chisepo, V. Adebayo, D. Oyedokun, and C. T. Gaunt, “Transformer models and meters in MATLAB and PSCAD for GIC and leakage dc studies,” *2020 Int. SAUPEC/RobMech/PRASA Conf. SAUPEC/RobMech/PRASA2020*,2020,doi:10.1109/SAUPEC/RobMech/PRASA48453.2020.9041060.

[81] S. Guillon, P. Toner, L. Gibson, and D. Boteler, “A Colorful Blackout: The Havoc Caused by Auroral

Electrojet Generated Magnetic Field Variations in 1989," *IEEE Power Energy Mag.*, vol. 14, no. 6, pp. 59–71, 2016, doi: 10.1109/MPE.2016.2591760.

[82] S. E. Zirka, Y. I. Moroz, and C. M. Arturi, "Once again about the Steinmetz transformer model and the ongoing subdivision of its leakage inductance," *COMPEL - Int. J. Comput. Math. Electr. Electron. Eng.*, 2021, doi: 10.1108/COMPEL-06-2021-0190.

[83] A. A. Hussein, "Mitigation of geomagnetically induced currents by variable series reactor," *2017 North Am. Power Symp. NAPS 2017*, 2017, doi: 10.1109/NAPS.2017.8107277.

[84] Office of Risk Management and Analysis, "Geomagnetic Storms : An Evaluation of Risks and Risk Assessments By the Office of Risk Management and Analysis," *Off. Risk Manag. Anal.*, May, pp. 1–12, 2011.

[85] P. Jankee, "Synchronous generator modelling and excitation voltage control for GIC studies," *Asia-Pacific Power Energy Eng. Conf. APPEEC*, 2021.

10. Appendices

10.1 Appendix A: QXP 1200 SP Watt DC Power Supply

Table 10.1: Specifications of the QXP power supply

Atrribute	Value
Output Voltage	0 → 60V
Output Current	0 → 50A
Bench Power Supply Type	Laboratory Power Supply
Number of Outputs	1
Type	Digital
Power Rating	1.2kW
Supply Voltage	110 → 240V ac
Number of Displays	1
Input Connector	IEC 320
Output Connector	Binding Post Terminal
Minimum Temperature	+5°C
Maximum Temperature	+40°C
Digital/Analogue	Digital

10.2 Appendix B: Magnetization Characteristics

The following figures show the magnetization curves of phase B and phase C obtained from O.C tests conducted on both 3p3L and 3p5L.

10.2.1 3p3L Magnetization Curves

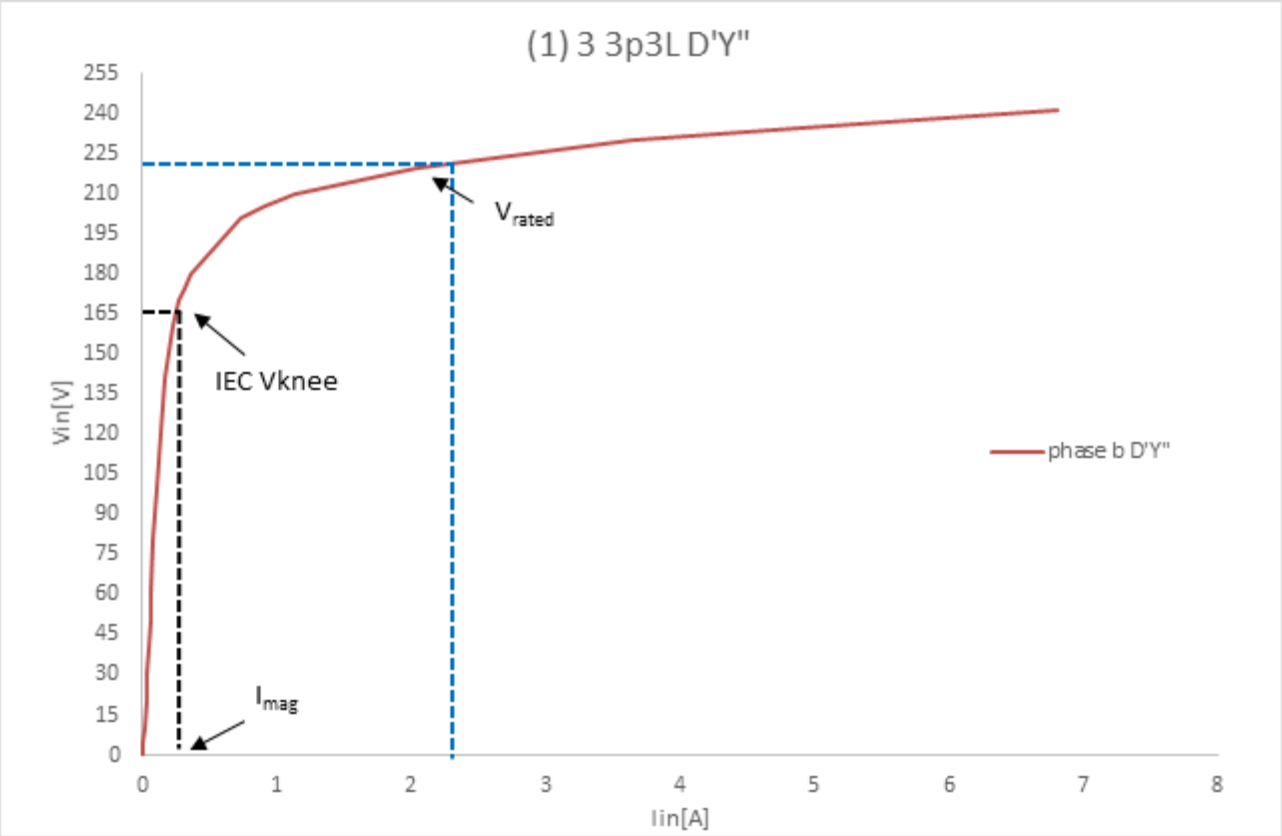

Figure 10.1: 3p3L Phase B Magnetization curve

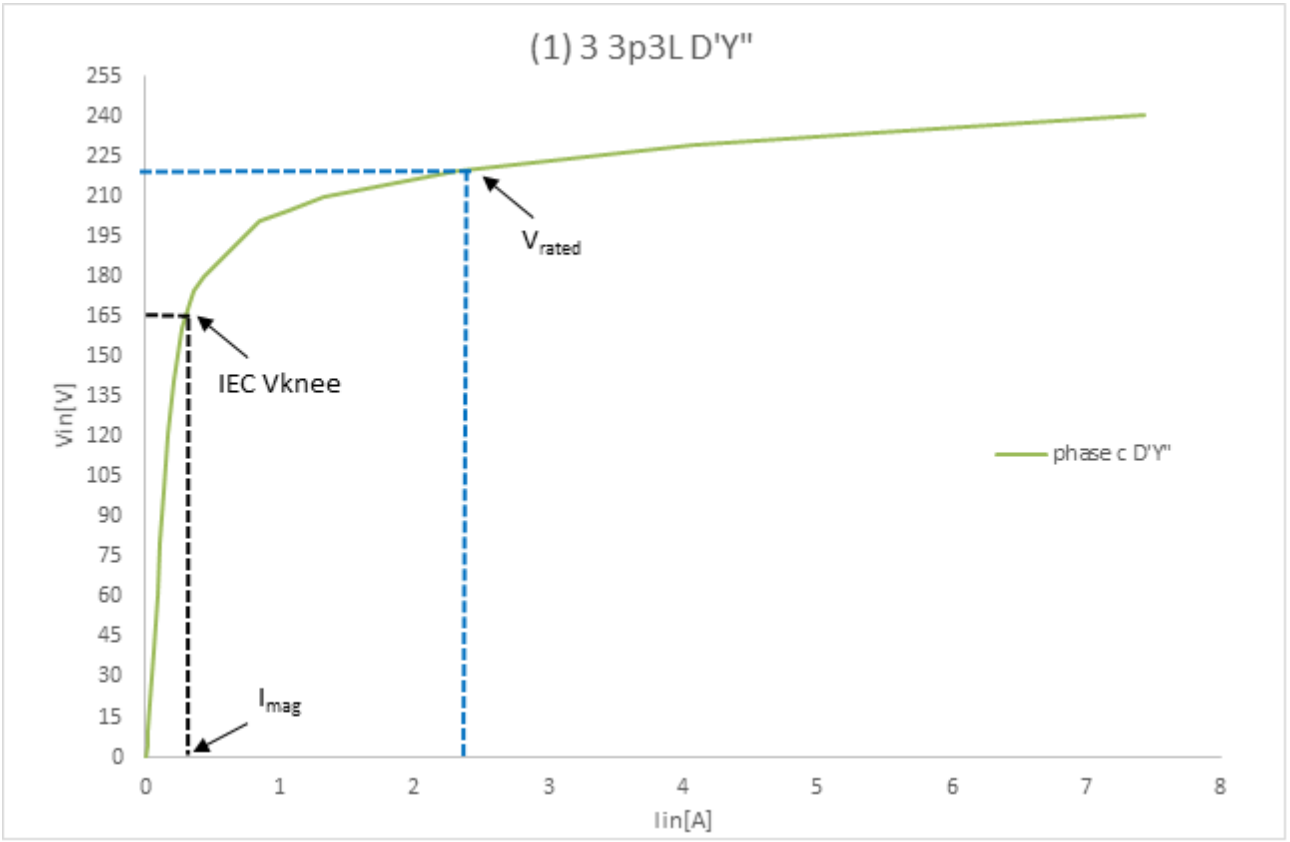

Figure 10.2:3p3L Phase C Magnetization Curve

10.2.2 3p5L Magnetization Curves

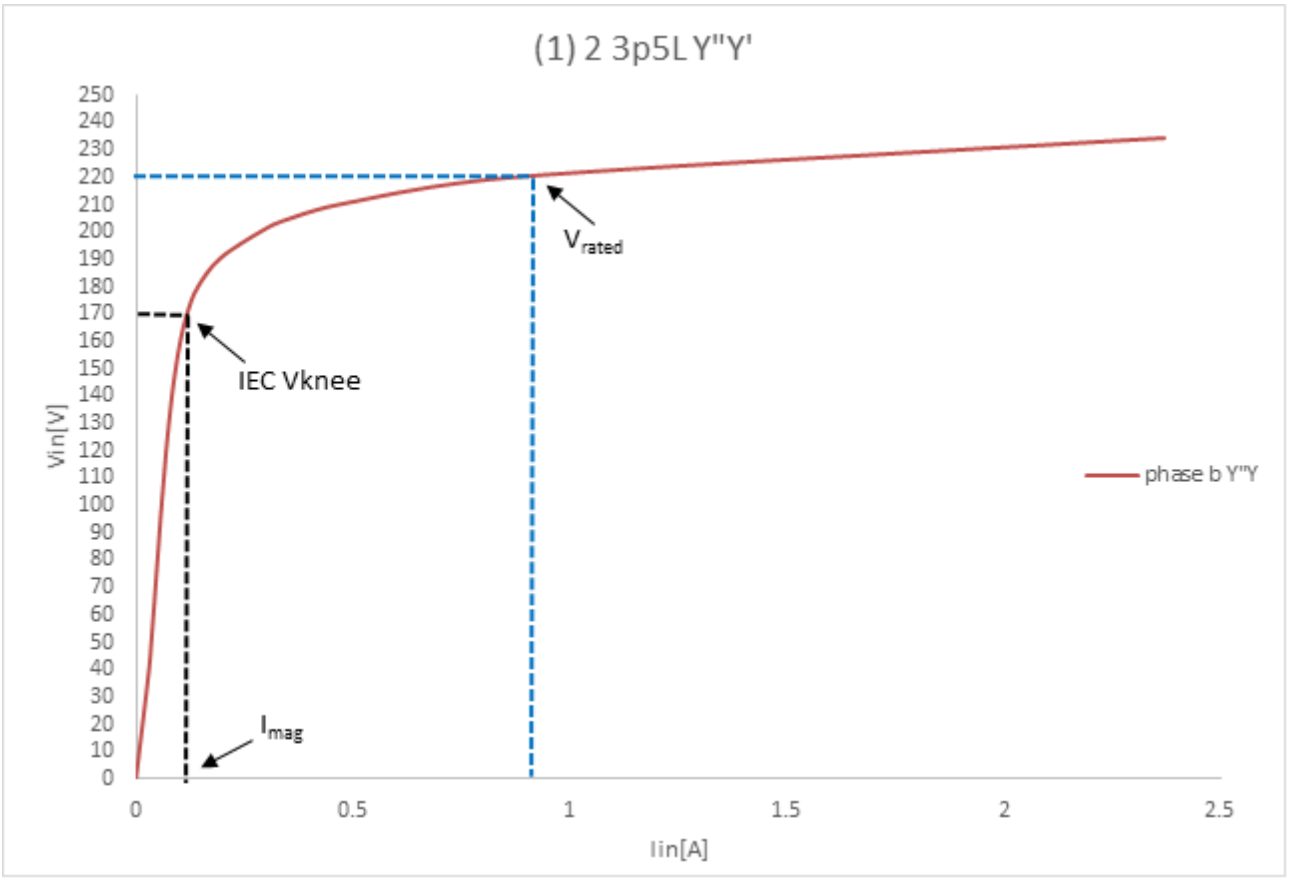

Figure 10.3:3p5L Phase B Magnetization Curve

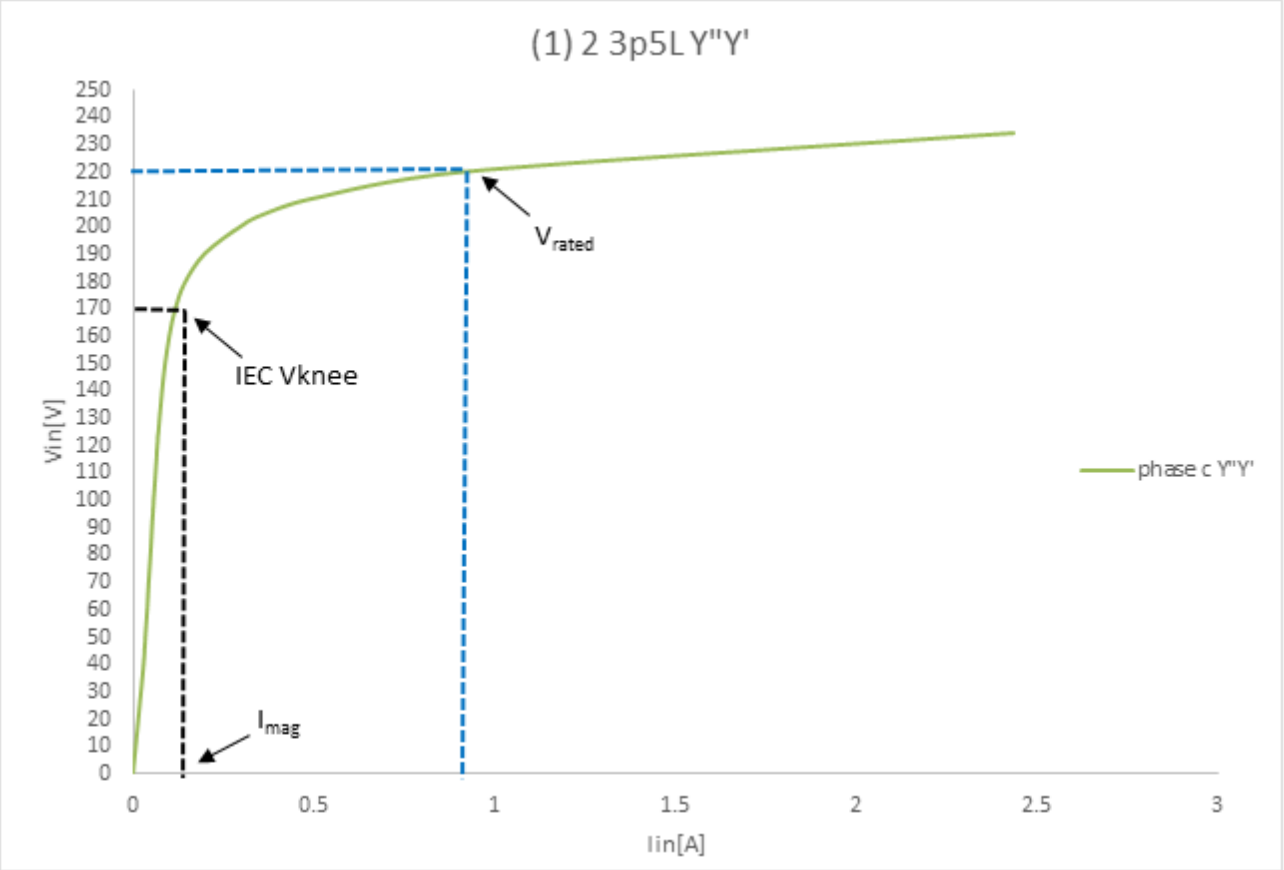

Figure 10.4: Phase C Magnetization Curve

10.3 Appendix C: Bus 3 Peak acGIC vs dcGIC Voltage and Current Harmonics at Different Loading Conditions

10.3.1 No Load Conditions

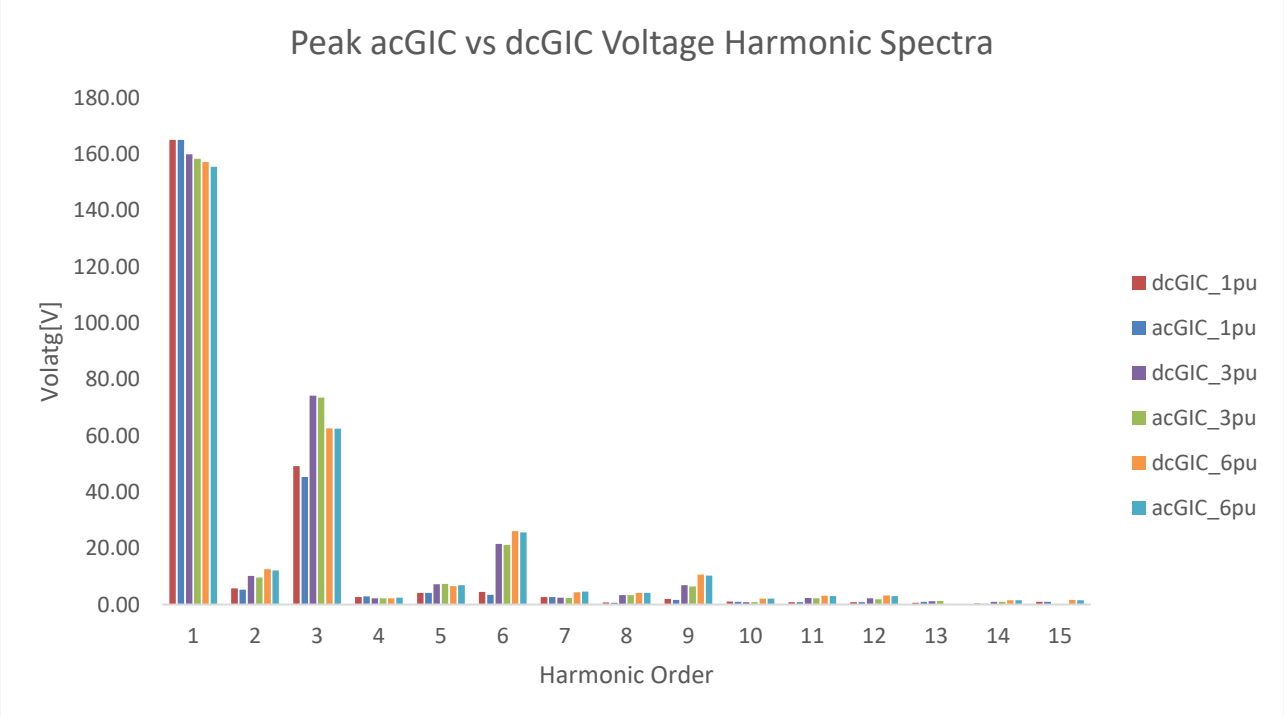

Figure 10.5: Phase A Peak acGIC vs dcGIC Voltage Harmonic Spectra at No Load

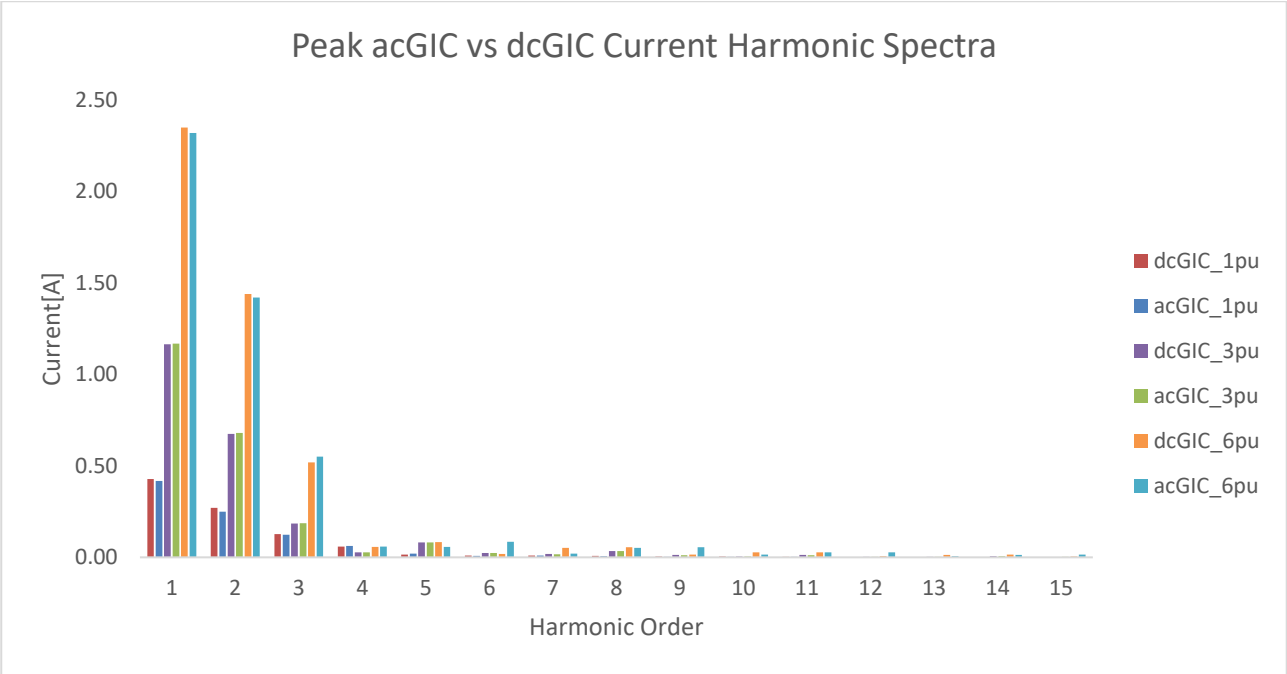

Figure 10.6: Phase A Peak acGIC vs dcGIC Voltage Harmonic Spectra at No Load

10.3.2 Lightly Loaded Conditions

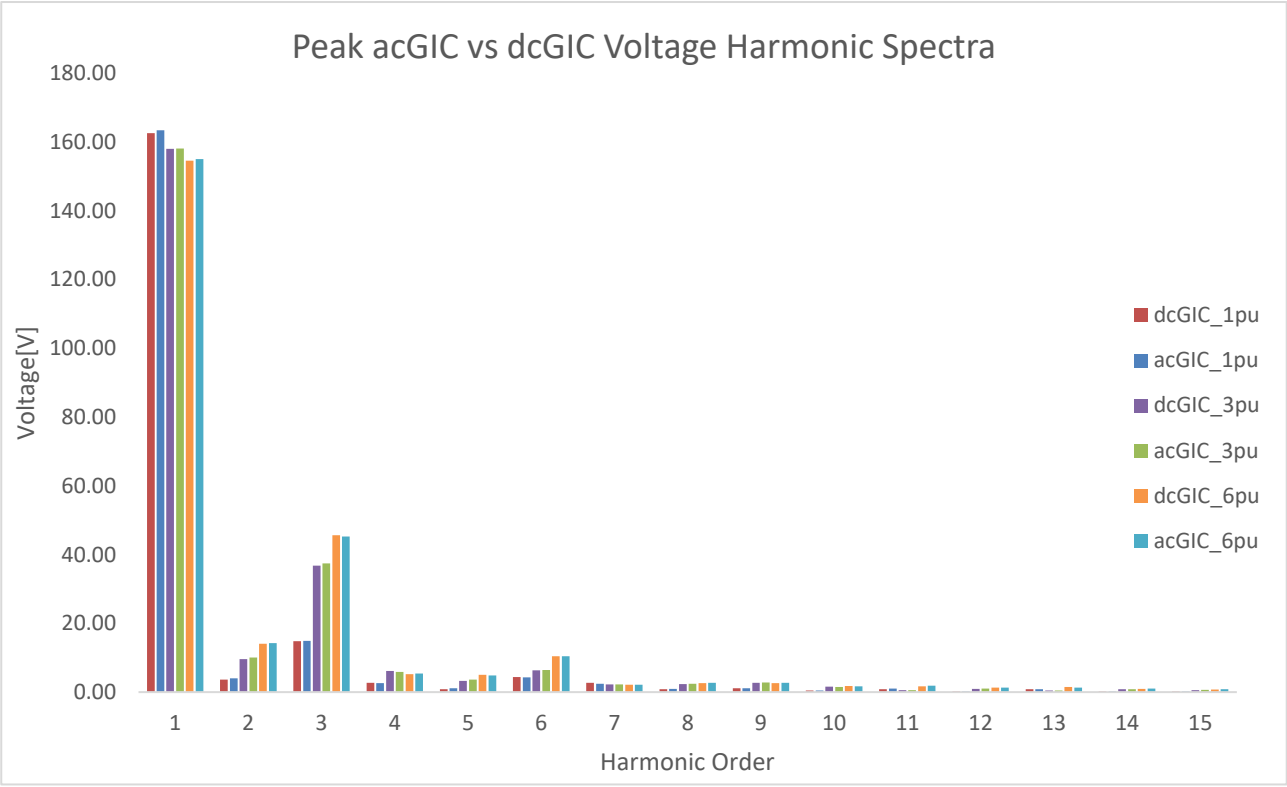

Figure 10.7: Phase A Peak acGIC vs dcGIC Voltage Harmonic Spectra for a Lightly Loaded System

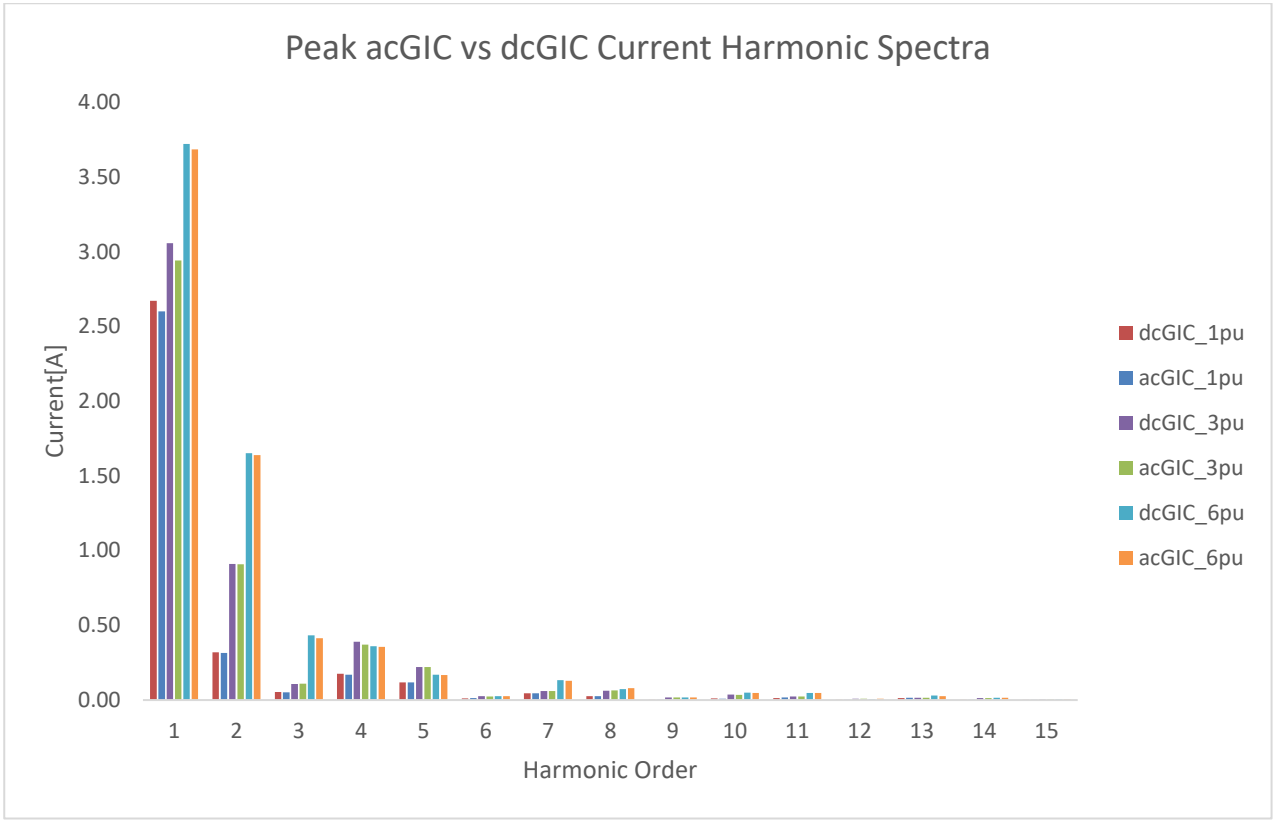

Figure 10.8:Phase A Peak acGIC vs dcGIC Voltage Harmonic Spectra for a Lightly Loaded System

10.4 Load Modelling Validation

10.4.1 1pu dcGIC

i. Heavily Loaded System

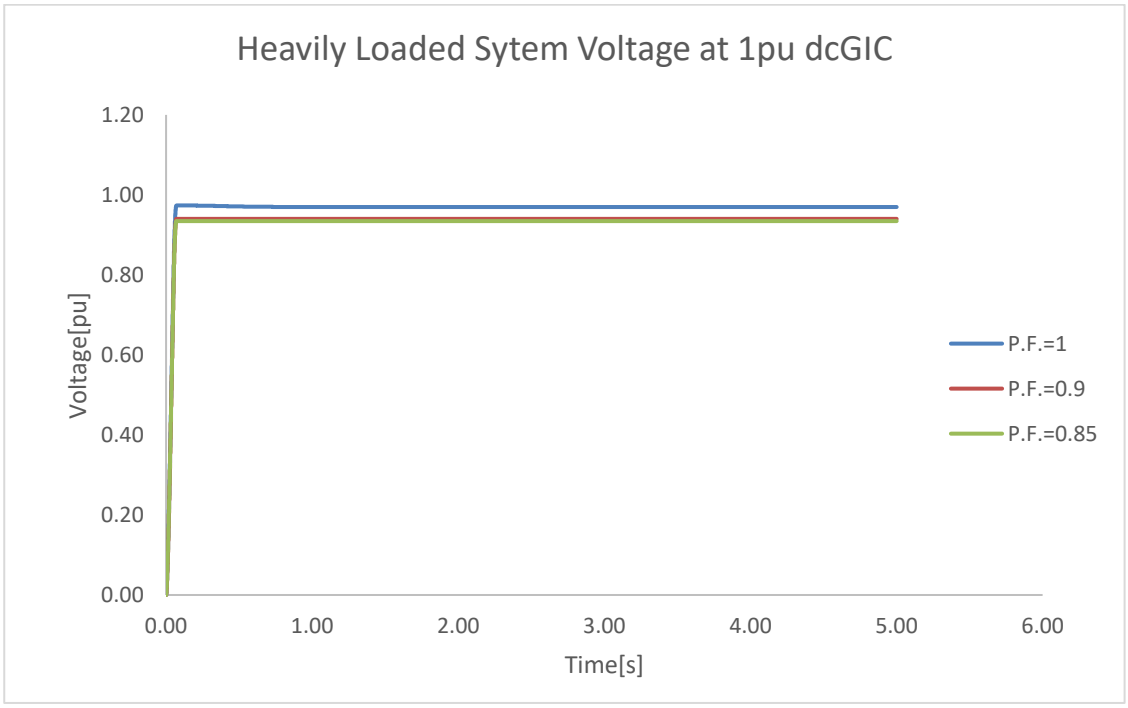

Figure 10.9: Heavily Loaded System voltage plots at different power factors with 1pu dcGIC injected

ii. Lightly Loaded System

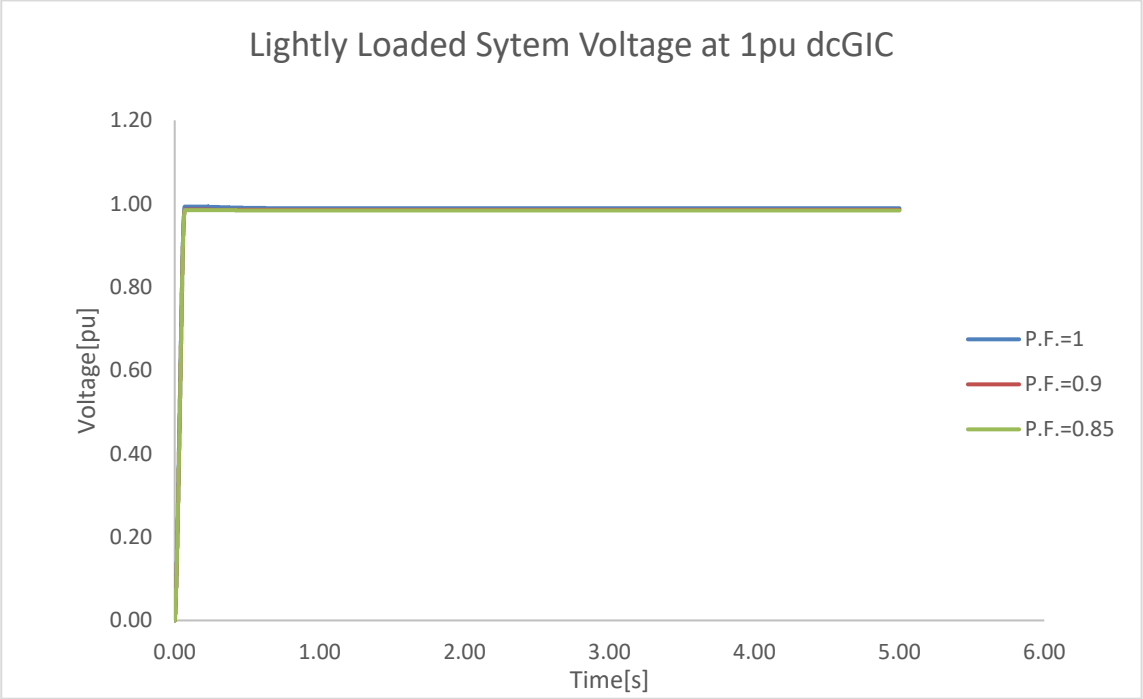

Figure 10.10: Lightly Loaded System voltage plots at different power factors with 1pu dcGIC injected

10.4.2 6pu dcGIC

i. Heavily Loaded System

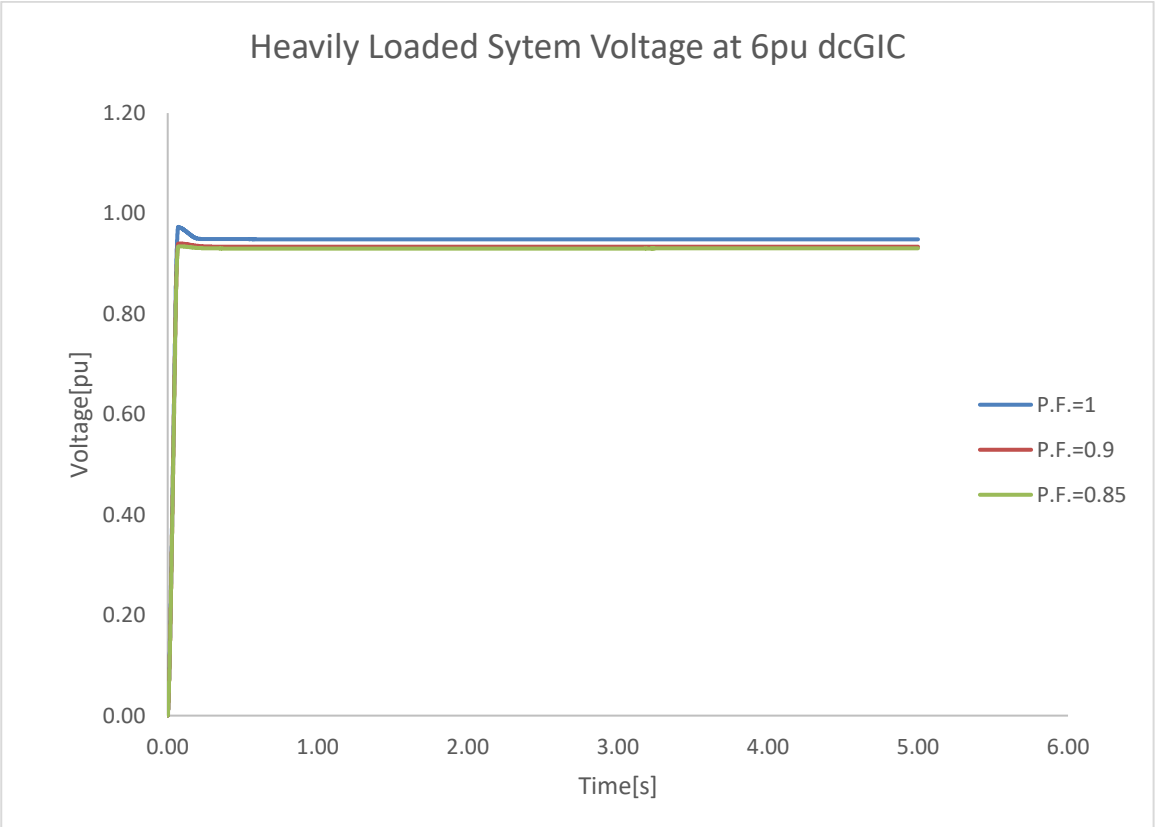

Figure 10.11: Heavily Loaded System voltage plots at different power factors with 6pu dcGIC injected

ii. ***Lightly Loaded System***

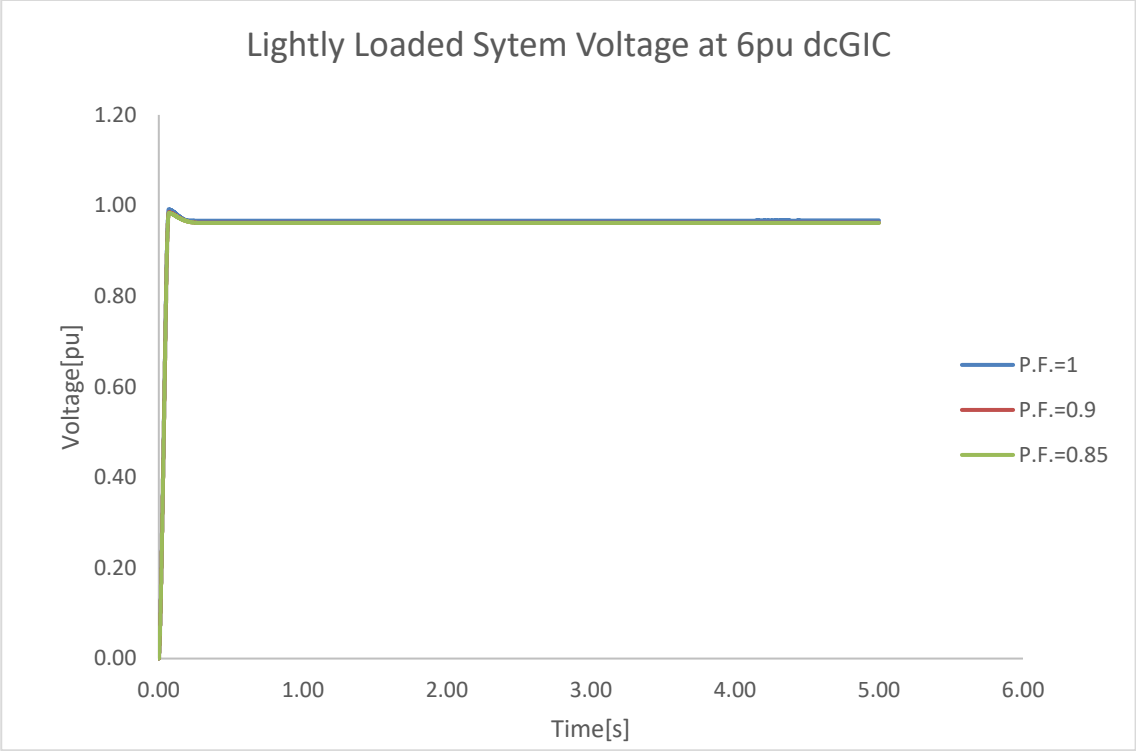

Figure 10.12: Lightly Loaded System voltage plots at different power factors with 6pu dcGIC injected